



Adsorption/Retention of Polymer Solution in Porous Media

Bauyrzhan Satken

► To cite this version:

Bauyrzhan Satken. Adsorption/Retention of Polymer Solution in Porous Media. Mechanics [physics]. Université de Bordeaux, 2021. English. NNT : 2021BORD0145 . tel-03267834

HAL Id: tel-03267834

<https://theses.hal.science/tel-03267834>

Submitted on 22 Jun 2021

HAL is a multi-disciplinary open access archive for the deposit and dissemination of scientific research documents, whether they are published or not. The documents may come from teaching and research institutions in France or abroad, or from public or private research centers.

L'archive ouverte pluridisciplinaire **HAL**, est destinée au dépôt et à la diffusion de documents scientifiques de niveau recherche, publiés ou non, émanant des établissements d'enseignement et de recherche français ou étrangers, des laboratoires publics ou privés.

THESIS PRESENTED
TO OBTAIN THE QUALIFICATION OF
**DOCTOR OF
THE UNIVERSITY OF BORDEAUX**

DOCTORAL SCHOOL OF PHYSICAL SCIENCES AND
ENGINEERING

Mechanical engineer

By Bauyrzhan SATKEN

**Adsorption/Retention of Polymer Solution in
Porous Media**

Under the supervision of Henri BERTIN

co-supervisor: Abdelaziz OMARI

Viva on 19 May 2021

Jury

Mr. Daniel BROSETA Professor, University de Pau et des Pays de l'Adour	Reviewer
Ms. Irina PANFILOV MCF HDR, University of Lorraine	Reviewer
Ms. Azita AHMADI Professor, ENSAM	Jury President
Mr. Thierry LEBLANC Resercher Engineer, SNF Floerger	Examiner
Mr. Henri BERTIN Research Director,CNRS	Supervisor
Mr. Abdelaziz OMARI Professor, Bordeaux INP	Co-Supervisor

Table of content

1.	Introduction	11
1.	Chapter I : General features & literature review	14
1.1.	Porous media	14
1.2.	Flow in porous media	16
1.2.1.	Pore scale.....	16
1.2.2.	Local scale.....	18
1.3.	Miscible flows	19
1.3.1.	Molecular diffusion	19
1.3.2.	Dispersion.....	19
1.4.	Diphasic flows	22
1.4.1.	Concept of saturation	22
1.5.	Interfacial tension and wettability	22
1.5.1.	Wettability measurement.....	24
1.5.2.	Influence of ageing of rock in contact with oil on the wettability	28
1.5.3.	Generalized Darcy's model.....	29
1.5.4.	Capillary pressure.....	30
1.5.5.	Relative permeability hysteresis.....	32
1.5.6.	Parameters that influence wettability	32
1.5.7.	Wettability of porous media.....	34
1.6.	Polymer.....	36
1.6.1.	Conformation of polymers in solution state	37
1.6.2.	Entanglement concentration	39
1.6.3.	Viscosity of polymer solutions.....	40
1.7.	Polymer at the surface	41
1.7.1.	Adsorption from quiescent solution	41
1.8.	Polymer solution in Porous medium	45
1.8.1.	Mechanical entrapment	45
1.8.2.	Hydrodynamic retention.....	47
1.8.3.	Polymer adsorption	48
2.	Chapter II: Experimental Study.....	55
2.1.	Porous media	55
2.2.	Brine	57

2.3.	Polymer.....	57
2.3.1.	Polymer solution	58
2.4.	Experimental setup	60
2.5.	Experimental equipment.....	61
2.5.1.	Pressure transducers	61
2.5.2.	Pumps	62
2.5.3.	Spectrophotometer	63
2.5.4.	TOC-L/TNM-L	64
2.6.	Experimental procedure.....	65
2.6.1.	Characterization of porous media.....	65
2.6.2.	Monophasic experimental procedure	65
2.6.3.	Diphasic experimental procedure.....	66
3	Chapter III – Results and Discussion	67
3.1	Composition of brine	67
3.2	Viscosity of polymer solutions	67
3.2.1	Influence of concentration on viscosity	68
3.3	Characterization of porous media.....	71
3.3.1	Porosity, pore volume and homogeneity of PM.....	71
3.3.2	Permeability	73
3.4	Monophasic experiments	75
3.4.1	Polymer flooding.....	75
3.4.2	Mobility reduction.....	77
3.4.3	Brine flush	80
3.4.4	Permeability reduction	80
3.4.5	Second polymer flooding	82
3.4.6	The retention of polymer.....	84
3.4.7	Inaccessible pore volume	96
3.5	Diphasic experiments: Water-wet condition	98
3.5.1	Oil drainage	98
3.5.2	Waterflooding.....	99
3.5.3	Dispersion test in diphasic.....	100
3.5.4	Polymer flooding.....	101
3.5.5	Mobility reduction.....	102

3.5.6	Brine flush and permeability reduction	103
3.5.7	Second polymer injection.....	103
3.5.8	Retention of polymer.....	104
3.5.9	IPV	105
3.6	Diphasic experiments: Altered wettability porous media.....	106
3.6.1	Permeability to oil after ageing	107
3.6.2	Waterflooding.....	108
3.6.3	Polymer flooding.....	109
3.6.4	Retention of polymer.....	111
4.	Chapter IV: Conclusions and perspectives.....	114
5.	Nomenclature	117
6.	Bibliography.....	120
7.	Appendix A	125
8.	Appendix B	127

Table of figures

Figure 1-1. The diagram of the types of pores in a porous medium [Rouquerol et al., 1994].	14
Figure 1-2. Representative diagram to show the difference in tortuosity	15
Figure 1-3. The different scales of observation of the porous media [Chiara, 2009]	16
Figure 1-4. The concentration profile as a function of dispersion and diffusion.	21
Figure 1-5. Relationship between Pe and dispersion [Perkins and Johnson, 1963]	21
Figure 1-6. Contact angle θ between immiscible fluids and the solid.	22
Figure 1-7. Wettability of oil/water/rock systems	23
Figure 1-8. Representations of fluid phases as a function of wettability [Meybodi et al., 2011]	24
Figure 1-9. Amott wetting technique [Glover, 2010]	26
Figure 1-10. Wettability test data [Glover, 2010]	27
Figure 1-11. USBM wettability test capillary pressure curve (numbers indicate the progress of the test from $S_w = 100\%$)	28
Figure 1-12. Relative permeabilities	29
Figure 1-13. Thipycal curves of relative permeabilities: a) in water-wet PM b) in oil-wet PM [Anderson, 1986b]	30
Figure 1-14. Capillary pressure in a Berea [Anderson, 1986c]	31
Figure 1-15. Capillary pressure as a function of the permeability type	31
Figure 1-16. Precipitation of asphaltenes as a function of the solvent [Buckley et al, 1998] ..	33
Figure 1-17. Surface/brine/oil interaction [Buckley et al 1998]	33
Figure 1-18. Influence of multivalent ions on the adsorption of surfactants [Buckley et al 1998]	34
Figure 1-19. Capillary pressure vs saturation as a function of wettability. a) water-wet, b) oil- wet, c) mixed-wet [Lenormand, 2013]	35
Figure 1-20. Water flow oil saturated PM a) water-wet, b) oil-wet [Anderson, 1986d]	35
Figure 1-21. Schematic representation of linear (a), branched (b), and cross-linked (c) polymers	36
Figure 1-22. Types of copolymers: brown and orange represents the different type of monomers	36
Figure 1-23. Conformations of polymers in dilute solutions [Colby, 2010]	37
Figure 1-24. Schematic of dilute, overlap and semi dilute solutions	38
Figure 1-25. Schematic structure of a semi-dilute solutions and correlation length, ξ	39
Figure 1-26. Comparison of overlap concentrations and entanglement concentrations of polystyrene in toluene [Kulicke and Kniewske, 1984; Onogi et al., 1967]	40
Figure 1-27. Qualitative plot of the polymer volume fraction (ϕ) vs distance from an adsorbing (a) and repelling (b) walls. Full line (a): profile $\phi(z)$ for a finite volume fraction ϕb in the bulk solution. Dotted line (a): profile extrapolated to $\phi b = 0$	42
Figure 1-28. Relationship between the polymer volume fraction versus distance and the polymer concentration on the surface with tails, loops and trains	43
Figure 1-29. Pancake and Brush conformations of polymer	44
Figure 1-30. Sketch of mushroom, a pancake, and a brush.	44

Figure 1-31. Schematic diagram of polymer retention mechanisms in porous media (Willhite and Dominguez, 1977)	45
Figure 1-32. Distribution of retained HPAM along a sandpack after polymer flood. Conditions: 0.4PV brine, 0.2PV polymer, continuous brine injection, $k=1200\text{mD}$, $v=6\text{ft/day}$ [Szabo, 1975]	46
Figure 1-33. The effect of flow rate on the hydrodynamic retention of HPAM [Chauveteau and Kohler, 1974].....	47
Figure 1-34. Two methods (A and B) for evaluating polymer adsorption in porous media from the core effluent profiles [Willhite and Dominguez, 1977]	49
Figure 1-35. Polymer adsorption for different types of polymers [Sheng, 2011]	50
Figure 1-36. Adsorption isotherms of acrylamide-based polymers a function of the anionicity degree (PAM, $M_w=167\text{kg/mol}$, Dispersity=1.11), HPAM-10 ($M_w=181\text{kg/mol}$, Dispersity=1.09) and HPAM-30 ($M_w=149\text{kg/mol}$, Dispersity=1.07)) on natural quartz [Bessaies-Bey et al., 2018]	51
Figure 1-37. Model of polymer adsorption/retention on the rock surface proposed by Zhang and Seright (2013)	52
Figure 1-38. Impact of the thermal treatment of the adsorption of HPAM ($M_w=7.6 \cdot 10^6\text{g/mol}$, 30% of anionicity) on silicon carbide with an oxidized surface [Lecourtier, 1990]	53
Figure 1-39. Variation of the free silanol groups density compared to the total amount of silanol groups as a function of the thermal treatment [Dugas et al., 2003].....	53
Figure 2-1. Bentheimer (a) and Berea (b) sandstones.....	56
Figure 2-2. Metallic plates with cross channels used to homogenize the fluid injection.....	56
Figure 2-3. Prepared porous media	57
Figure 2-4. Rheometers ARG2(a) and Kinexus(b), and Ostwald viscometer(c)	59
Figure 2-5. Typical plot of relative viscosity versus shear rate.....	60
Figure 2-6. Experimental setup	60
Figure 2-7. Differential pressure transducer Rosemount 3051	62
Figure 2-8. Pressure taps location in porous media with different length: 20cm and 15cm	62
Figure 2-9. Pumps used in the experiments	63
Figure 2-10. Spectrophotometer UV-3100PC.....	63
Figure 2-11. Calibration curve of concentration of KI vs Absorbance of light at 226nm	64
Figure 2-12. TOC-L/TNM-L analyser	64
Figure 2-13. Calibration curve	65
Figure 3-1. Dynamic viscosity of Flopaam 5115 BPM as a function of the shear rate at different concentrations at $T = 25^\circ\text{C}$	68
Figure 3-2. Viscosity of polymers at Newtonian plateau as a function of concentration. Solid line: power-law fits to dilute and semi-dilute regimes. Dashed line: the overlap concentrations	69
Figure 3-3. Relative specific viscosity, $\eta r - 1Cp$, vs concentration of polymer 3130S	70
Figure 3-4. Relative plateau viscosity of polymers 3630S and 3130S at various concentrations versus $C_p[\eta]_0$ and fitting Huggins model	71
Figure 3-5. Dispersion test carried out on a sample of Bentheimer	72
Figure 3-6. The dispersion curves of every Bentheimer sample.....	72

Figure 3-7. Permeability measurement of Bentheimer sample. Evaluation of pressure for different flow rates	73
Figure 3-8. Pressure gradients as a function of flow rates for Bentheimer core	73
Figure 3-9. Permeability vs porosity of Bentheimer and Berea	74
Figure 3-10. Pore size distributions for Bentheimer and Berea sandstones, determined by mercury porosimetry	75
Figure 3-11. Calibration curve giving concentration of polymer 5115BPM versus concentration of carbon and nitrogen.....	76
Figure 3-12. The break-through curve of first polymer flooding and its analytical fitting.....	76
Figure 3-13. The pressure drop data during polymer injection; Bentheimer and 3630S at $C_p=1500\text{ppm}$, $Q=10\text{ml/h}$	77
Figure 3-14. Pressure drop during polymer injection at various flow rates in a range of 5 to 300ml/h to estimate the RM.....	78
Figure 3-15. Mobility reduction and relative viscosity versus shear rate	79
Figure 3-16. The RM value of polymer 3630S in Bentheimer and η_r of 3630S in bulk solution	79
Figure 3-17. Pressure drop data during brine flush, Bentheimer-3630S.....	80
Figure 3-18. Evolution of RM and R_k , relative viscosity, η_r , and relative apparent viscosity, η_{rapp} as a function of shear rate.....	81
Figure 3-19. Breakthrough curves of first and second polymer flooding	83
Figure 3-20. Breakthrough curves of second polymer flooding and KI dispersion	84
Figure 3-21. Retention of polymer 3630S in Bentheimer versus concentration and Freundlich fitting (black solid line)	85
Figure 3-22. Sketch of polymer adsorption mechanism in dilute regime at low and high concentrations.....	85
Figure 3-23. Adsorption kinetics of polymer 3630S in Bentheimer at various concentration as a function of injected Pore volume (PV).....	86
Figure 3-24. Adsorption rate, $d\Gamma/dPV$, versus concentration of polymer 3630S in Bentheimer in log-log scale and the typical adsorption kinetics of colloids(dashed line) versus concentration	87
Figure 3-25. The difference between the colloids deposition and polymer adsorption on the surface of the collector	88
Figure 3-26. Sketch of polymer bridging [Zaitoun and Chauvteau, 1998]	89
Figure 3-27. Adsorption kinetics of polymer 3130S in Berea at various concentrations	89
Figure 3-28. Retention of polymer 3130S in Berea at various concentration.....	90
Figure 3-29. Sketch of coverage of the same surface with the polymer molecules of different size.....	90
Figure 3-30. Retention of polymer 3130S at various concentration in Bentheimer and Berea.....	92
Figure 3-31. Sketch of capillary model with the capillary tubes of radius R_p and length L	93
Figure 3-32. Corrected retention data of polymer 3130S in Bentheimer and Berea at concentrations 3500, 5000 and 7000ppm.....	93
Figure 3-33. Retention of polymers 5115XV and 5115BPM at concentrations 1000ppm and 2500ppm that corresponds to viscosity around 10cP	94
Figure 3-34. Possible calcium mediated adsorption on silica (Mohan et al., 2021)	95

Figure 3-35. Retention of polymer 5115XV and 3630S in Bentheimer at concentration 1000ppm.....	95
Figure 3-36. Adsorption rate of polymers 5115XV and 3630S in Bentheimer at concentration 1000ppm.....	95
Figure 3-37. Inaccessible pore volume versus polymer concentration for 3630S in Bentheimer	96
Figure 3-38. Inaccessible pore volume for polymer 3130S in Berea.....	97
Figure 3-39. Pressure drop and Water saturation versus injected oil volume during the oil drainage and injecting at higher flow rates to estimate the effective permeability to oil	98
Figure 3-40. Oil recovery and Pressure drop data during water imbibition and at various flow rates to determine the $k_w(S_{or})$	99
Figure 3-41. Dispersion curve before oil drainage and at S_{or} versus injected volume of brine in Bentheimer	100
Figure 3-42. Dispersion curve in monophasic, before oil drainage, and in diphasic versus PV in Bentheimer	101
Figure 3-43. Intermediate pressure drop data during first polymer flooding in presence of oil and without oil.....	101
Figure 3-44. Normalized pressure drop data for monophasic and diphasic polymer flooding at 10ml/h; The data for diphasic is corrected to S_{or}	102
Figure 3-45. Pressure drop data during polymer flooding at various flow rates to estimate the RM in Bentheimer	103
Figure 3-46. RM values of 3630S in Bentheimer and η_r in a bulk solution at $C_p=1000\text{ppm}$	103
Figure 3-47. The retained polymer of monophasic and diphasic experiments with polymers 3630S and 5115XV in Bentheimer	104
Figure 3-48. Sketch of adsorption of polymer in pores with oil droplet in the center	105
Figure 3-49. Sketch of possible adsorption of polymer on to the oil-water interface.....	105
Figure 3-50. IPV of monophasic and diphasic (water-wet) experiments with 3630S and 5115XV	106
Figure 3-51. The pore repartition of S_{or} (black) and S_{wi} (blue) in water-wet and oil-wet porous media	107
Figure 3-52. Injection of oil at various flow rates after ageing to estimate the $ko_2(S_{wi})$ in Bentheimer	107
Figure 3-53. Pressure drop during waterflooding and at various flow rates to calculate the water permeability at S_{or} , $k_w(S_{or})$, and oil recovery data.....	108
Figure 3-54. Oil recovery in water-wet and altered wettability cores experiments.	109
Figure 3-55. Pressure drop data during flooding polymer 3630S at $C_p=1000\text{ppm}$ in 100% brine-saturated core, water-wet and aged diphasic cores	110
Figure 3-56. Normalized pressure drop during polymer flooding in 100% brine saturated core, diphasic water-wet core and diphasic aged core	111
Figure 3-57. The retention of polymers 3630S and 5115XV in Bentheimer at monophasic and diphasic cases	111
Figure 3-58. The adsorption of polymer and oil location in oil-wet core	112
Figure 3-59. The pore repartition of S_{or} (black) and S_{wi} (blue) in water-wet and oil-wet porous media	112

Figure 7-1. Dynamic viscosity of Flopaam 3630S as a function of the shear rate at different concentrations at $T = 25^{\circ}\text{C}$	125
Figure 7-2. Dynamic viscosity of Flopaam 3130S as a function of the shear rate at different concentrations at $T = 25^{\circ}\text{C}$	126
Figure 7-3. Dynamic viscosity of Flopaam 5115XV as a function of the shear rate at different concentrations at $T = 25^{\circ}\text{C}$	126
Figure 8-1. Breakthrough curves of first and second polymer flooding at $C_p=200\text{ppm}$ of 3630S in Bentheimer and KI dispersion	127
Figure 8-2. Breakthrough curves of first and second polymer flooding at $C_p=300\text{ppm}$ of 3630S in Bentheimer and KI dispersion	128
Figure 8-3. Breakthrough curves of first and second polymer flooding at $C_p=500\text{ppm}$ of 3630S in Bentheimer and KI dispersion	128
Figure 8-4. Breakthrough curves of first and second polymer flooding at $C_p=1000\text{ppm}$ of 3630S in Bentheimer and KI dispersion	129
Figure 8-5. Breakthrough curves of first and second polymer flooding at $C_p=2000\text{ppm}$ of 3630S in Bentheimer and KI dispersion	129
Figure 8-6. Breakthrough curves of first and second polymer flooding at $C_p=5000\text{ppm}$ of 3630S in Bentheimer and KI dispersion	130
Figure 8-7. Breakthrough curves of first and second polymer flooding at $C_p=500\text{ppm}$ of 3130S in Berea and KI dispersion	130
Figure 8-8. Breakthrough curves of first and second polymer flooding at $C_p=700\text{ppm}$ of 3130S in Berea and KI dispersion	131
Figure 8-9. Breakthrough curves of first and second polymer flooding at $C_p=2000\text{ppm}$ of 3130S in Berea and KI dispersion	131
Figure 8-10. Breakthrough curves of first and second polymer flooding at $C_p=3500\text{ppm}$ of 3130S in Berea and KI dispersion	132
Figure 8-11. Breakthrough curves of first and second polymer flooding at $C_p=5000\text{ppm}$ of 3130S in Berea and KI dispersion	132
Figure 8-12. Breakthrough curves of first and second polymer flooding at $C_p=7000\text{ppm}$ of 3130S in Berea and KI dispersion	133
Figure 8-13. Breakthrough curves of first and second polymer flooding at $C_p=3500\text{ppm}$ of 3130S in Bentheimer and KI dispersion	133
Figure 8-14. Breakthrough curves of first and second polymer flooding at $C_p=5000\text{ppm}$ of 3130S in Bentheimer and KI dispersion	134
Figure 8-15. Breakthrough curves of first and second polymer flooding at $C_p=7000\text{ppm}$ of 3130S in Bentheimer and KI dispersion	134
Figure 8-16. Breakthrough curves of first and second polymer flooding at $C_p=1000\text{ppm}$ of 5115XV in Bentheimer and KI dispersion	135
Figure 8-17. Breakthrough curves of first and second polymer flooding at $C_p=2500\text{ppm}$ of 5115BPM in Bentheimer and KI dispersion	135
Figure 8-18. Breakthrough curves of first and second polymer flooding at $C_p=1000\text{ppm}$ of 3630S in Bentheimer (water-wet) and KI dispersion	137
Figure 8-19. Breakthrough curves of first and second polymer flooding at $C_p=1000\text{ppm}$ of 3630S in Bentheimer (aged) and KI dispersion	137

Figure 8-20. Breakthrough curves of first and second polymer flooding at $C_p=1000\text{ppm}$ of 5115XV in Bentheimer (water-wet) and KI dispersion	138
Figure 8-21. Breakthrough curves of first and second polymer flooding at $C_p=1000\text{ppm}$ of 5115XV in Bentheimer (aged) and KI dispersion.....	138

Introduction

Oil has become the world's most important source of energy since the mid -the 1950s. Its products mainly supply energy to the power industry, heat homes, and provide fuel for vehicles. Besides, oil's refined products are used to manufacture almost all chemical products, such as plastics, fertilizers, detergents, paints, and even medicines. However, the oil reserves are not limitless and new sources of energy are developing, and one day they might overtake oil.

Oil is a fossil fuel, meaning that it has been created by the decomposition of organic matter over millions of years. It is formed when large quantities of dead organisms – primarily zooplankton and algae – underneath sedimentary rock are subjected to intense heat and pressure. In permeable soils where oxygen-laden water can circulate freely, such as sands, the destruction of organic matter is observed (carbon mineralization in the form of dioxide, CO₂). This is the reason why sands and sandstones, which are good reservoir rocks, are not favorable rocks (parent rocks) for the formation of petroleum. On the other hand, underwater systems such as clays, limestones are good places to develop an anaerobic microbiological activity for the formation of kerogen (an intermediate substance between organic matter and fossil fuels and unassimilable by microorganisms). To have an exploitable deposit, the oil must be expelled from the bedrock to accumulate on adjacent more porous rocks where the hydrocarbons will be trapped. The increased pressure within the fluids formed in the bedrock (kerogen degradation) eventually exceeds the resistance of the rock by making cracks through which the oil flows to the traps.

Oil recovery is carried out in several stages. There are three different phases of oil recovery, i.e., primary, secondary and tertiary. This way to describe oil production is “classical”, and in some cases, the production can start directly by the secondary stage even by the tertiary stage.

In the first step to recovering the oil in place, the well is drilled in such a way that the oil naturally rises thanks to the pressure difference between the pressure of the reservoir and the surface. This pressure decreases over time and the production rate drops. At the end of this step, the recovery rate is around 10% of OOIP (Original oil in place), which depends on the characteristics of each reservoir.

Secondary processes consist of injecting water or gas to maintain the pressure in the reservoir and continue oil extraction. The choice between water or gas injection is made according to two criteria, economic and technical. Secondary recovery achieves a recovery rate of between 35% -45% of the oil in place.

When a reservoir has already been exploited by primary and secondary techniques, it may in certain cases be subject to economic criteria to continue its exploitation through tertiary recovery, enhanced oil recovery (EOR). These processes make it possible to extract between 5 and 20% more of the oil in place in the reservoir. The improved recovery methods are considerably more expensive than the conventional methods. Four techniques are used during tertiary recovery:

- Thermal recovery, which involves the injection of hot water or steam to lower the viscosity of oils, and to improve the mobility of the oil in the reservoir.
- Injection of gases, such as CO₂, to increase the pressure and reduce the viscosity of hydrocarbons. This technique can combine the recovery of oil and the geological storage of CO₂ because of its solubility in an adjacent aquifer.
- The injection of microorganisms that reduce the length of carbon chains while generating in situ surfactants and CO₂, which reduce water/oil interfacial tension but also the viscosity of the oil.
- The chemical EOR consists of improving the flushing of petroleum by water as surfactants by reducing the interfacial tension, nanoparticles, water-soluble polymers that increase the viscosity of displacing fluid.

Polymer injection is the most used EOR technique, commonly characterized by a more favorable mobility ratio than for water. The viscoelastic character of the polymer solutions helps to improve the mobilization of the trapped oil at the microscopic scale of the pores and therefore to reduce the residual oil saturation. Due to these advantages, polymer flooding has many successful applications in sandstone reservoirs. However, polymer flooding through carbonatic rock formations is challenging because of heterogeneity, high anionic polymer retention, low matrix permeability, and hardness of the formation water. While injecting the polymer solution the injectivity could be one of the crucial factors. Therefore, the polymer solution should be a non-Newtonian and shear-thinning fluid, that is, the viscosity decreases with increasing shear rate. It is worth noting that the shear rate is inversely proportional to the distance from the well. So we have low viscosity in the vicinity of the well (good injectivity) and high viscosity far from the well. However, close to the well elongation rate may be so high that polymer may be mechanically degraded there. In that respect, rigid polymers appear to be attractive since they have a very pronounced shear-thinning and are less sensitive to mechanical degradation in addition to their high tolerance to salt and elevated temperature. The economic success of the polymer flooding technique depends on the minimization of polymer loss due to retention. The retention of the polymer causes the decreasing of the viscosity of the polymer slug, consequently decreasing the overall sweep efficiency. Several laboratory studies have been dedicated to this issue for decades focusing on different parameters, i-e: polymer type, molecular weight, concentration, salinity and hardness of the aqueous solution, and flow conditions to optimize the ratio between oil recovery and polymer retention. However, most of the studies have been performed in monophasic conditions [Lecourtier et al., 1990; Lakatos et al., 1981; Zhang and Seright, 2014; Bessaies-Bey et al., 2018; Ferreira et al., 2019] showing that polymer retention is mostly due to adsorption of polymer chains on the surface of the porous medium. The experiments in presence of oil or oil-wet porous media are more sparse [Lakatos et al., 1981; Broseta et al., 1995; Wever et al., 2018] but generally show that oil presence may prevent polymer retention.

Polymer retention is a general term that includes adsorption, mechanical entrapment, and hydrodynamic retention. The first two phenomena are generally irreversible while the last is reversible since such retention occurs where the flow is stagnant as in the rear of solid particles. According to the literature, it occurs when the flow rate was adjusted to a new value

or after stopping and recommencing the flooding [Desremaux et al., 1971; Chauveteau and Kohler, 1974; Maerker, 1973].

However, adsorption is the most studied phenomenon among other retention processes. There are two main approaches in the experimental study, static and dynamic. During static experiments, the polymer solution is put into contact with solid particles (sand, silicon carbide, and other minerals) to study the adsorption of polymer molecules under different conditions. In static experiments only adsorption takes place. While in dynamic experiments usually all three phenomena can occur and it is referred to as retention. Several studies distinguish the adsorption from mechanical entrapment by performing the static and dynamic experiments using the same sand [Szabo, 1975; Dominguez and Willhite, 1977]. Another approach to study the mechanical entrapment is by silane treatment of the silica sand to make them non-adsorptive surface [Cohen and Christ, 1986]. Adsorption also can cause the mechanical trapping of polymer, when polymer molecule is adsorbed between the two silica particles perpendicularly to the flow direction forming a bridge, which can lead to accumulation of polymer molecules and plugging the pore channel eventually. It is possible to avoid mechanical entrapment by choosing the high permeable porous medium and pre-shearing or pre-filtering the polymer solution that removes the undissolved micro-gels and any impurities. Hydrodynamic retention depends on the flow rate, and it is not a well-defined phenomenon. Usually, the mechanical entrapment and hydrodynamic retention are negligibly low and retention is mostly due to adsorption.

The objective of our study is to investigate polymer retention in natural porous media considering various system conditions. If polymer retention is quite easy to measure in batch conditions or monophasic conditions, experiments in two-phase flow close to reservoir conditions considering crude oil and the ageing process are more complex and more time-consuming. One question to be addressed is to know if and how polymer retention in monophasic conditions can be representative and extrapolated to predict polymer retention that would be expected in presence of oil. So, to that end, we will consider the retention of various polymers under monophasic conditions before performing experiments in two-phase flow conditions.

The manuscript organized as follows:

- First we start with the general features and literature review of natural porous media and polymer, which includes the monophasic and diphasic flow in porous media, polymer adsorption and depletion to the surface, polymer flow through porous media, and finally retention of the polymer.
- In the second chapter we present the materials, experimental setup, and the equipment used in experiments. In the end, the experimental procedures for monophasic and diphasic experiments are described step by step.
- In the third chapter, we start with the characterization of porous media, brine, and polymer solution used in this work. Then we present and discuss the results obtained during experiments following the order that is given in chapter II.
- Final chapter is the conclusions and perspectives of this work.

1. Chapter I : General features & literature review

1.1. Porous media

A porous medium is an assembly of solid particles containing empty spaces called pores that can be occupied by fluids. The morphological and physicochemical properties of the pore structure control the resistance to fluid flow through the porous medium.

Porous media is classified into consolidated and unconsolidated media. Unconsolidated structures are characterized by the absence of grain bonds (such as sand), while solid consolidated matrices are formed from cemented grains such as limestone and sandstone.

Porosity

The porosity of a porous medium is the ratio between the volume of pores V_0 and the total volume of medium V_T .

$$\phi = \frac{V_0}{V_T} \quad \text{Eq. 1-1}$$

In porous systems, the pores can be interconnected or separated according to Figure 1-1 below. In this pore system, we distinguish the residual porosity that is constituted by the isolated pores and the effective or useful pores, constituted by the interconnected pores.

Typical porosity values depend on the pore system. For consolidated sandstones, the porosity value is between 0.1 and 0.3, and for unconsolidated sands between 0.3 and 0.4 [Corey 1994].

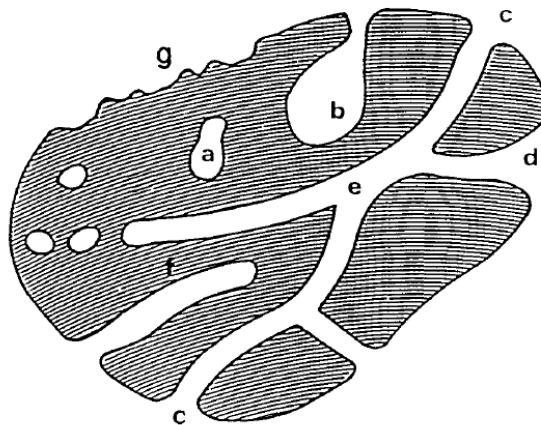


Figure 1-1. The diagram of the types of pores in a porous medium [Rouquerol et al., 1994].

a – isolated pores or closed pores. They influence the macroscopic properties of the porous medium such as the density of the solid, the mechanical resistance, or the thermal conductivity, on the other hand, these pores do not intervene in the flows or the absorption processes.

b,c,d,e, and f – connected pores or open pores. Some can be open at one end (b and f, that described as blind) or at two ends (e). Depending on geometry: cylindrical c or f, bottle-shaped b or funnel d.

Another remarkable property is the roughness of the surface (g). A rough surface is not a porous surface, but it has irregularities that can influence the flow, especially adsorption.

Tortuosity

The tortuosity characterizes the structure of porous media about hydraulic conductivity and dispersivity.

Porous media, particularly natural media such as rocks and soils, are disordered systems with many pore sizes and different grain shapes. The flow paths in these media are not straight, and a particle travels a distance that is greater than the length of the sample.

Tortuosity τ [Tye, 1983; Epstein, 1989; Sahimi, 1993; Moldrup et al., 2001] is an intrinsic property of each medium. It is a function of the ratio of the length of the real path traveled between two points L_g to the rectilinear distance L_s that separates them [Scheidegger, 1974; Clennell, 1997;]. Since $L_g > L_s$, the tortuosity factor τ is greater than 1.

$$\tau = \left(\frac{L_g}{L_s} \right)^2 \quad \text{Eq. 1-2}$$

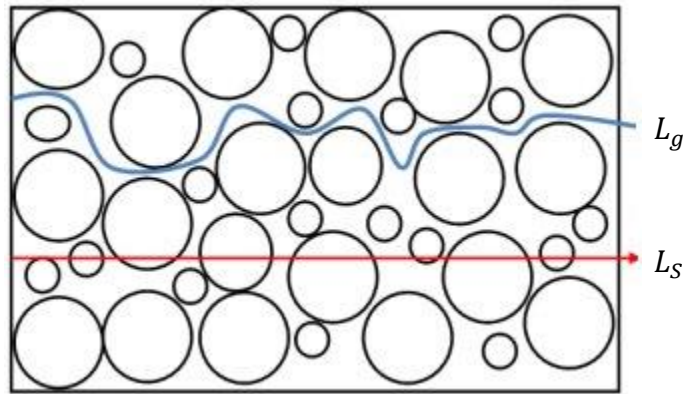


Figure 1-2. Representative diagram to show the difference in tortuosity

Specific surface

The specific surface is the total surface area of the solid in contact with the fluids. Its unit is m^2/g .

In a cubic pore system of volume V in which are placed \tilde{n} spheres of radius r and density ρ such that a volume H^3 can be associated with each sphere in the pore system [Besnard, 2004]. So the porosity is

$$\phi = \frac{V_p}{V} = \frac{H^3 - \frac{4}{3}\pi r^3 \tilde{n}}{H^3} = 1 - \frac{4}{3}\pi \left(\frac{r}{H} \right)^3 \tilde{n} \quad \text{Eq. 1-3}$$

And the specific surface S_{sp} of each sphere can be expressed by the following equation:

$$S_{sp} = \frac{S_{sphere}}{M_s} = \frac{4\pi r^2}{\rho \frac{4}{3}\pi r^3} = \frac{3}{\rho r} \quad \text{Eq. 1-4}$$

Logically the smaller the particle size, the larger the specific surface area, for example, the value of the specific surface area for sandstones is between $0.5 - 5 \text{ m}^2/\text{g}$ and around $100 \text{ m}^2/\text{g}$ for clays [Bear, 1988].

1.2. Flow in porous media

Fluid mechanics in porous media studies the phenomena of mass, momentum, and energy transfer, of fluids, taking into account the configuration of the medium and the chosen scale.

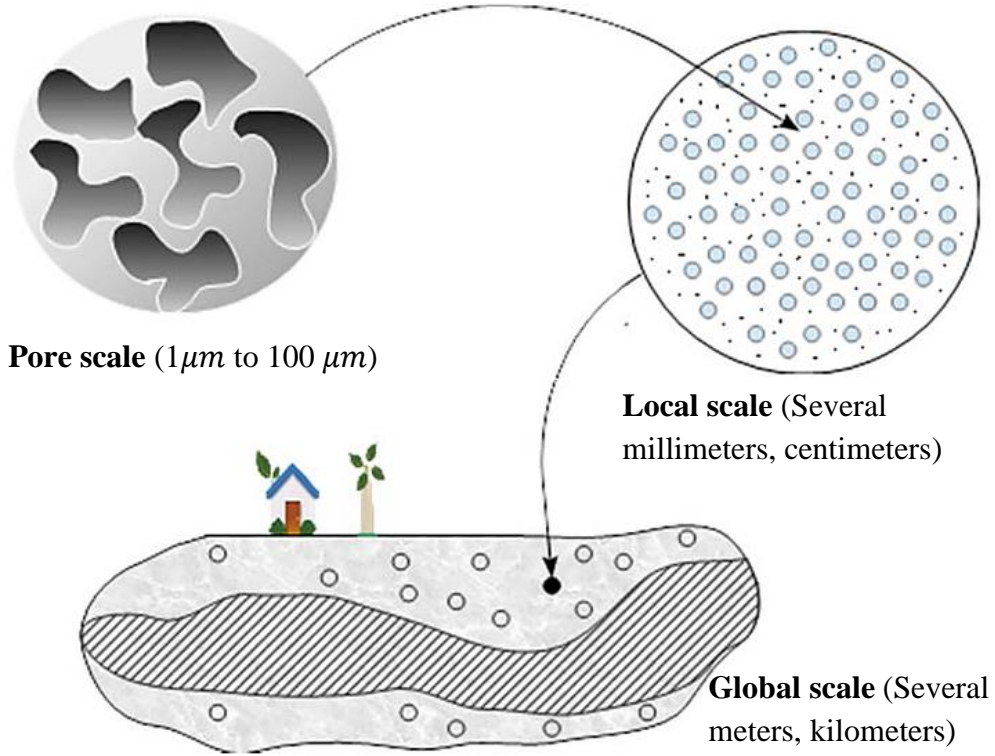


Figure 1-3. The different scales of observation of the porous media [Chiara, 2009]

1.2.1. Pore scale

The characteristic dimension at this scale is the grain diameter in unconsolidated media and the average pore diameter for consolidated media. At this scale, flow is described by the Navier-Stokes equation.

For a fluid of density ρ and dynamic viscosity η , the Navier-Stokes equation is expressed in terms of velocity in the field of gravity given by:

$$\rho \left(\frac{\delta \vec{v}}{\delta t} + (\vec{v} \nabla) \vec{v} \right) = -\nabla \vec{p} + \eta \nabla^2 \vec{v} + \rho \vec{g} \quad \text{Eq. 1-5}$$

The non-linearity of the Navier-Stokes equation is due to two terms, the term of inertia or momentum convection $(\vec{v}\nabla)\vec{v}$ and the viscous diffusion term $\nabla\vec{v}$. The Reynolds number allows these two terms to be compared and is written as the ratio of the inertia to the viscosity.

$$Re = \frac{\text{inertia}}{\text{viscosity}} = \frac{\|\rho(\vec{v}\nabla)\vec{v}\|}{\|\eta\Delta\vec{v}\|} \quad \text{Eq. 1-6}$$

The Reynolds number can be evaluated from the equation 1-6 as follows:

$$Re = \frac{\|\rho(\vec{v})\vec{v}\|}{\|\eta\Delta\vec{v}\|} = \frac{\rho v^2/D_H}{\eta v/D_H^2} = \frac{\rho D_H v}{\eta} = \frac{D_H v}{\psi} \quad \text{Eq. 1-7}$$

Where ψ is the kinematic viscosity $\psi = \eta/\rho$, v – the average velocity, D_H – hydraulic diameter. For $Re \gg 1$, momentum transfer by inertia is higher than by viscosity, so the term inertia predominates. For $Re \ll 1$ the viscous effects predominate over the inertial effects. Low Reynolds number flows correspond to very low velocities, very small dimensions, or very viscous fluids.

If we assume the slow flow of an incompressible Newtonian fluid, then flow is governed by the Stokes equation:

$$0 = -\nabla\vec{p} + \eta\nabla^2\vec{v} + \rho\vec{g} \quad \text{Eq. 1-8}$$

Which is associated with the continuity equation (conservation of mass) for an incompressible fluid:

$$0 = (\nabla^2 \cdot \vec{v}) \quad \text{Eq. 1-9}$$

Poiseuille equation: capillary bundle model

To establish practical correlations between the different properties of the flows in porous systems, we can represent these porous media through simplified models. One of the most widely used models is to consider the porous medium as a bundle of rectilinear capillary tubes with identical radii. Poiseuille's equation describes the flow of a fluid in a capillary tube through the equation 1-10. If we consider the medium as a bundle of n_t parallel capillaries of radius R_p and the same length L , we can write the flow rate using Poiseuille's law:

$$Q = \frac{n_t \pi R_p^4}{8\eta} \frac{\Delta P}{L} \quad \text{Eq. 1-10}$$

Where the cross-section of the flow is:

$$A\phi = n_t \pi R_p^2 \quad \text{Eq. 1-11}$$

Using the relations 1-10 and 1-11, we obtain the expression [Sorbie, 1991]:

$$R_p = \sqrt{\frac{8k}{\phi}} \quad \text{Eq. 1-12}$$

If the bundle instead of being parallel is randomly distributed in all directions, then the pressure gradient is corrected by the tortuosity factor τ , and permeability is written as [Nooruddin and Hossain, 2011]:

$$k = \frac{\phi R_p^2}{8\tau} \quad \text{Eq. 1-13}$$

1.2.2. Local scale

The transition to the local scale makes it possible to describe the flow of an incompressible fluid with a low Reynolds number by applying Darcy's law [Whitaker, 1986; Scheidegger, 1960; Dullien, 1979].

$$\langle \vec{v} \rangle = -\frac{\mathbf{K}}{\eta} (\nabla \langle \vec{P} \rangle - \rho \vec{g}) \quad \text{Eq. 1-14}$$

Where $\langle \vec{v} \rangle = \frac{1}{V} \int_{(V_p)} \vec{v} dV$ is Darcy's velocity, and $\langle \vec{P} \rangle = \frac{1}{V_p} \int_{(V_p)} \vec{P} dV$ is the average pressure of the fluid phase. \mathbf{K} is the permeability tensor, the intrinsic physical quantity of the porous medium which quantifies the disposition of the rock to allow a fluid to pass through anisotropic media. \mathbf{K} strongly depends on the direction of the flow, in common reservoirs the vertical permeability is often lower than horizontal permeability due to the presence of strata.

In the case of isotropic porous media, the permeability tensor is expressed as a function of the absolute permeability k and the identity tensor \mathbf{I} , and it is expressed in Darcy ($1 \text{ Darcy} = 0.987 \times 10^{-12} \text{ m}^2$).

$$\mathbf{K} = k\mathbf{I} \quad \text{Eq. 1-15}$$

where k depends only on the topology of the porous medium, and Darcy's law can be expressed by:

$$Q = -\frac{kA}{\eta} \frac{dP}{dl} + \rho g \sin \alpha \quad \text{Eq. 1-16}$$

where A is the cross-section of the flow, l is the length and α is the angle of inclination of the flow. For the particular case of unidirectional, horizontal flow, the equation 1-16 is written in the following form:

$$Q = \frac{kA}{\eta} \frac{\Delta P}{l} \quad \text{Eq. 1-17}$$

ΔP is the pressure drop between the inlet and the outlet of the medium, and A is the cross-section of the medium of length l . It shows a linear relationship between volume flow and differential pressure.

The Kozney-Carman model

Starting from Poiseuille's model of capillary tubes, permeability as a function of specific internal surface area can be expressed by Kozeny-Carman's model (1937), in which a characteristic shape factor of the medium f_g is integrated, that takes into account the

microstructure, then permeability is written as [Nooruddin and Hossain 2011; Nelson 1994]:

$$k = \left(\frac{1}{f_g \tau S_{sp}^2} \right) \frac{\phi^3}{(1 - \phi)^2} \quad \text{Eq. 1-18}$$

The model of Carman (1937) and Kozeny (1927) established for a column filled with spheres of diameter d at maximum compactness, and $S_{sp} = 6/d$; the permeability expressed by the relation of Ergun (1952):

$$k = \frac{\phi^3 d_p^2}{180(1 - \phi)^2} \quad \text{Eq. 1-19}$$

1.3. Miscible flows

This paragraph deals with the transport of miscible fluids in a saturated porous medium where one of the fluids contains a non-reactive tracer. The spatial and temporal distribution of the solution concentration results from its molecular diffusion and mechanical dispersion.

1.3.1. Molecular diffusion

Diffusion is a physical phenomenon related to molecular motion. In a fluid at rest, the thermal motion sends particles in all directions in space. If there is a concentration gradient between two neighboring points, a mass flow is observed. This phenomenon is described by the classical Fick's law [Fick, 1855] (equation 1-20) where the molecular diffusion coefficient D_d expresses the proportionality of the mass flow as a function of the concentration gradient in 1D :

$$F = -D_d \frac{\delta c}{\delta x} \quad \text{Eq. 1-20}$$

In porous media, the presence of grains slows diffusion because the ions must then follow longer paths than in free water. The so-called effective molecular diffusion coefficient D_d considers this phenomenon and is associated with the free water coefficient. In addition, the coefficient depends on the nature of the ion, the temperature (according to an Arrhenius law), the pressure and the composition of the fluid. Diffusion is generally negligible compared to kinematic dispersion, except at low flow velocities.

1.3.2. Dispersion

In practice, the mechanisms of mechanical dispersion and diffusion coexist giving rise to an overall dispersion of the solution and with dispersion coefficients of :

$$D_L = \alpha_L v + D_d \quad \text{Eq. 1-21}$$

$$D_T = \alpha_T v + D_d \quad \text{Eq. 1-22}$$

Moreover, if D_x is the total dispersion in the x direction. D_x can be expressed by two components, the mechanical dispersion D and the effective diffusion D_d which depends on the tortuosity of the system [Bear, 1988], so that the parameter of the dispersion in equations 1-21 and 1-22, and can be expressed in the form:

$$D_x = \alpha_T \bar{v}_x + D_d \quad \text{Eq. 1-23}$$

To describe the transport of a conventional flow of a solution, a mass balance should be performed on a unit elementary volume of the porous medium.

If we define the general transport equation:

$$\frac{\delta c}{\delta t} = -\frac{\delta}{\delta x} J \quad \text{Eq. 1-24}$$

J is the sum of the convective flux component

$$\vec{J}_C = c \vec{v}_x \quad \text{Eq. 1-25}$$

And the dispersive flux component:

$$\vec{J}_D = -D_x \frac{\delta c}{\delta x} \quad \text{Eq. 1-26}$$

From the equations 1-25, 1-26 and 1-24 we can obtain the expression for the conservation of mass:

$$\frac{\delta}{\delta x} \left(D_x \frac{\delta c}{\delta x} \right) - \frac{\delta}{\delta x} (\bar{v}_x c) = \frac{\delta c}{\delta t} \quad \text{Eq. 1-27}$$

The equation above is modified for reactive flow [Runkel and Bencala 1995; Runkel 1996] where Kc is the reaction rate:

$$-Kc + \frac{\delta}{\delta x} \left(D_d \frac{\delta c}{\delta x} \right) - \frac{\delta}{\delta x} (\bar{v}_x c) = \frac{\delta c}{\delta t} \quad \text{Eq. 1-28}$$

The diffusion-dispersion equation describes the transport of a solution in a saturated porous medium. The analytical solution of this equation with the following boundary conditions provides the concentration of the solution as a function of space and time and corresponds to the non-reactive case, Eq 1-27.

$$\text{boundary conditions} \begin{cases} c(x, 0) = 0 \\ c(0, t) = C_0 \\ c(\infty, t) = 0 \end{cases}$$

That corresponds to the permanent injection of solution at the C_0 concentration at the inlet of a semi-infinite 1D porous medium. If we consider a constant dispersion coefficient, the solution is expressed in the form [Ogata and Banks 1961]:

$$c(x, t) = \frac{c_0}{2} \left[\text{erfc} \left(\frac{x - \bar{v}t}{2\sqrt{D_x t}} \right) + \exp \left(\frac{\bar{u}_x}{D_x} \right) \text{erfc} \left(\frac{x + \bar{v}t}{2\sqrt{D_x t}} \right) \right] \quad \text{Eq. 1-29}$$

where erfc is the complementary error function.

If the time and/or the length of the sample are large enough, then the second term is negligible and the mass conservation equation is described by Fick's equation:

$$D_d \frac{\delta^2 c}{\delta x^2} = \frac{\delta c}{\delta t} \quad \text{Eq. 1-30}$$

and therefore, the solution of equation 1-29 (Figure 1-4) is limited to:

$$c(x, t) = \frac{c_0}{2} \left[\operatorname{erfc} \left(\frac{x - \bar{v}t}{2\sqrt{D_x t}} \right) \right] \quad \text{Eq. 1-31}$$

The concentration profile is controlled by mechanical dispersion and diffusion.

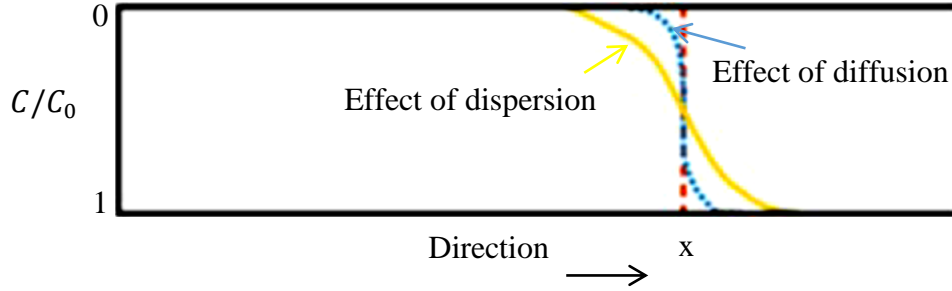


Figure 1-4. The concentration profile as a function of dispersion and diffusion.

At a very low flow rate, diffusion is the phenomenon that controls the process and the dispersion coefficient is $D_x \approx J$. On the other hand, for high flow rates, mechanical dispersion becomes the dominant phenomenon. The ratio of the mechanical dispersion and molecular diffusion leads to the definition of dispersion, the Péclet number of grain.

$$Pe = \frac{\bar{v}d_p}{D_d} \quad \text{Eq. 1-32}$$

Where d_p is the diameter of a grain, \bar{v} the interstitial flow velocity ($\bar{v} = Q/A\phi$), and D_d is the molecular diffusion coefficient of the order of $10^{-9} \text{m}^2/\text{s}$. In Figure 1-5 we show the relation between the longitudinal dispersion and the Péclet number where D_d is the diffusion coefficient in pure water.

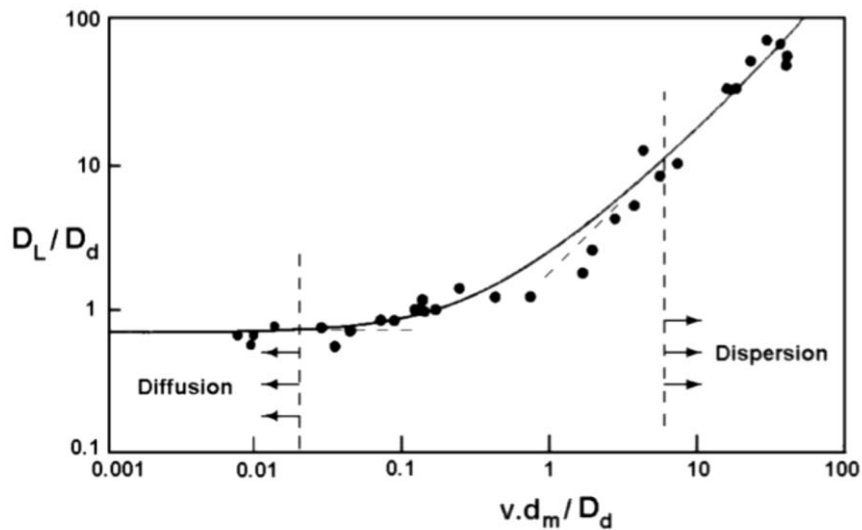


Figure 1-5. Relationship between Pe and dispersion [Perkins and Johnson, 1963]

In the figure above we see three regimes according to the value of the Péclet number. For low Pe , molecular diffusion is predominant, when Péclet number is high, the predominant phenomenon becomes mechanical dispersion.

1.4. Diphasic flows

We now consider the case where the porous medium is saturated with two immiscible phases, one $\langle o \rangle$ oil phase, and another $\langle w \rangle$ aqueous phase. In this case, we also consider the fluid-solid interactions, and the fluid-fluid interactions. We also introduce the different parameters that describe the two-phase flows.

1.4.1. Concept of saturation

In a pore volume V_p , the saturation S_β defines the proportion of the pore volume occupied by a fluid β :

$$S_\beta = \frac{V_\beta}{V_p} \quad \text{Eq. 1-33}$$

In a water/oil system we have $S_o + S_w = 1$.

1.5. Interfacial tension and wettability

When a system has two immiscible phases, the interfacial tension measures the minimum energy required to create a unit area at the interface of these two fluids. If the fluids are highly immiscible, the interfacial tension is high and low if the fluids are poorly immiscible. In the water/oil system, the interfacial tension in the reservoir has a value between 15 and 35 dynes/cm [Cossé, 1988].

In the case of a drop of liquid deposited on a solid surface and surrounded by an immiscible fluid, the wetting of the liquid is characterized by the contact angle θ . This geometric parameter is used to measure the affinity between the solid phase and one of the liquid phases. This angle depends on the surface tensions involved in the equilibrium of the drop and it can be determined by Young's equation:

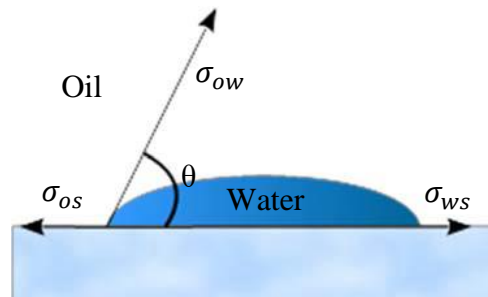


Figure 1-6. Contact angle θ between immiscible fluids and the solid.

$$\cos\theta = \frac{\sigma_{os} - \sigma_{ws}}{\sigma_{ow}} \quad \text{Eq. 1-34}$$

Where σ_{os} is the interfacial tension between the oil phase and the solid surface, σ_{ws} is the interfacial tension between the water phase and solid, and σ_{ow} is the interfacial tension between the immiscible fluids.

The value of the contact angle makes it possible to identify the wettability of a surface.

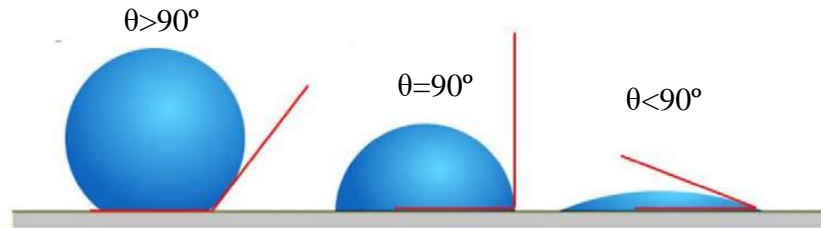


Figure 1-7. Wettability of oil/water/rock systems

Anderson (1986b) established a series of contact angle values to define the wettability that can be found in porous media according to the following table:

Contact angle	Water-wet	Neutral wettability	Oil-wet
Minimum	0°	60-75°	105-120°
Maximum	60-75°	105-120°	180°

Table 1-1. Contact angle values [Anderson, 1986b]

The wettability has an impact on the distribution of immiscible fluids in porous media and flow of these fluids. Oil reservoirs are porous, permeable rocks that contain water and hydrocarbons. Their wettability can change from water-wet to oil-wet through different situations with intermediate wettabilities [Anderson, 1986a].

In general, it is assumed that reservoir rocks are water-wet before the migration of hydrocarbons by density difference. If the medium is water-wet, water coats the pore surface and saturates the small pores, while the oil is in the center of the large pores in the form of drops.

The oil-wet porous media show the opposite distribution of fluids than in the water-wet case. The oil saturates the small pores and will cover the surface of the large pores. Oil wettability results from the effect of the adsorption of certain molecules of crude oil on the surface of the pore surface.

Due to the interactions between rock, oil, and the water phase, there are different types of wettability. When the rock does not show a preference for water or oil, the system becomes neutral (neutral wettability).

The mineralogical composition of the solid surfaces of the porous medium can vary locally and alter the ion exchange and adhesion processes of fluids on the surface. Some minerals are more likely to interact with crude oils and brine than others. This diversity in the mineralogical and chemical composition of the surface causes heterogeneous wettability, also called fractional wettability. In this case, the rock surface has some areas with high wettability in oil and others with high wettability in water.

If the small pores are water-saturated with clean water wettability, while large pores are oil-filled with strong oil wettability, then it is called mixed wettability.

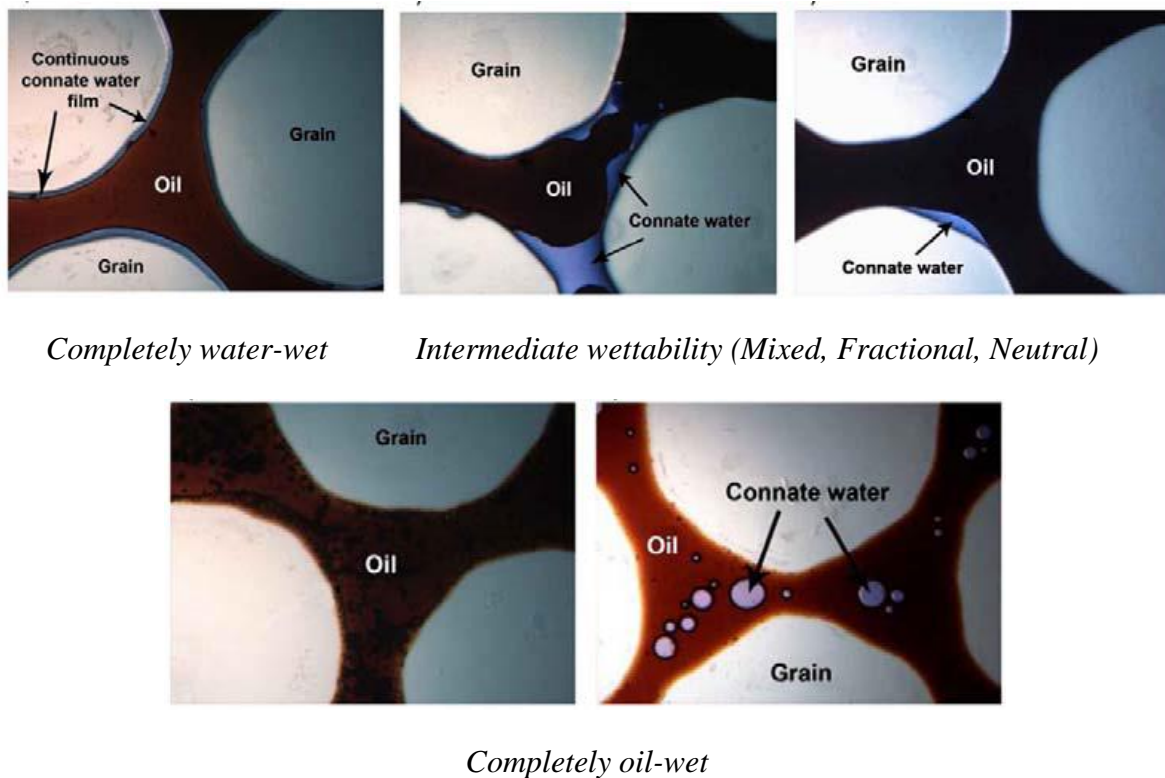


Figure 1-8. Representations of fluid phases as a function of wettability [Meybodi et al., 2011]

1.5.1. Wettability measurement

There are several methods for determining wettability of a rock to various fluids. The main ones are:

- (i) Microscopic observation. This involves the direct observation and measurement of wetting angles on small rock samples. Either a petrographic microscope or SEM fitted with an environmental stage is used.
- (ii) Amott wettability measurements. This is a macroscopic mean wettability of a rock to given fluids. It involves the measurement of the amount of fluids spontaneously and forcibly imbibed by a rock sample. It has no validity as an absolute measurement, but is industry standard for comparing the wettability of various core plugs.
- (iii) USBM (U.S. Bureau of Mines) method. This is a macroscopic mean wettability of a rock to given fluids. It is similar to the Amott method but considers the work required to do a forced fluid displacement. As with the Amott method, it has no validity as an absolute measurement, but is industry standard for comparing the wettability of various core plugs.
- (iv) NMR longitudinal relaxation and other wettability methods. These are briefly summarised in Table 1-2.

Measurement technique	Physical observation
Amott and Amott-Harvey	Amounts of oil and water imbibed by a sample spontaneously and by force
U.S. Bureau of Mines (USBM)	Work required to imbibe oil and water
Microscopic examination	Microscopic examination of the interaction between the fluids and the rock matrix
Nuclear Magnetic Resonance	Changes in longitudinal relaxation time
Flotation method	The distribution of grains at water/oil or air/water interfaces
Glass slide method	Displacement of the non-wetting fluid from a glass slide
Relative permeability method	Shape and magnitudes of k_{ro} and k_{rw} curves
Reserved logs	Resistivity logs before and after injection of a reverse wetting agent
Dye adsorption	Adsorption of a dye in an aqueous solvent

Table 1-2. Summary of wettability measurement techniques

a) Amott Wettability Measurements

The Amott method (Figure 1-9) involves four basic measurements. Figure 1-9 shows the data produced with the water-wetting index given by AB/AC and the oil-wetting index by CD/CA .

- (i) The amount of water or brine spontaneously imbibed, AB.
- (ii) The amount of water or brine forcibly imbibed, BC.
- (iii) The amount of oil spontaneously imbibed, CD
- (iv) The amount of oil forcibly imbibed, DA

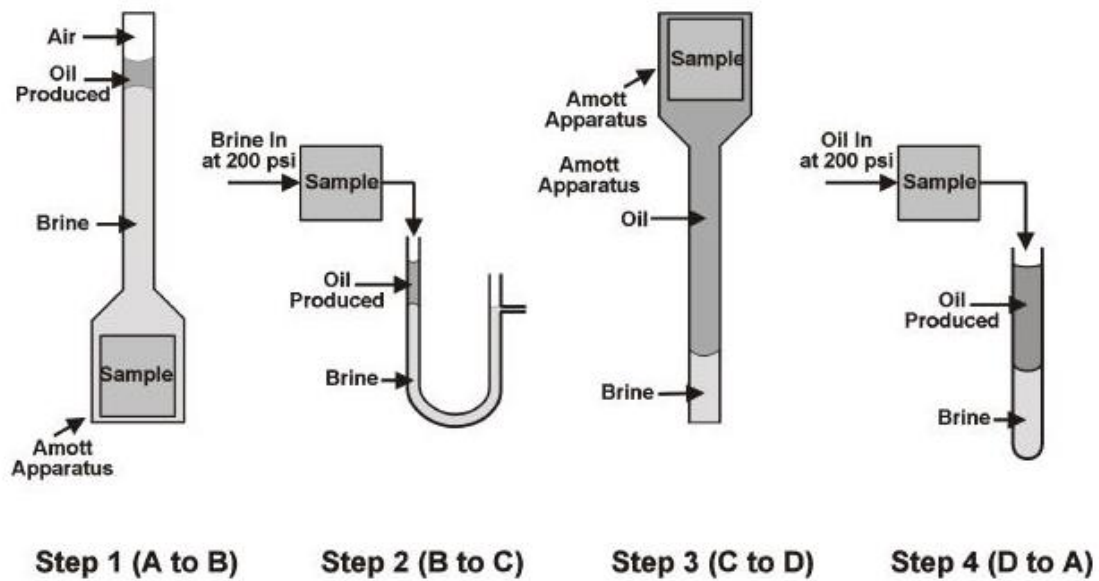


Figure 1-9. Amott wetting technique [Glover, 2010]

Figure 1-10 shows the initial conditions of the sample (point X) to be oil saturated at S_{wi} . The spontaneous measurements are carried out by placing the sample in a container containing a known volume of the fluid to be imbibed such that it is completely submerged (steps 1 and 3 in Figure 1-9 for water and oil respectively), and measuring the volume of the fluid displaced by the imbibing fluid (e.g. oil in step 1 of Figure 1-9). The forced measurements are carried out by flowing the ‘imbibing’ fluid through the rock sample and measuring the amount of the displaced fluid (steps 2 and 4 in Figure 1-9), or by the use of a centrifuge. The important measurements are the spontaneous imbibition of oil and water, and the total (spontaneous and forced) imbibition of oil and water. Water-wet samples only spontaneously imbibe water, oil-wet samples only spontaneously imbibe oil, and those that spontaneously imbibe neither are called neutrally wet. The wettability ratios for oil (AB/AC) or water (CD/CA) are the ratios of the spontaneous imbibition to the total imbibition of the each fluid.

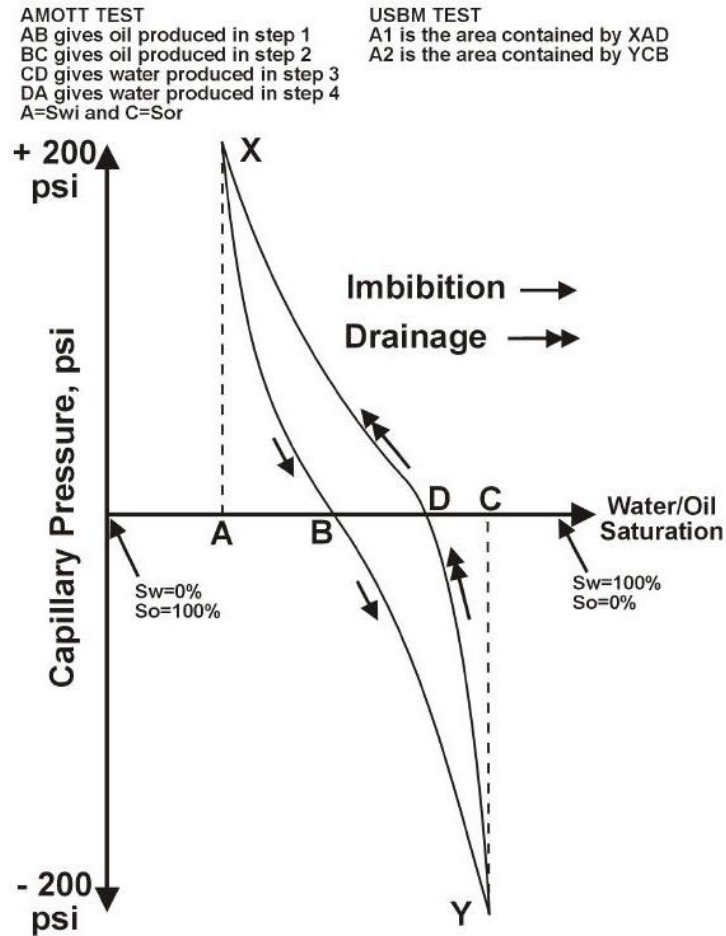


Figure 1-10. Wettability test data [Glover, 2010]

At the end of the experiment, the so-called Amott-Harvey wettability index is calculated:

$$Index = \frac{\text{Spontaneous Water Imbibition}}{\text{Total Water Imbibition}} \frac{\text{Spontaneous Oil Imbibition}}{\text{Total Oil Imbibition}} \quad \text{Eq. 1-35}$$

$$= \frac{AB}{AC} \frac{CD}{CA}$$

Wettability indices are usually quoted to the nearest 0.1 and are often further reduced to weakly, moderately or strongly wetting. The closer to unity the stronger the tendency.

b) USBM Wettability Measurements

This method is very similar to the Amott method, but measures the work required to do the imbibitions. It is usually done by centrifuge, and the wettability index W is calculated from the areas under the capillary pressure curves $A1$ and $A2$:

$$W = \log \frac{A1}{A2} \quad \text{Eq. 1-36}$$

where, $A1$ and $A2$ are defined in Figure 1-10. Note that in this case the initial conditions of the rock are $S_w = 100\%$ and an initial flood down to S_{wi} is required (shown as step 1 in Figure 1-10), although either case may be necessary for either the Amott or USBM methods. Figure 1-11 shows typical USBM test curves for water wet, oil wet and neutrally wet cores.

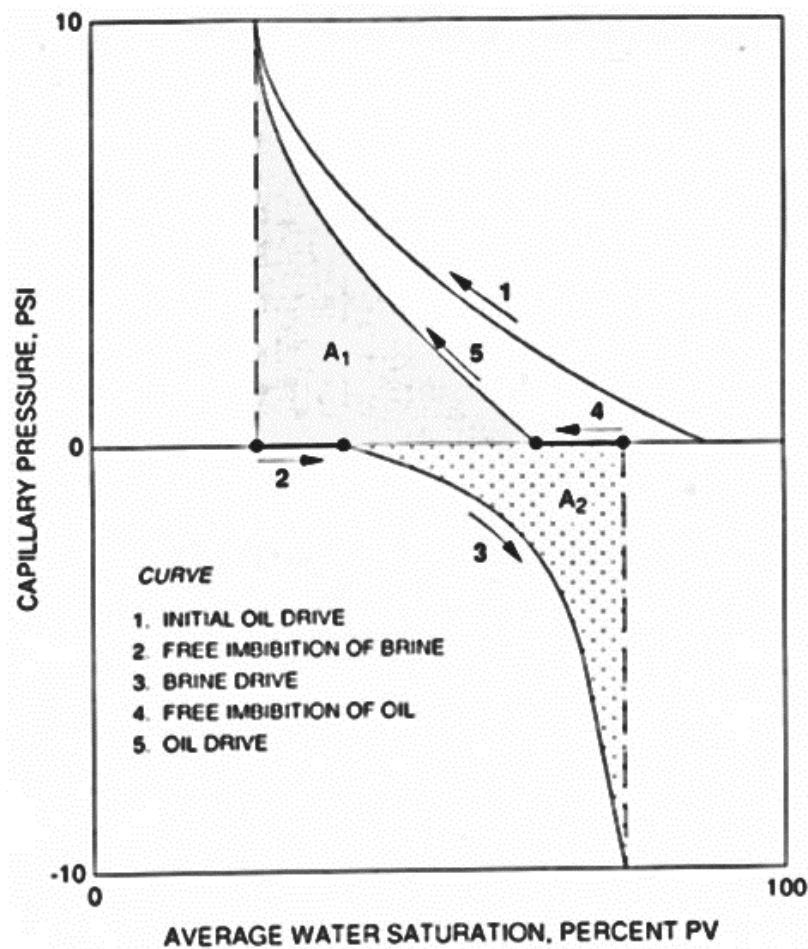


Figure 1-11. USBM wettability test capillary pressure curve (numbers indicate the progress of the test from $S_w = 100\%$)

	Oil wet	Neutral wet	Water wet
Amott wettability index water ratio	0	0	>0
Amott wettability index oil ratio	>0	0	0
Amott-Harvey wettability index	-1.0 to -0.3	-0.3 to 0.3	0.3 to 1.0
USBM wettability index	about -1	about 0	about 1
Minimum contact angle	105° to 120°	60° to 75°	0°
Maximum contact angle	180°	105° to 120°	60° to 75°

Table 1-3. Comparison of the Amott and USBM wettability methods

1.5.2. Influence of ageing of rock in contact with oil on the wettability

A quartz surface is water-wet due to the presence of hydroxyl and hydrophilic groups. If this surface is brought into contact with crude oil, it is possible to change its wettability [Skauge and Fosse 1994]. This phenomenon is explained by the adsorption of polar oil molecules

(typically asphaltenes) on the quartz surface [Valat et al., 1993; Bousseau et al., 1995], and it depends on the temperature, pressure, and duration of the process.

In a case of mixed wettability, the water film depends on an equilibrium that is established between the Van der Waals forces, the electric double layer forces, and the solvation forces [Morrow, 1990]. A crude oil disturbs this balance, which can then lead to the breaking of the film and therefore to the adsorption of oil molecules to the solid surface.

1.5.3. Generalized Darcy's model

If we consider a 1D two-phase flow in a homogeneous and isotropic medium, this flow can be described by generalized Darcy's law through the flows of water and oil:

$$v_w = -\frac{k_w}{\eta_w} \left(\frac{dP_w}{dx} + \rho_w g \sin\beta \right) \quad \text{Eq. 1-37}$$

$$v_o = -\frac{k_o}{\eta_o} \left(\frac{dP_o}{dx} + \rho_o g \sin\beta \right) \quad \text{Eq. 1-38}$$

where k_w and k_o are the effective permeabilities of water and oil, respectively. This quantity represents the flow quality of a fluid under a pressure gradient in the presence of another fluid. These permeabilities are linked to the absolute permeability of the medium through the following expressions:

$$k_w = k k_{rw}(S_w) \quad \text{Eq. 1-39}$$

$$k_o = k k_{ro}(S_o) \quad \text{Eq. 1-40}$$

where k_{rw} and k_{ro} are the relative permeability to water and oil, respectively. These relative permeabilities also depend on the saturation of the corresponding phase. Relative permeability represents the ratio between the effective permeability of a fluid at a given saturation and the absolute permeability of the medium.

For a water-oil system, where water is the wetting fluid, the shape of the relative permeability curves, as a function of saturation, is presented in the following imbibition:

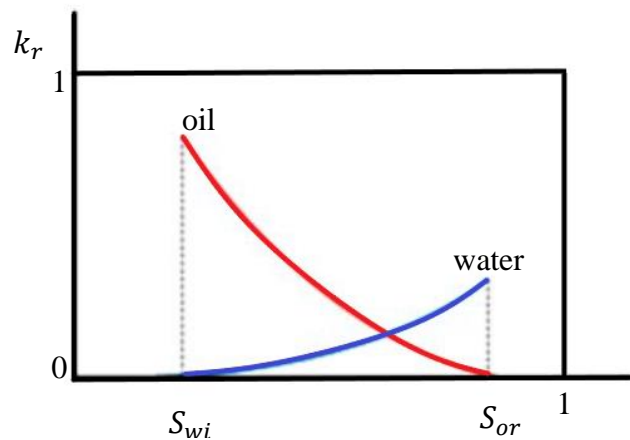


Figure 1-12. Relative permeabilities

The shape of the relative permeability curves depends on the porous media. Note that the relative water permeability at residual oil saturation, S_{or} , has very low value, while the permeability to oil has a value close to 1. That means that the presence of irreducible water, S_{wi} , does little to interfere with the flow of water. While the presence of residual oil significantly impedes the flow of water.

These curves can be obtained experimentally by steady or unsteady methods.

The wettability of a medium plays an important role in the relative water/oil permeabilities.

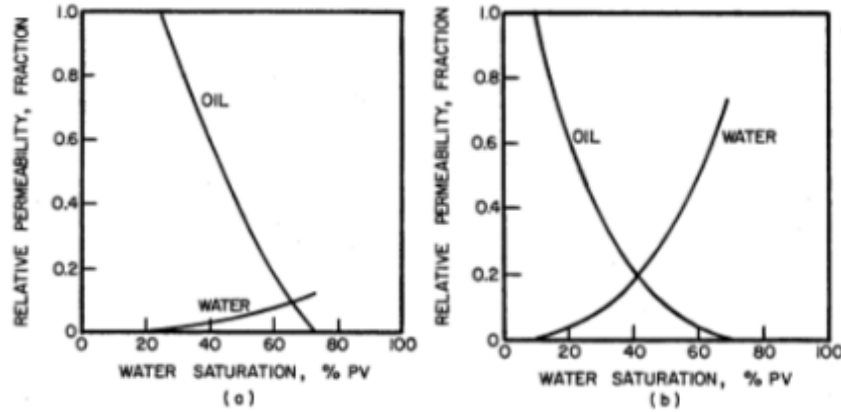


Figure 1-13. Typical curves of relative permeabilities: a) in water-wet PM b) in oil-wet PM [Anderson, 1986b]

1.5.4. Capillary pressure

The pore scale capillary pressure P_c is defined as the pressure difference existing between two neighboring points located on either side of an interface delimited by a non-wetting fluid 1 and a wetting fluid 2 in equilibrium.

$$P_c = P_1 - P_2 \quad \text{Eq. 1-41}$$

Capillary pressure highlights the influence of phenomena observed at the pore scale such as surface forces or wettability. The capillary pressure is related to the curvature of the R interface which separates the two fluids and to the interfacial tension σ (for an oil / water system the interfacial tension has a value of around 30 mN/m). This relationship is expressed by the Laplace equation:

$$P_c = P_1 - P_2 = \frac{2\sigma}{R_p} \quad \text{Eq. 1-42}$$

In the case of a capillary tube of radius R_p containing oil and water, applying the Laplace and Young equation gives the relation:

$$P_c = P_1 - P_2 = \frac{2\sigma \cos\theta}{r} \quad \text{Eq. 1-43}$$

P_c function of saturation

The drainage and imbibition are defined as the displacement of a non-wetting fluid by a wetting fluid and vice versa.

The capillary pressure curve for drainage is established by reducing the saturation of the wetting phase to its irreducible value by an increment of the capillary pressure. The capillary pressure is then gradually decreased during imbibition and the wetting fluid displaces the non-wetting fluid until its saturation is in its residual form.

It is important to note that the first part of the imbibition curve is spontaneous imbibition until the value of $P_c = 0$ is reached. The second part corresponds to forced imbibition where the capillary pressure reaches negative values.

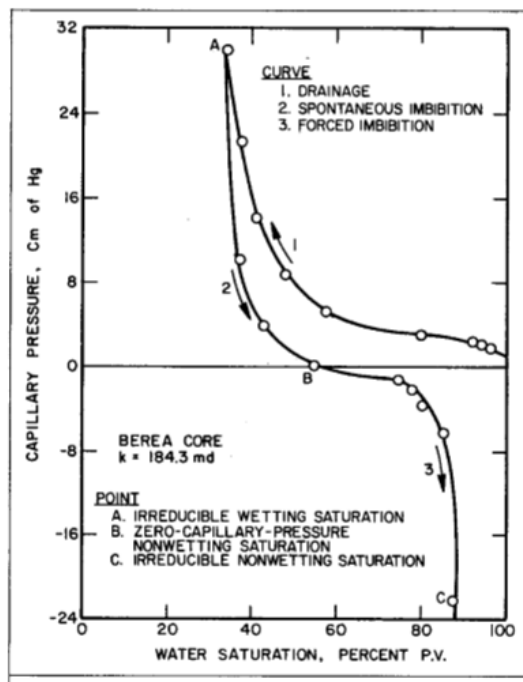


Figure 1-14. Capillary pressure in a Berea [Anderson, 1986c]

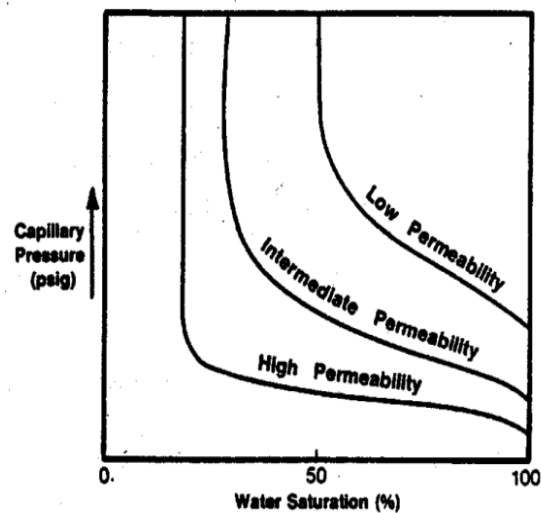


Figure 1-15. Capillary pressure as a function of the permeability type

Capillary pressure during drainage is the pressure applied of the non-wetting fluid to the fluid that saturates the sample. The amount of wetting fluid displaced is measured as a function of the capillary pressure applied. This pressure is increased to irreducible saturation (S_{wi}), and we obtain the primary curve. The capillary pressure is then gradually decreased and the wetting fluid re-enters the sample and displaces the non-wetting fluid. This process is phase 2 in Figure 1-14 and is called spontaneous imbibition, and in phase 3 it is forced imbibition. A residual saturation S_{or} of non-wetting fluid is reached when capillary pressure reaches point C at the end of forced imbibition (phase 3) (Figure 1-14).

The shape of the capillary pressure curves also depends on the permeability of the porous media, the size of the grains, and the distribution of the pores.

1.5.5. Relative permeability hysteresis

Both relative permeabilities and capillary pressure depend on the distribution of the two fluids at the pore scale. It is possible to have several distributions at equilibrium at the same saturation value; therefore, several pairs of relative permeabilities are possible.

If we assume a medium completely saturated with a wetting fluid (1), which is partially driven by non-wetting fluid (2) until the simultaneous flow of the two fluids is possible, and we can measure the relative permeabilities. The fluid (1) is moved a little more by the fluid (2), the relative permeabilities are then measured again, and so on. First by decreasing the saturation and then by increasing it.

It is noted that the relative permeability to the wetting fluid changes little with the direction of variations in saturation. The relative permeability of the non-wetting fluid, on the other hand, is lower in imbibition than in drainage.

1.5.6. Parameters that influence wettability

In a water/oil system, several factors determine the wettability of a surface: the chemical composition of the oil, the pH, the composition of water, the chemical nature of the medium, the topography of the surface, the pressure and temperature [Anderson, 1986b; Buckley et al, 1998].

Composition of the oil

Polar components present in crude oil such as resins and asphaltenes play a crucial role in wettability. Asphaltenes are hydrocarbon compounds consisting of (82 ± 3) wt% carbon and (8.1 ± 0.7) wt% hydrogen. The H/C ratio, close to 1.15 ± 0.05 , is characteristic of the presence of condensed aromatic rings. In addition, nitrogen, oxygen, and sulfur are present in significant proportions within asphaltene molecules.

Asphaltenes are black and are the heaviest fractions of petroleum. The colloidal theory [Leontaritis and Mansoori, 1987] considers that asphaltenes are dissolved in crude oil (solvent) with a layer of resin around them. This resin behaves like an agent that helps the dispersion of the asphaltene molecules in the solvent and prevents the asphaltenes from coming into contact with each other and precipitating. These aggregates are called micelles, and the rate of aggregation will depend on the composition of the crude oil and its aromatic character. Asphaltenes are a heterogeneous material in chemical composition and polydisperse in aggregate size.

Asphaltenes are soluble in aromatic solvents and insoluble in paraffinic solvents, the latter can cause its precipitation of asphaltenes. Therefore, the adding of a certain amount of flocculant such as n-pentane can destroy the micelle and cause the precipitation of asphaltenes.

The adsorption of the oil on the surface will depend on the precipitation of the asphaltenes and therefore on the quality of the solvent. If the oil is a poor solvent (paraffinic), the asphaltenes present in the oil will tend to precipitate and change the wettability of the surface.

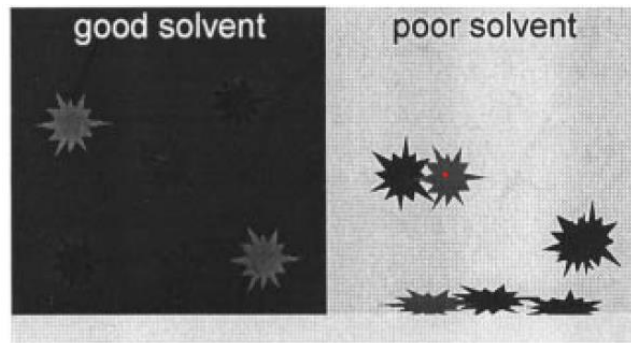


Figure 1-16. Precipitation of asphaltenes as a function of the solvent [Buckley et al, 1998]

Surface composition and acid-base interactions

The chemical composition of the porous medium is also very important [Cuiec, 1984] because it plays an important role in the phenomena of adsorption and wettability. The surface mineralogy of porous media interacts with the polar components of crude oil. Saraji et al (2010) studied the adsorption kinetics of asphaltenes from different crude oils on calcite, quartz, and dolomite under anhydrous conditions. The authors observed that asphaltenes show high adsorption on calcite, while quartz and dolomite have the same low adsorption amounts.

If we do not take into account the effects of the chemical composition of the brine, then the organic bases are adsorbed on the surfaces of silica (SiO_2), and the acidic components are adsorbed on the surfaces of the carbonates because the surfaces of silica are negatively charged.

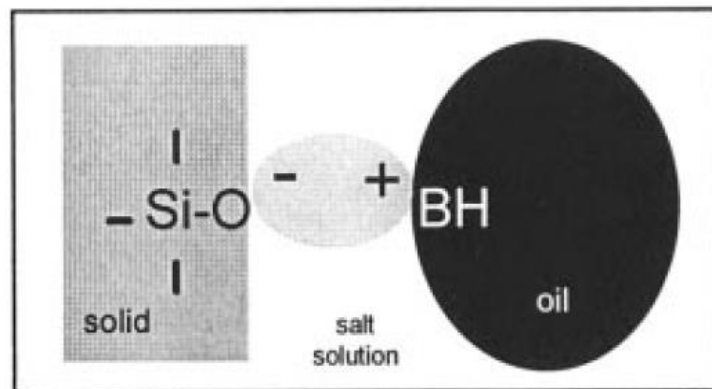


Figure 1-17. Surface/brine/oil interaction [Buckley et al 1998]

On the other hand, carbonate surfaces are positively charged at pH below 9.5 [Buckley et al., 1998].

Several studies show that the adsorption of asphaltenes also depends on the specific surface. The presence of impurities reduces the number of active centers by reducing the probability of adsorption.

Composition of the brine and the presence of multivalent ions

The composition of brine, like the composition of oil, plays an important role in the wettability of the surface [Buckley et al., 1998; Liu et al., 2007].

In silica/crude oil/brine systems, the presence of multivalent ions in the brine composition can reduce the solubility of crude oil surfactants and promote their precipitation and adsorption to the surface. Several interactions can take place with the presence of multivalent ions.

The first two types of interactions can limit impaired wettability while the third type promotes adsorption of surfactant components. This physicochemical bond is the result of van der Waals forces through the formation of a double layer of ions in equilibrium on the surface.

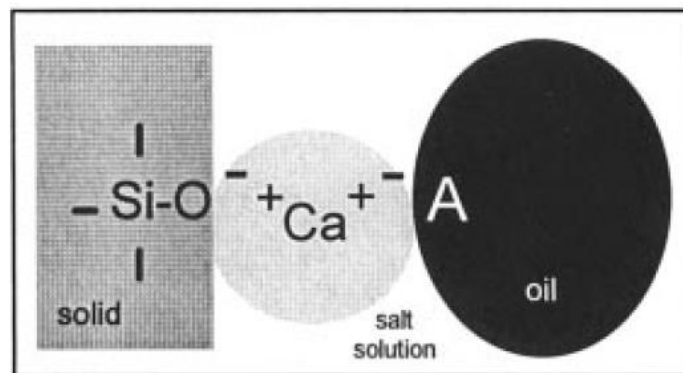


Figure 1-18. Influence of multivalent ions on the adsorption of surfactants [Buckley et al 1998]

The radius of hydration of the ions present in the brine (such as Ca^{2+} , Mg^{2+} , Na^+) also influences the phenomenon of absorption. A high hydration ratio promotes the presence of ions in the double layer.

The hydrodynamic radius of a Ca^{2+} ion is smaller than the radius of a Na^+ ion explains that the divalent ions are more strongly adsorbed than the monovalent in the double layer. This selectivity, which favors the adsorption of more charged ions, decreases with ionic strength [Harris, 2007].

1.5.7. Wettability of porous media

Relationship between wettability and capillary pressure

Figure 1-19 shows this influence, as well as the capillary pressure that depends on the wettability.

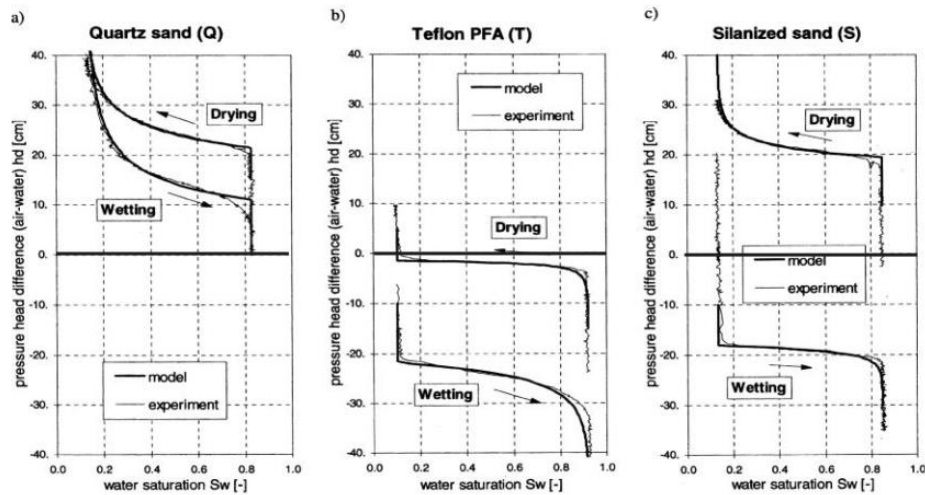


Figure 1-19. Capillary pressure vs saturation as a function of wettability. a) water-wet, b) oil-wet, c) mixed-wet [Lenormand, 2013]

An ageing process can modify the wettability of a porous medium saturated with crude oil. Under the effect of temperature, asphaltene-type compounds can adsorb to the solid surface over time and modify the wettability of the rock.

Influence of wettability on relative permeability

Wettability plays an important role in the pore-scale phase distribution and in the way two-phase flow is structured [Anderson, 1986e].

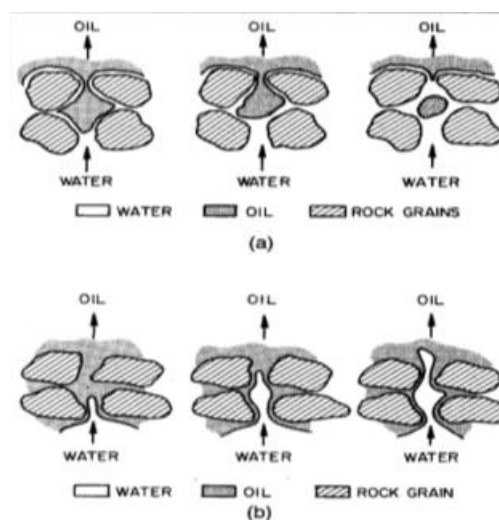


Figure 1-20. Water flow oil saturated PM a) water-wet, b) oil-wet [Anderson, 1986d]

In a water-wet medium, oil flows into large pores, and water flows into smaller pores as well as to the surface of solid grains. It results in a high relative permeability to oil and a low relative permeability to water, making it difficult for water to flow through PM.

In an oil-wet medium, the situation is reversed, and the water flow will be with less resistance than in a water-wet medium. Therefore a high relative permeability to water and a low relative permeability to oil.

1.6. Polymer

Polymers are large molecules composed of small simple structural units or monomers. Polymer chain depending on connectivity can be linear, branched and cross-linked. It is linear when each monomer is connected only to two monomers, and branched when it is connected to three or more monomers. If the monomers are interconnected resulting in a three-dimensional network then it is called cross-linked polymer.

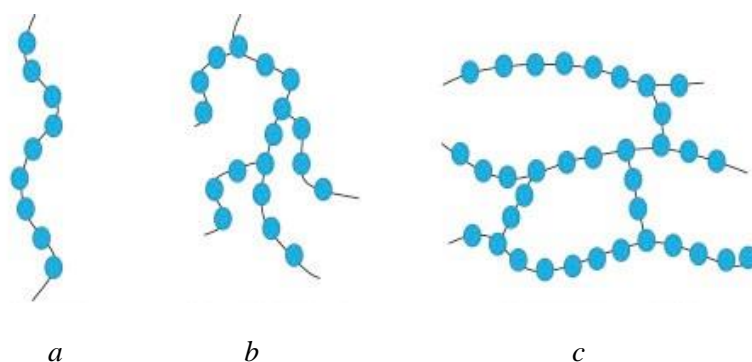


Figure 1-21. Schematic representation of linear (a), branched (b), and cross-linked (c) polymers

There are two main types of polymers, synthetic polymers such as hydrolyzed polyacrylamide (HPAM) and biopolymers such as xanthan gum. Synthetic polymers are obtained through a polymerization process and when they are built from a single monomer, it is called homopolymer. If in contrast the polymer is built from two or more different monomers, then it is called copolymer. Copolymers in turn are classified as random copolymers, block copolymers, or graft copolymers.

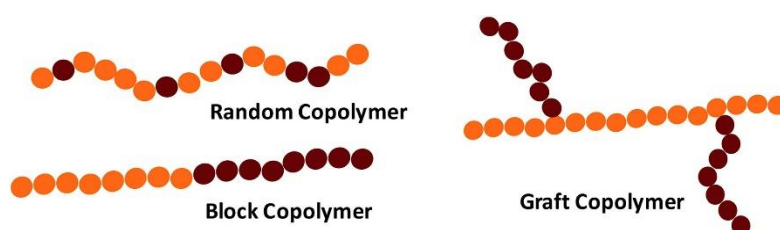


Figure 1-22. Types of copolymers: brown and orange represents the different type of monomers

The motivation for producing copolymers is to obtain materials with a wider range of mechanical properties than is possible with the homopolymers alone. For example, amphiphilic polymers are made of surface-active units and hydrosoluble monomers. Moreover, depending on the structure and electrostatic charge of monomers, polymers range from neutral to polyelectrolyte types and from flexible to rigid shapes as well.

The molecular weight of a macromolecule is the product of the molecular weight of a structural unit and the number of structural units in the molecule, say the polymerization index. In addition, inherently to polymerization reaction, the obtained polymer is rarely

monodisperse and has a polymerization index greater than 1. Typical synthetic polymer molecules may have molecular weights between 10.000 and 1.000.000 g/mol or more. Besides molecular weight, the properties of polymer solutions depend mainly on concentration and the solvent quality that is a function of its chemical composition and temperature.

In the remainder of this part, we will restrict ourselves to consider linear flexible polymers.

1.6.1. Conformation of polymers in solution state

To investigate the conformation of flexible linear chains, the common approach is to consider the random walk configurations of the chain units on a 3D lattice of given coordination using a Monte-Carlo method. Hence, the geometric characteristics of isolated chains are determined by determining first the mean end-to-end distance and the average gyration radius of the chain. In a first approximation, chain parts are allowed to cross each other and R_G is then dependent on N though $N^{0.5}$ for such a phantom chain. This situation corresponds only to an athermal solvent, or theta solvent and the conformation is said ideal. In a good solvent, however, the excluded volume effect should be taken into account allowing chains to adopt an expanded self-avoiding walk configuration, and R_G is now related to N (or molecular weight) through $R_G \cong N^v$ where v is the excluded volume exponent that is close to 0.6. In case of poor solvent isolated chain collapse into a dense coil with a size $R_G \cong N^{1/3}$.

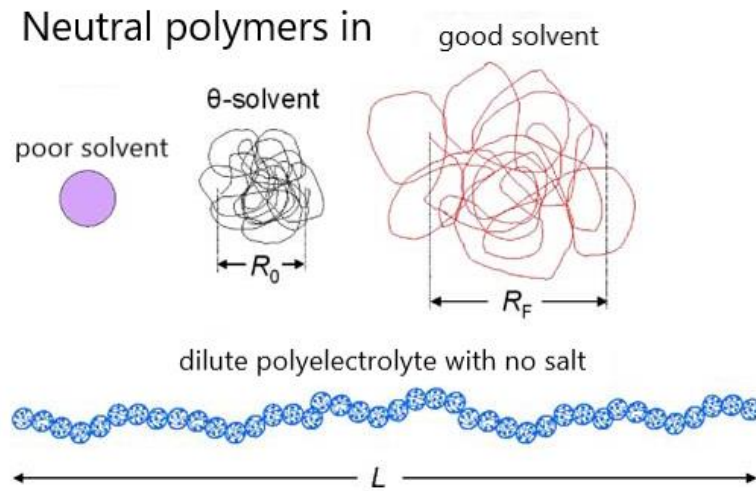


Figure 1-23. Conformations of polymers in dilute solutions [Colby, 2010]

For low polymer concentration, the solution is dilute and macromolecules are, on average, so far apart that they have a negligible influence on each other. As concentration is increased, a remarkable concentration is reached where chains began to overlap by sharing space. Such a critical concentration is called the overlap concentration and is usually noted as C^* and is given by $C^* \cong N/R_G^3$ say $C^* \cong N^{1-3v}$. Beyond C^* the concentration regime is termed semi-dilute. More precisely, two semi-dilute regimes are defined as a non-entangled semi-dilute regime where chains do only weakly overlap just above C^* and an entangled semi-dilute regime where chains fully overlap when polymer concentration exceeds a critical value C_e which is reported to equal approximately $9C^*$. In such entangled semi-dilute regime, polymer solution is seen as a collection of polymer blobs each of size of ξ (see Figure1-25) and contains g monomers. The blob size is then given by $\xi \cong R_G(C_p/C^*)^{-v/(3v-1)}$, say $R_G \cong$

$(C_p/C^*)^{-3/4}$ for linear polymer in a good solvent. Moreover, the size of chains in that entangled semi-dilute regime is given by $R_G \cong N^{1/2} C_p^{-(\nu-0.5)/(3\nu-1)}$ which for a good solvent ($\nu=0.6$) reduces to $R_G \cong N^{1/2} C_p^{-0.12}$.

If a solvent is precisely poor enough to cancel the effects of excluded volume expansion, the θ -condition is satisfied, and such solvent is called θ -solvent. Neutral polymers in θ -solvent are random walks with ideal end-to-end distance (Figure 1-23), and this individual chain statement is true when two chains approach each other, with zero net excluded volume, and cause three-body repulsion and some temporary association occurs that influences properties such as Huggins coefficient [Bohdanecky and Kovar, 1982]. With zero net excluded volume, two chains can overlap occasionally in dilute θ -solvent and temporarily entangle [Semenov, 1988].

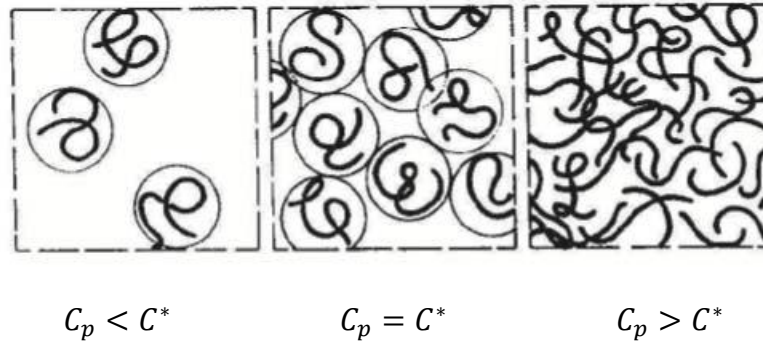
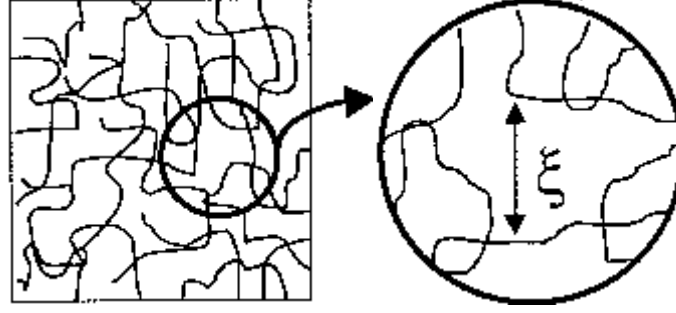


Figure 1-24. Schematic of dilute, overlap and semi dilute solutions

Correlation length, ξ , is the distance between neighbor chains in polyelectrolyte solutions without salt in semi-dilute regime. Nevertheless, in case of neutral polymers in good and θ -solvent it is the distance between the crosslink of chains (Figure 1-25).

De Gennes showed that the correlation length, ξ , is the key to understanding the structure of solutions above C^* , termed semi dilute [Daoud et al., 1975; de Gennes, 1979]. On scales smaller than ξ , there are only monomers from the same chain and lots of solvent molecules. The chains adopt a local conformation similar to the dilute solution conformations and dilute solution rules apply to both structure and dynamics inside ξ (Figure 1-25). On scales larger than ξ , there are many other chains, and the chain adopts a conformation that is a random walk of correlation blobs of size ξ , with melt-like rules applying for both structure and dynamics on large scales. Excluded volume interactions, hydrodynamic interactions, and for polyelectrolytes also charge repulsion interactions, all are screened at the correlation length ξ , causing it also be termed the screening length. Inside ξ , the different solutions have quite different chain conformations, but the large-scale conformation of the chain in semi-dilute solution is always a random walk of correlation blobs.



Neutral polymer in good solvent and θ -solvent

Figure 1-25. Schematic structure of a semi-dilute solutions and correlation length, ξ

In all solutions, de Gennes showed that the correlation length does not depend on chain length, and its concentration dependence can be inferred from a simple scaling argument:

$$\xi \approx R_{dilute} \left(\frac{C_p}{C^*} \right)^{\nu} \sim C_p^{-\nu/(3\nu-1)} \quad \text{Eq. 1-44}$$

where the last result was obtained requiring ξ to be independent of N (since at the scale of ξ , there is no information about how long the chain is). For θ -solvent, $\nu = 1/2$ and $\xi \sim C_p^{-1}$, for good solvent, $\nu = 0.588$ and $\xi \sim C_p^{-0.76}$, and for polyelectrolytes without salt, $\nu = 1$ and $\xi \sim C_p^{-0.5}$.

In entangled semi-dilute state, chains consists in N/n_ξ blobs each of size ξ and due to screening effect induced by the presence of the others are ideal. So, the end-to-end distance of a chain is written as:

$$R_G \approx \xi (N/n_\xi)^{1/2} \sim N^{1/2} C_p^{-(\nu-1/2)/(3\nu-1)} \quad \text{Eq. 1-45}$$

where $n_\xi = c_n \xi^3$ is the number of monomers per correlation blob (c_n is the number density of monomers), making N/n_ξ the number of correlation blobs per chain. For θ -solvent, $\nu = 1/2$ and $R_G \sim N^{1/2} C_p^0$, so the ideal random walk persists at all concentrations. For good solvent, $\nu = 0.588$ and $R_G \sim N^{1/2} C_p^{-0.12}$. It was well established experimentally in works of Daoud et al., 1975; Nierlich et al., 1985; Graessley, 2003; Rubenstein and Colby, 2003; Dobrynin and Rubenstein, 2005.

1.6.2. Entanglement concentration

Entanglement occurs at concentrations significantly larger than overlap concentration, C^* . There is an abrupt change (by roughly a factor of 3) in power law exponent for the concentration dependence of viscosity at the entanglement concentration C_e . Entanglement concentrations from such changes in the concentration dependence of viscosity are shown in Figure 1-26. Clearly in this case $C_e > C^*$, meaning that there is a range of concentration that is semi-dilute where the chains are not entangled [Graessley, 1980, 2008; Rubenstein and Colby, 2003].

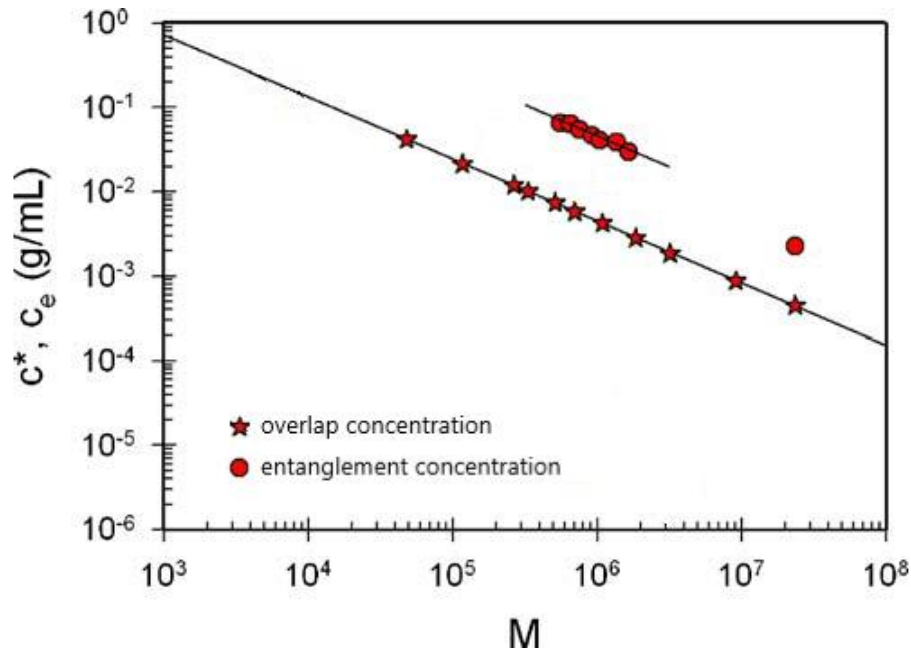


Figure 1-26. Comparison of overlap concentrations and entanglement concentrations of polystyrene in toluene [Kulicke and Kniewske, 1984; Onogi et al., 1967]

The existing models expect C_e to be larger than but proportional to C^* [Dobrynin et al., 1995; Rubenstein and Colby, 2003; Dobrynin and Rubenstein, 2005].

1.6.3. Viscosity of polymer solutions

To describe the viscosity of polymer solutions we define the relative viscosity η_r as the ratio of the solution viscosity η to the solvent viscosity η_s :

$$\eta_r = \frac{\eta}{\eta_s} \quad \text{Eq. 1-46}$$

Various empirical formulas are proposed in literature that link η_r to polymer concentration C_p but the most used one is the Huggins one that expands η_r in a Taylor series in the concentration C_p :

$$\eta_r = 1 + [\eta]_0 C_p + k' [\eta]_0^2 C_p^2 + \dots \quad \text{Eq. 1-47}$$

in which $[\eta]$ is the intrinsic viscosity that represents the volume occupied by polymer chain at infinite dilution and is expressed in terms of volume per unit mass. By using Eq. 1-47 it is then given by:

$$\lim_{C_p \rightarrow 0} \frac{\eta_r - 1}{C_p} = [\eta]_0 \quad \text{Eq. 1-48}$$

where $(\eta_r - 1) / C_p$ is the reduced specific viscosity. Hence $[\eta]_0$ may be experimentally determined by measuring the relative viscosity at successive dilutions. It is also related to C^* since at close packing situation we should have $C^* [\eta]_0 \approx 0.77$ Note that the intrinsic viscosity has dimensions of reciprocal concentration and does in general, depends on the shear rate $\dot{\gamma}$.

At very low shear rates the intrinsic viscosity approaches a limiting value $[\eta]_0$ known as the zero-shear-rate intrinsic viscosity. Writing that $C^*[\eta]_0 \approx 1$ and since we have $C^* \sim N^{1-3\nu}$, it is found that for homologous series of fractionated linear polymers, the relation between $[\eta]_0$ and polymerization index N (or molecular weight) can be expressed as:

$$[\eta]_0 = K'N^a \quad \text{Eq. 1-49}$$

With $a=3\nu-1$ that is close to 0.8 in case of a linear polymer in good solvent. This relationship is known as the Mark-Houwink formula. The pre-factor K' here above is solvent quality dependent.

In other respects, The Huggins constant k' in Eq. 1-47 is also dependent on solvent quality and its typical values are 0.4 in case of a good solvent and may be higher than unity in case of poor solvents. It is to be mentioned that the C^* value is sometimes obtained from viscosity measurement by stating that the viscosity of polymer solution should be twice that of the solvent at that concentration.

The zero-shear-rate intrinsic viscosity is also related to the molecular dimension of the polymer. For a broad spectrum of polymer-solvent systems the relation:

$$[\eta]_0 = \phi' \frac{R_G^3}{M_w} \quad \text{Eq. 1-50}$$

for $M_w > 10^6$. That means that almost all the chain mass is comprised within a volume of R_G^3 ; R_G being the gyration radius. This relationship holds for linear polymers provided that $M_w > 10^6$. The parameter ϕ' is nearly a universal constant (but depend on polydispersity index) and is equal to 2.5×10^{23} for monodisperse polymers.

1.7. Polymer at the surface

1.7.1. Adsorption from quiescent solution

It has been found that if the energy of adsorption per segment is too small, coils arriving at the wall by diffusion are reflected like balls. On the other hand, if the adsorption energy exceeds a certain threshold value, the coils are retained. If the change in enthalpy because of adsorption exceeds the entropy loss associated with the collapse of the three-dimensional coils to two-dimensional formations, the macromolecules are deformed and adsorbed with almost all of their segments. It is defined as dimensionless excess energy per monomer on the surface, δ .

When a solution of neutral, flexible polymer chain is put in contact with a solid surface, two regimes can occur: (a) the polymer sticks to the wall; (b) the polymer repelled by the wall, and depletion layer is expected to build up.

The mean-field theory of the profile $C(z)$ that give the concentration of monomers at distance z from the wall has been constructed by Jones and Richmond (1977) in the attractive case and Joanny and Leibler (1979) in the repulsive case.

The concentration profiles are shown qualitatively on Figure 1-27a for the attractive case and on 1-27b for the repulsive case. There are three distinct regions in each figure.

- i. Proximal ($a \ll z \ll D$). Where D is the adsorption region or extrapolation region. It is defined as a tangent to the profile at point C_s , which is the monomer fraction per unit area on the surface. This region has a characteristic adsorption behavior:

$$C(z) \simeq C_s \left(\frac{z}{a} \right)^{-m} \quad \text{Eq. 1-51}$$

where $m = \frac{v+\phi-1}{v} \approx 1/3$.

- ii. Central ($D < z < \xi_b$). Here the profile is strongly universal and becomes independent of the bulk concentration C_b .
- iii. Distal ($z > \xi_b$). Here the concentration relaxes exponentially towards the bulk value:
 $\frac{C(z)-C_b}{C_b} \sim \exp\left(-\frac{z}{\xi_b}\right)$.

The polymer volume fraction Φ is related to polymer concentration C through $\Phi \cong C a^3$, where a is the monomer size.

iv.

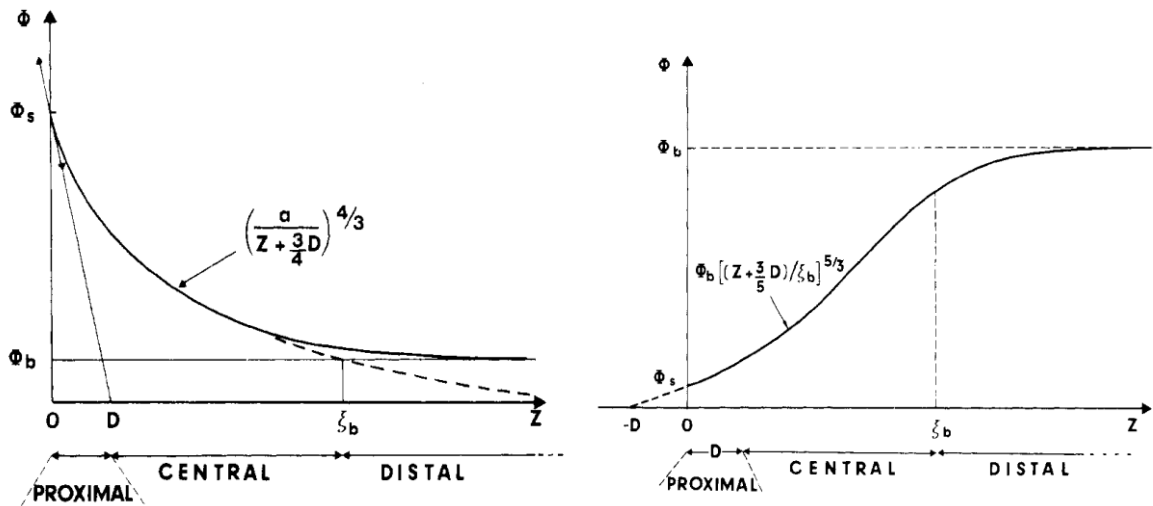


Figure 1-27. Qualitative plot of the polymer volume fraction (ϕ) vs distance from an adsorbing (a) and repelling (b) walls. Full line (a): profile $\phi(z)$ for a finite volume fraction ϕ_b in the bulk solution. Dotted line (a): profile extrapolated to $\phi_b = 0$.

The precise definition of the length D will be by an extrapolation of the slope of the central profile toward $z \rightarrow 0$.

$$\left| \frac{1}{\phi} \frac{d\phi}{dz} \right|_{\text{central } z \rightarrow 0} = \frac{1}{D} \quad \text{Eq. 1-52}$$

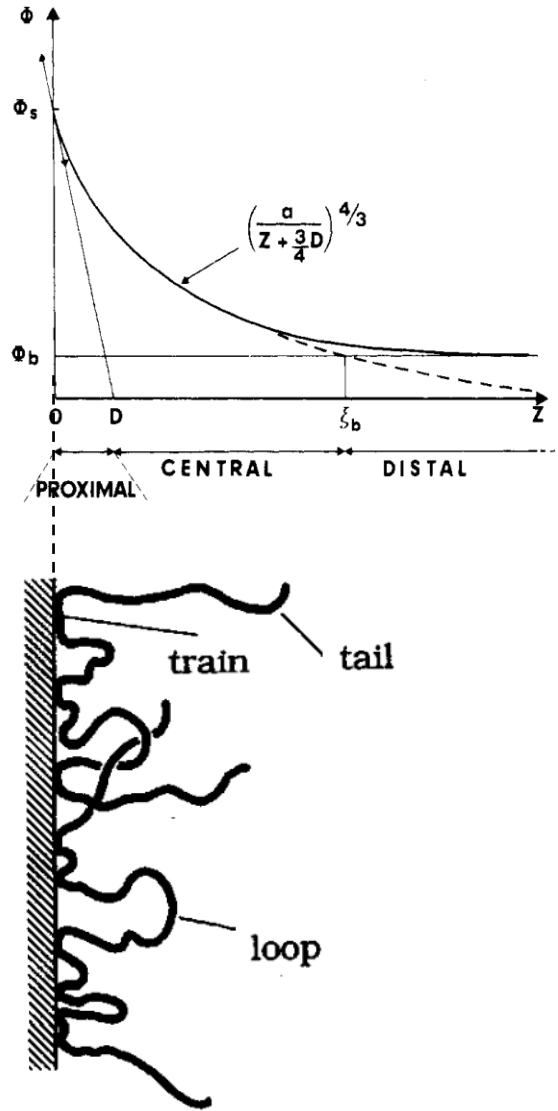


Figure 1-28. Relationship between the polymer volume fraction versus distance and the polymer concentration on the surface with tails, loops and trains

a) Polymer adsorption

In central region as we can see in Figure 1-28a the concentrations are $\phi \gg \phi_b$ ($C \gg C_b$), and thus we can let $C_b \rightarrow 0$. In this situation, it is useful to define a local correlation length $\xi(C)$ can be defined as

$$\xi(C) = aC^{-3/4} \quad \text{Eq. 1-53}$$

And

$$C = (a/z)^{4/3} \quad (D \ll z \ll \xi_b) \quad \text{Eq. 1-54}$$

Thus, the profile is defined by

$$\xi[C(z)] \cong z \quad \text{Eq. 1-55}$$

Equation 1-53 is typical of a self-similar structure.

Conformation of polymer chains on the surface

At low polymer concentrations, when the individual adsorbed polymers are far apart on the surface, the whole chain can adsorb on the surface and assume a low profile. These low profile polymers have been referred to as “pancakes” [De Gennes, 1987; Marques et al., 1988]. When polymers concentrations in solution are increased, the number density of polymers at the surface will also increase. At this point, the pancakes start to touch each other. Since these polymers are in a good solvent, the chains repel each other, and they cannot overlap very much. For homopolymers beyond this overlapping concentration, adsorption will slow down and stop. On the other hand, the polymers with a strong adsorbing end-group can continue to adsorb because the strongly adsorbing group can displace the weakly adsorbed backbones already on the surface. This competition between the end-groups and the backbones will continue to drive, or “pop”, the polymer backbones into solution by anchoring more chains onto the surface until the energy gained by adsorbing another chain is balanced by the pressure in the polymer layer. When process is ended, the backbones have a relatively stretched configuration, which are usually referred as “brushes” for diblock copolymers near saturated adsorption (Figure 1-29) [De Gennes, 1987; Ligoure and Leibler, 1990].

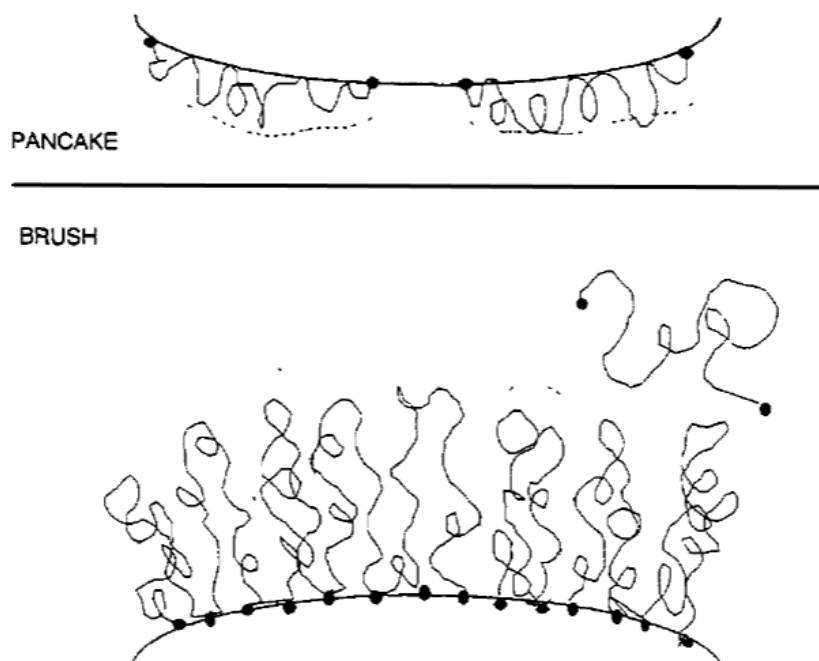


Figure 1-29. Pancake and Brush conformations of polymer.

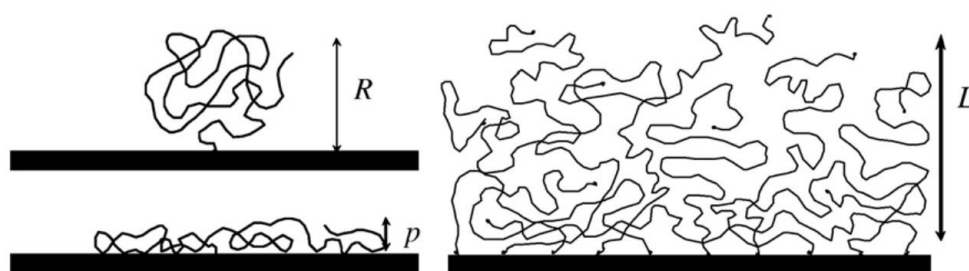


Figure 1-30. Sketch of mushroom, a pancake, and a brush.

Another approach that took Fler (2010) was three types of conformation on a solid surface (Figure 1-30). A mushroom is an isolated end-grafted chain on a repelling surface, where the typical length scale is the size of R . On an attractive surface the mushroom collapses to a pancake with thickness p , which is of order unity. When the end-grafted chains are densely packed a brush is formed, with thickness L which is proportional to the chain length N .

1.8. Polymer solution in Porous medium

There are three main retention mechanisms which take place when polymer solution flows through porous media.

- Polymer adsorption
- Mechanical entrapment
- Hydrodynamic retention

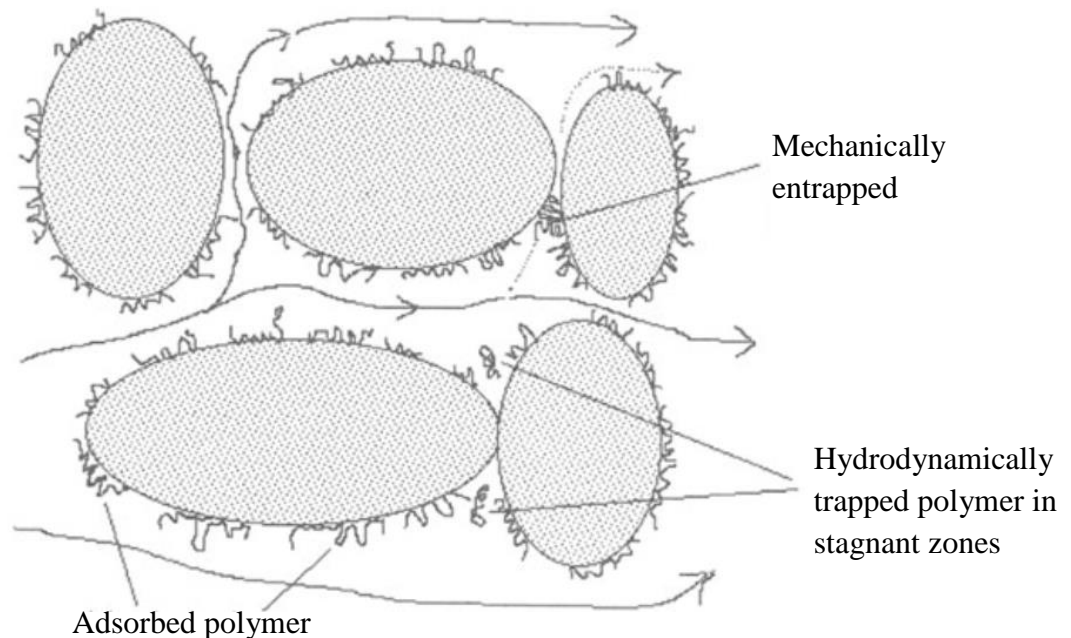


Figure 1-31. Schematic diagram of polymer retention mechanisms in porous media (Willhite and Dominguez, 1977)

These different mechanisms were reviewed by Willhite and Dominguez (1977), and each illustrated in Figure 1-31.

1.8.1. Mechanical entrapment

Retention by entrapment occurs when larger polymer molecules become lodged in narrow flow channels. The pore structure is a large interconnected network with vast number of possible paths connecting the inlet and the outlet of a core. A certain fraction of the network elements would consists of narrow pore throats. When the polymer solution is flowing through this complex network some of the molecules would be trapped in the narrow pores. These would block, and flows in these elements would consequently reduce, probably trapping more molecules upstream of the blockage.

The distribution of mechanically entrapped polymer along the core should be largest close to the inlet and decrease along the core. Besides, if there were above a critical number of 'entrapment sites' in the network, the core would ultimately block completely and the permeability would fall to practically zero.

Experimental studies by Szabo (1975) and Dominguez and Willhite (1977) have presented results in which they have tried to separate the effects of mechanical entrapment and polymer adsorption. Szabo (1975) studied the retention of HPAM in both sandpacks and in Berea cores. He performed static adsorption experiment with sand and then used the same sand to perform dynamic experiment in sandpack. The retained amount of polymer in static experiment was in order of 3-4 $\mu\text{g/g}$ and independent of concentration. While in the dynamic flow experiments were up to five times larger than in static experiment, indicating the dominant role of mechanical entrapment.

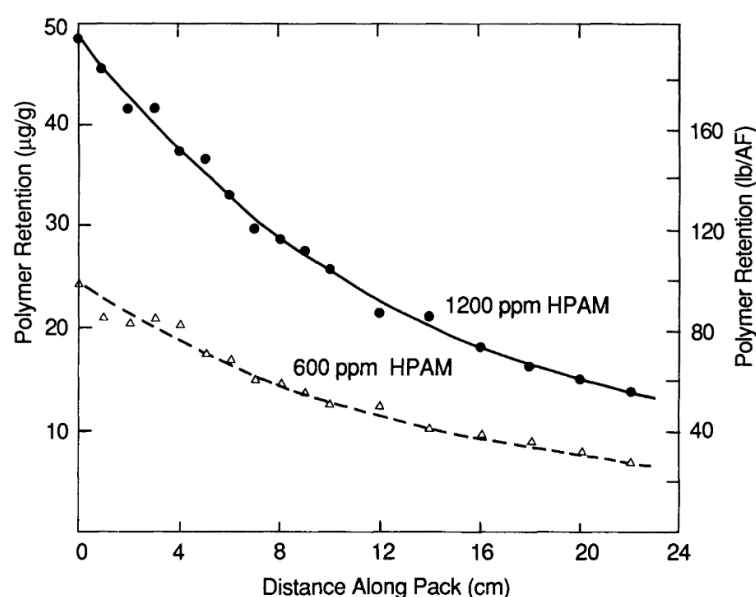


Figure 1-32. Distribution of retained HPAM along a sandpack after polymer flood. Conditions: 0.4PV brine, 0.2PV polymer, continuous brine injection, $k=1200\text{mD}$, $v=6\text{ft/day}$ [Szabo, 1975]

Figure 1-32 shows the distribution of retained polymer along the sandpack after 0.2PV of polymer solution was followed by injection of 5PV of brine. In the particular cases illustrated in Figure 1-32 for the two HPAM concentrations ($C_p=600\text{ppm}$ and 1200ppm), the mechanically retained levels ranged from 6 and $15\mu\text{g/g}$ at the outlet end to between 24 and $50\mu\text{g/g}$ at the inlet for the lower and higher polymer concentrations respectively. The fact that in static test the adsorption is independent from concentration and in dynamic flow the retention depends on concentration (Figure 1-32) also further evidence that mechanical entrapment is the retention mechanism operating here.

Cohen and Christ (1986) quantified the adsorptive retention by surface treatment technique. This was done by using a silane treatment of the silica in their sandpacks, which changed the surface such that it no longer adsorbs HPAM. They found that the adsorption is 32.5% of the total retention.

Mechanical entrapment is more likely mechanism for polymer retention for lower permeability materials where the pore sizes are smaller. Therefore, it is very important to know the hydrodynamic size of the polymer relative to the pore size distribution. To avoid this undesirable phenomenon the polymer solution should be pre-filtered or pre-sheared to reduce the molecular size. In any such treatment of the polymer solution to reduce the retention by mechanical entrapment, it is important to maintain other target properties such as solution viscosity.

1.8.2. Hydrodynamic retention

The physical picture of the hydrodynamic retention mechanism is illustrated in Figure 1-33. Here, some of the polymer molecules are thought to be trapped temporarily in stagnant flow regions by hydrodynamic drag forces. In such regions it is possible for the local polymer concentration to exceed that of the injected fluid. The idea of hydrodynamic retention arose from the observation that, after steady state was reached in a polymer retention experiment in a core, the total level of retention changed when the fluid flow rate was adjusted to a new value [Maerker, 1973; Chauveteau and Kohler, 1974; Dominguez and Willhite, 1977]. When the flow stops, these molecules may diffuse into the main flow channels and, when the flow recommences, they are produced as a peak in polymer concentration.

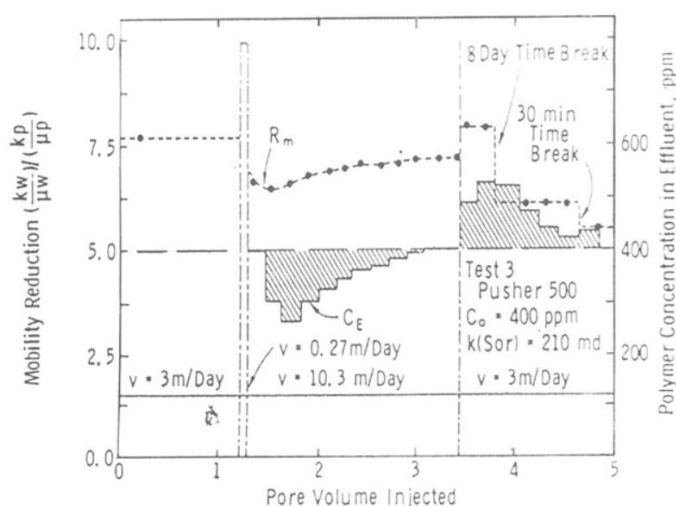


Figure 1-33. The effect of flow rate on the hydrodynamic retention of HPAM [Chauveteau and Kohler, 1974]

In Figure 1-33 illustrated an example of hydrodynamic retention in a core experiment using HPAM from the work of Chauveteau and Kohler (1974). As the flow rate increased from 3m/day to 10.3m/day in this experiment, more polymer was retained from the mobile aqueous phase, as shown by the dip in the polymer effluent concentration. When the flow rate is lowered back to 3m/day the polymer effluent concentration rises above the input value (400ppm), denoting a drop in the retained level. This kind of behaviour was observed by other researches as well [Maerker, 1973; Dominguez and Willhite, 1977]. In addition, the very similar effect can be observed for HPAM and xanthan by simply stopping the flow and then restarting it [Zaitoun and Kohler, 1987; Sorbie et al., 1989]. In the experiments of Sorbie et al.

(1989) results were presented for both high (0.85D-1.2D) and low (0.127D) permeability cores. The retention mechanism appeared to be different for the lower permeability core since the effluent concentration did not reach the input value and some flow rate dependence of retention level observed. From these experiments it appears that the retention by mechanical entrapment and hydrodynamic retention is more significant for the lower permeability material. The difficulty with the hydrodynamic retention is properly quantifying the exact value, we can see this effect only through the change in the effluent concentration while changing the flow conditions. Generally, hydrodynamic retention is small and can be neglected in most practical applications.

1.8.3. Polymer adsorption

We defined the adsorption in previous section as an attractive interaction between the polymer molecules and the solid surface. This interaction causes polymer molecules to be bound to the surface of the solid mainly by physical adsorption – van der Waals and hydrogen bonding. The polymer occupies surface adsorption sites, and the higher the surface area available the higher the levels of adsorption that are observed. Adsorption is the only mechanism that occurs during static experiment, when the bulk polymer solution is introduced to solid powder, such as silica sand or latex beads, and stirred until equilibrium is reached.

The measurement of polymer retention in a core flow experiment essentially involves measuring the effluent polymer concentration. There are two approaches to quantify the retained polymer using either the polymer frontal breakthrough only (method A) or with a complete post flush until no further polymer is produced (method B). As may be seen in Figure 1-34, in method A, the amount of polymer in the core is estimated at a point where the normalized effluent concentration reaches unity [Willhite and Dominguez, 1977]. This might be complicated by the fact that there may be some inaccessible pore volume [Dawson and Lantz, 1972]. Therefore, to quantify the retention value a postflush must be carried out and further polymer floods must be performed.

In method B, it is a simple subtraction of mass of produced polymer from the injected amount. A point about this method compared with method A is that it gives the total amount of irreversibly retained polymer.

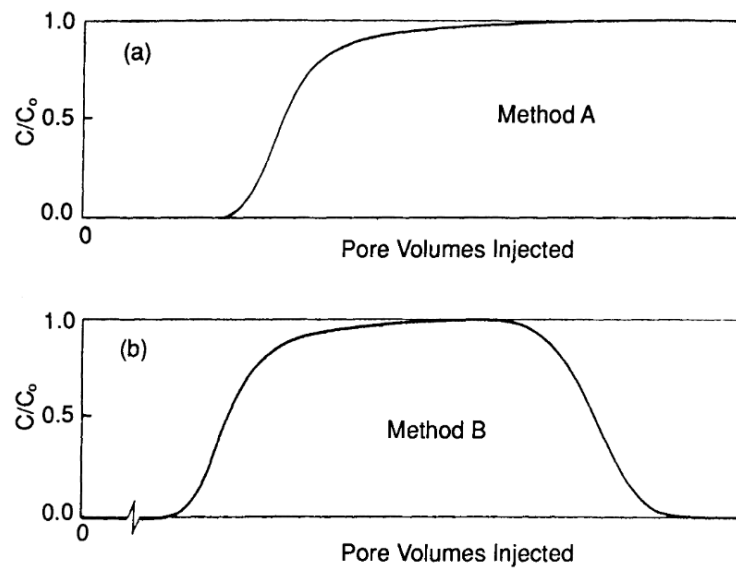


Figure 1-34. Two methods (A and B) for evaluating polymer adsorption in porous media from the core effluent profiles [Willhite and Dominguez, 1977]

Polymer adsorption mainly depends on:

- The polymer: the type of polymer, the polymer properties such as molecular weight, molecular size and hydrolysis degree.
- The solvent: the pH, salinity (Na^+ , Cl^- etc.) and hardness (Ca^{2+} , Mg^{2+} , etc.).
- The surface: the specific surface area and the type of surface (silica, calcium carbonate, clay, etc.), the wettability.

The studies of Lecourtier and Chauveteau (1985) and Zaitoun and Kohler (1987) showed that the polymer adsorption may be modified by changing the pH, temperature, brine composition, hydrolysis degree and the nature of the adsorbing substrate surface.

Polymer type. In early studies by Szabo (1975) for dynamic adsorption, it was shown that 2-acrylamide-2-methyl propane sulfonate (AMPS) adsorption is lower than HPAM. Broadly, xanthan adsorption in porous media is much lower than that of HPAM and tends to show less sensitivity to the salinity/hardness conditions of the solvent [Sorbie, 2013; Green and Willhite, 1998]. Figure 1-35 shows more adsorption examples for different types of polymers which illustrates the vast variation in adsorption as a function of the type of the polymer.

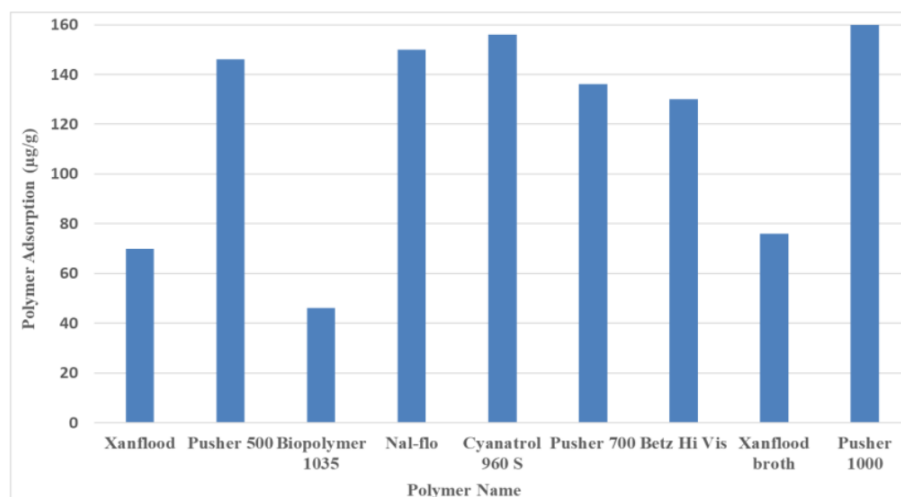


Figure 1-35. Polymer adsorption for different types of polymers [Sheng, 2011]

Molecular weight. The results obtained for sulfonated polymer in static adsorption showed that level of adsorption was increased by increasing molecular weight [Hlady et al., 1982; Rashidi et al., 2009]. This is in accordance with theory since a polymer with a higher molecular weight would lead for a thicker layer of the polymer when adsorbed on a surface [Hlady et al., 1982]. However, dynamic adsorption in silica sand decreased with increasing molecular weight. The effect of molecular weight on retention of sulfonated polyacrylamide copolymers studied by Rashidi (2009, 2011) led to the conclusion that by increasing the molecular weight of the polymer, fewer polymers was retained. The observation was explained by inaccessible pore volume concept; larger polymers are unable to enter the smaller pores of the rock. Lakatos et al. (1979) found that the level of HPAM retention in the sandpack decreased slightly with increasing molecular weight but decreased even more sharply as the degree of hydrolysis increased [Lakatos et al., 1981].

Hydrolysis degree. MacWilliams et al. (1973) reported that HPAM adsorption onto Miocene sand was around 30µg/g when the degree of hydrolysis was between 25% and 70%. However, as the degree of hydrolysis was reduced from 15% to 2%, HPAM adsorption increased from ~60µg/g to ~700µg/g. It was presumed that adsorption was reduced by charge repulsion between the acrylate groups and anionic groups on the quartz.

Bessaies-Bey et al. (2018) found that adsorption of HPAM depends on the anionicity degree of the polymers (Figure 1-36). Indeed, the adsorption of HPAM is lower than the one for for neutral PAM at low ionic strength. However the polymer adsorption could be restored by increasing the salt concentration.

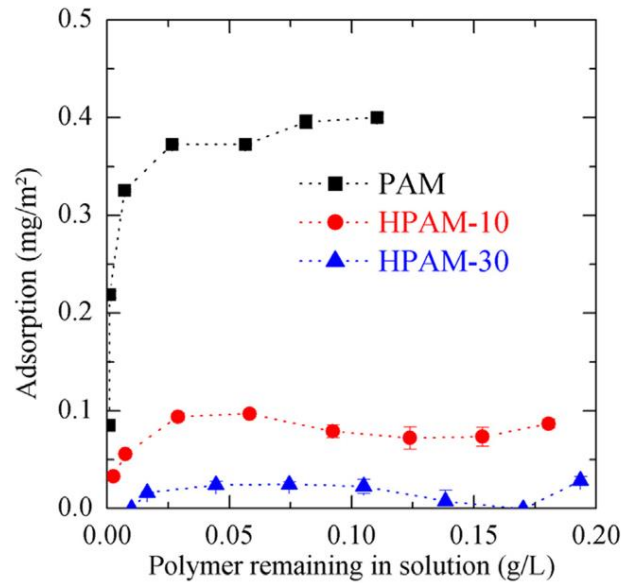


Figure 1-36. Adsorption isotherms of acrylamide-based polymers as a function of the anionicity degree (PAM, $M_w=167\text{kg/mol}$, Dispersity=1.11), HPAM-10 ($M_w=181\text{kg/mol}$, Dispersity=1.09) and HPAM-30 ($M_w=149\text{kg/mol}$, Dispersity=1.07)) on natural quartz [Bessaies-Bey et al., 2018]

Salinity. Chiappa et al. (1999) noted that HPAM adsorption on quartzite increased from $\sim 60\mu\text{g/g}$ with no CaCl_2 present to $\sim 750\mu\text{g/g}$ with 8% CaCl_2 in the brine. To explain this behaviour, they proposed calcium bridging from the anionic rock to the anionic polymer. Consistent with their hypothesis, they also noted that adsorption of cationic polyacrylamide was nearly independent of CaCl_2 content. In contrast to that, the content of monovalent salt NaCl showed no difference in retention in experiments of Mungan (1969) where he used distilled water and 2% NaCl . Smith (1970) showed that low concentration of calcium ion Ca^{2+} will promote HPAM adsorption on silica, as the divalent ions compress/squeeze the size of the molecules of the flexible HPAM and reduces the static repulsion between the silica surface and the polymer carboxyl group.

Polymer concentration. The adsorption amount dependence on the polymer concentration for a typical non-hydrolysed and a partially hydrolysed polyacrylamide shows similar behaviour. Generally, the adsorption increases with the increase in polymer concentration [Huang and Sorbie, 1993; Green and Willhite, 1998; Zheng et al., 2000]. During experiments with HPAM concentrations ranging from 10 to 6000ppm, Zhang and Seright (2013) reported three regimes of retention behaviour: (1) relatively low retention (but concentration insensitive) at low polymer concentrations (e.g., $\sim 20\mu\text{g/g}$ between 10 and 100ppm), (2) retention increasing with increased polymer concentrations. They proposed a conceptual model to explain this behaviour that is illustrated in Figure 1-37.

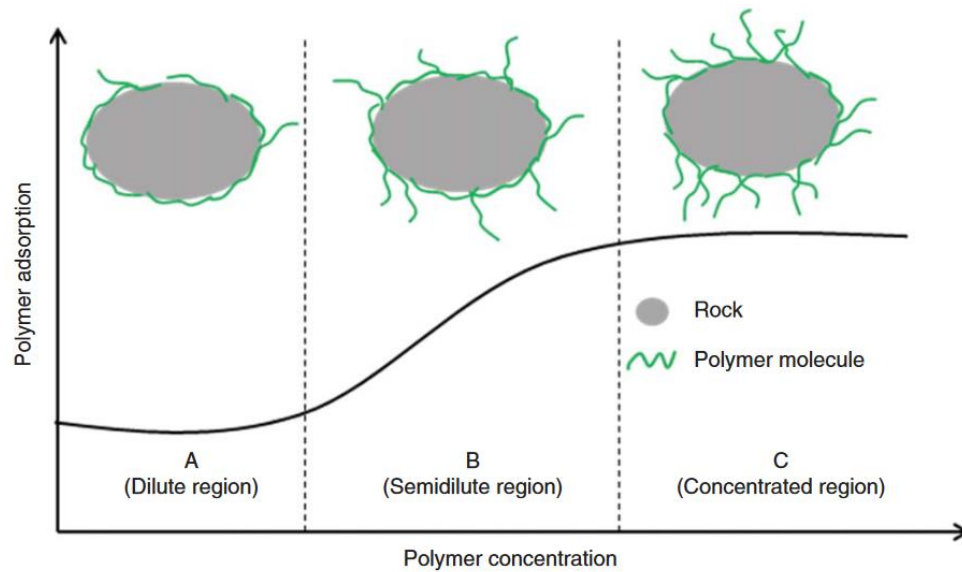


Figure 1-37. Model of polymer adsorption/retention on the rock surface proposed by Zhang and Seright (2013)

In a dilute regime, the adsorption is independent of polymer concentration. The retention in the dilute regime indicates the minimum amount of polymer needed to occupy the available vacant sites. However, in a semi-dilute regime, the intermolecular interaction in solution will result in mixed adsorption, where some molecules will be adsorbed with all the segments in contact with the surface, while others will be adsorbed with only partial segments in contact with the surface. Increasing the polymer concentration in this regime will increase the adsorption as shown by Region B in Figure 1-37.

In the concentrated regime, most polymer molecules are adsorbed with segments partially attached to the rock surface. Put another way, only the end of the polymer molecule is attached to the surface, while the majority of the molecule dangles free in the solution. In this case, almost no additional polymer molecules can be adsorbed with increasing concentration because all sites are taken. As shown by Region C in Figure 1-37, the adsorption is concentration-independent.

The experimental behavior did not appear to be consistent with the Langmuir isotherm. The Langmuir isotherm assumes that polymer retention approaches zero at low polymer concentrations and is reversible. Both of these assumptions have generally been proven false [Green and Willhite, 1998].

Rock surface effect. The retention is strongly affected by the iron and clay content of the porous medium. The HPAM adsorption on calcium carbonate is significantly higher than adsorption on the silica surface [Sheng, 2011]. During static adsorption studies, Chiappa et al. (1999) found adsorption for a cationic polyacrylamide to be $610\mu\text{g/g}$ on quartzite, $14500\mu\text{g/g}$ on quartzite with 8% clay, and $180000\mu\text{g/g}$ on pure clay. Clay particles are generally very small (fraction of μm) and contribute both to increasing specific area of the core and to decreasing its permeability.

HPAM retention increases by materials with a positively charged surface, such as dolomite, and decreases retention, when surface area remains constant, on materials with negatively charged surfaces, such as sandstones.

As the adsorption of PAM/HPAM on silica surface is induced by the formation of hydrogen bonds, the density and the accessibility of the silanol groups are crucial. In addition to silanol groups, siloxane groups are also present on the silica surface. According to the origin of silica, purity, surface treatment, storage condition, the density and accessibility of both silanol and siloxane groups strongly differ from one surface to another. Then, for siliceous materials the changes in surface groups composition obviously affect its reactivity and consequently its affinity with polymers. Lecourtier et al. (1990) investigated the adsorption behavior of hydrolyzed and of a neutral polyacrylamide on siliceous material treated at different temperatures. Figure 1-38 shows a drastic decrease in polymer adsorption when the temperature of thermal treatment increases. An absence of HPAM adsorption is observed onto the siliceous surface treated at 700°C. The depletion of silanol groups as observed in Figure 1-39 could explain the radical changes of polyacrylamide affinity toward the same siliceous materials. The correlation between the depletion of silanol and decrease in polyacrylamide adsorption suggest that silanol groups are the anchoring sites.

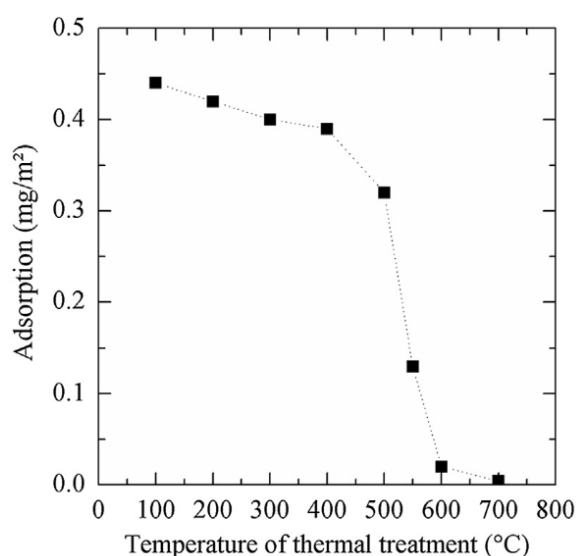


Figure 1-38. Impact of the thermal treatment of the adsorption of HPAM ($M_w=7.6 \cdot 10^6$ g/mol, 30% of anionicity) on silicon carbide with an oxidized surface [Lecourtier, 1990]

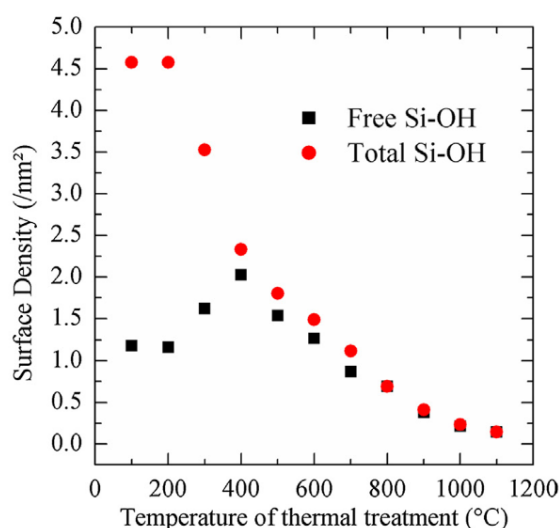


Figure 1-39. Variation of the free silanol groups density compared to the total amount of silanol groups as a function of the thermal treatment [Dugas et al., 2003]

As a function of origin (natural or synthetic), the surface of siliceous materials can support in some case a few amount of other oxides. According to their density, these oxides can strongly affect the macroscopic properties of siliceous materials (charges, solvation, acidity, hydrophobicity) and offer possible new sites for adsorption process.

Pefferkorn et al. (1985) were the first to show the occurrence of a strong adsorption of neutral PAM on natural (kaolinite) and synthetic aluminosilicates. They observed that PAM does

not adsorb on the basal face of kaolinite but only on the edge face where aluminol sites are located. They clearly established that the presence of aluminol sites on the surface of siliceous materials can considerably affect the amount of adsorbed polyacrylamide. The authors established that hydrogen bonds between amide groups and aluminol ones dominate polyacrylamide adsorption compared to adsorption on silanol groups. Thus important conclusion was supported by a decrease of the adsorbed amount when the solution pH was increasing thus breaking the hydrogen bonds responsible for adsorption.

The increase of adsorption ability as a function of oxide impurity was confirmed by Gravelling et al. (1997) who compared the adsorption of HPAM on quartz, feldspar and kaolinite having respectively increasing aluminum content. They showed that kaolinite adsorbs 3 times more of HPAM than quartz.

Bessais-Bey et al. (2018) found that the PAM or HPAM do not adsorb on synthetic silica particles (Sikasol) while they strongly adsorb on the natural quartz sample. To investigate the difference between these two siliceous materials, they characterised the two materials using XRD, SEM coupled with EDX analysis and AI NMR. The analysis showed the presence of octahedral aluminium thus suggesting the presence of surface impurities in the form of aluminol at the surface of the natural quartz sample.

Permeability effect. Generally, polymer retention decreases with higher permeability. This is due to mechanical entrapment in a low permeability rock compared to that in a high permeability rock. Moreover, a high clay content in low permeability rocks is also another possible reason for higher retention.

Presence of oil. Broseta et al (1995) examined the polyacrylamide retention in the water-wet system in presence of oil and found no change in retention compared to monophasic experiments at the same condition. They suggested the theory of the adsorption on the water-oil interface that will increase the overall retention and make up for inaccessible pore volume that decreases the adsorption of the polymer. These opposite effects together can give the same value of retention of the polymer as in monophasic experiments. However, the wettability has a big impact on retention level, in the oil-wet system, polymer retention of polyacrylamide at residual oil saturation will considerably decrease by factors of 2 to 5 compared to the retention if the core is 100% water-saturated. It agrees with the findings of Wever et al. (2018), they reported the retention level up to 3-4 times higher in the presence of oil than in fully water-saturated PM in the high permeable reservoir rock. As we mentioned before the experimental results dealing with retention in the presence of oil are scarce.

Chapter II: Experimental Study

In this chapter, we describe the materials and fluids chosen for carrying out the experiments, as well as the experimental setup and procedures followed during this work.

2.1. Porous media

The experiments were performed with 2 types of sandstones with different permeability. We chose these sandstones for their well-known mineralogy and homogeneous structure. Bentheimer is a high permeable porous medium with the permeability of 2.5-3 Darcy, while Berea is an intermediate permeable porous medium with the permeability of 80-120 mDarcy. Both porous media have a porosity of around 25%. The specific surface area for Bentheimer is $\approx 0.45 \text{ m}^2/\text{g}$ (Peksa et al. 2015), and for Berea is in the range of $\approx 0.8\text{-}1.2 \text{ m}^2/\text{g}$ (Churcher et al. 1991).

Minerals	Berea	Bentheimer
Quartz	87.5	90.6
Illite/Mica	3	3.2
Kaolinite	3.2	0
Chlorite	1.7	0
Feldspar	1.9	4.6
Plagioclase	0.9	0
Calcite		0.6
Dolomite	0.9	0
Siderite	0.9	1

Table 2-1. Mineral Composition of Bentheimer and Berea sandstones [Skauge, 2013]

These sandstones are considered ideal sedimentary rocks for reservoir studies due to their lateral continuity and homogeneous block-scale nature. They have a uniform grain size distribution, porosity, permeability, and dielectric properties, which makes them suitable for standard laboratory experiments and associated comparison with theory [Klein and Reuschle, 2003; Ruedrich and Siegesmund, 2007]. Therefore, Bentheimer and Berea sandstones are used to investigate a variety of reservoir topics ranging from passive and active properties of oil recovery processes to flow and transport in the groundwater zone and environmental remediation processes.

The mineral composition given in the table above can vary depending on where they have been extracted and the reservoir conditions. Different researchers report slightly different values of aluminum, iron, and other minerals, but quartz content is always around 90% and higher content of clay in Berea sandstones.

The sandstones samples used in our study were rectangular and cylindrical forms with a length in range of 15 to 20 cm and with cross section in range of 16 to 19.6 cm² (Figure 2-1).



Figure 2-1. Bentheimer (a) and Berea (b) sandstones

Before core flood experiments the porous media are prepared in the following way:

- Weigh the core
- Put the core between the two metallic plates that are covered by a thin layer of Teflon™ to avoid ionic exchange between metallic plates and flowing fluids (especially with iron which causes the degradation of polymer solution); These metallic plates have an inlet/outlet for injection/recovery of fluids and pressure tabs to measure the total pressure drop by means of differential pressure transducers



Figure 2-2. Metallic plates with cross channels used to homogenize the fluid injection.

- Cover laterally the sandstone with epoxy paste (Araldite, epoxy resin), and leave it to dry for a night
- Check the porous media for leakage with nitrogen and leak finder foam
- Drill the holes (for connections) on epoxy paste that is covering the sandstone
- Put the connections and seal the joints with epoxy paste, leave it to dry for one more night
- For mechanical rigidity purpose and safe use, cover it with fiberglass and resin, leave it to dry for another night
- Put all valves and weigh it
- It is ready for saturation



Figure 2-3. Prepared porous media

As you can see in Figure 2-3 there are 5 pressure taps to measure the pressure drop across the total length of porous media, and across sections in the internal part of it to follow the propagation of injected fluids.

2.2.Brine

The brine is a Synthetic Sea Water (SSW) which composition is presented in Table 2-2. We dissolved the salts in deionized water, then filtrated under low pressure through 0.45 μ m polycarbonate filter and degassed under gentle stirring and low pressure. The KI was added to serve as a tracer only for dispersion test experiments. As we can see, the ratio of divalent/monovalent salt content is about 2:1

Salts	Mass (g) per 1L of water
NaCl	23.907
KCl	0.743
MgCl ₂ -6H ₂ O	10.827
CaCl ₂ -2H ₂ O	1.525
Na ₂ SO ₄	3.994
NaHCO ₃	0.199

Table 2-2. Composition of used Synthetic Seawater

2.3.Polymer

The polymers provided by SNF Floerger were available considering different hydrolysis degree, molecular weight, chemical composition, and molecular structure. For our study we have chosen the polymers that vary by molecular weight, (high and low), and chemical structures (with or without ATBS, that will infer ionic characteristics to the polymer in solution state). Table 2-3 summarizes the different polymers available and those used in this study (framed ones).

Study	Polymer	Chemistry (mol%)			Molecular weight (MDa)
		AM	AA	ATBS	

Hydrolysis degree	A	100	0	0	3
	B	70	30	0	3
	C	30	70	0	3
	D	0	100	0	3
Molecular weight	Flopaam 3630S	70	30	0	19
	Flopaam 3130S	70	30	0	3
Chemical structure	Flopaam 3630S	70	30	0	19
	Flopaam 5115 XV	75	10	15	19
	Flopaam 5115 BPM	75	10	15	3
	Flopaam SAV 10 VHM	<60	0	>40	19
Molecular structure	Flopaam 3630S	70	30	0	19
	Microgel/branched HPAM	70	30	0	-
Dispersity	Flopaam 3130S	70	30	0	3
	Polymer B	70	30	0	3
	Flopaam 3430S	70	30	0	11
	Polymer SNF	70	30	0	11

Table2-3. Characteristics of Polymers provided by SNF

To investigate the influence of molecular weight on polymer adsorption/retention in porous media we used polymers Flopaam 3630S and 3130S with a molecular weight of 19MDa and 3MDa respectively. These are hydrolyzed polyacrylamides HPAM with a 30% hydrolysis degree. We also performed experiments with sulfonated HPAM polymers Flopaam 5115 XV and 5115 BPM with a molecular weight of 19MDa and 3MDa respectively. Both polymers have a hydrolysis degree of 10%, and a sulfonation degree of 15%. All polymers that were provided by SNF Floerger were in dry white powder form of various moisture content.

The amount of moisture in polymer powder was measured using an infrared balance to have pure polymer mass and prepare the right concentration of polymer.

2.3.1. Polymer solution

All polymer solutions were prepared by diluting a concentrated mother solution that is prepared beforehand according to the following procedure:

1. Pour 500ml of brine into a beaker
2. Place a stirring rod in the beaker. It should be placed in the middle of the beaker and as low as possible. Set rotor speed at 500 rpm to create a vortex
3. Pour the polymer powder gently into the vortex shoulder. It is recommended to do it grain by grain to ease the powder dispersion
4. Leave the solution under stirring for 2h

5. Decrease the stirring rate to ≈ 150 rpm, cover it with a plastic film and leave it for a night
6. Filter the mother polymer solution through polycarbonate filters in series: 10, 5, and 2 μm at constant flow rate 0.3ml/min using a volumetric pump
7. Keep the stock solution under nitrogen gas in a fridge. It is to be mentioned that 400ppm of NaN_3 were added to SSW in this case. Doing so, polymer was protected against oxidation, bacterial and chemical degradation.

To prepare the daughter solution, this mother solution was diluted with SSW.

The shear viscosity of each polymer solution was measured using a controlled shear stress rheometer ARG2 (TA Instruments, France) or Kinexus (Malverne, France). We measured viscosity at temperature $T=25^\circ\text{C}$ using a 2° cone/plate geometry by steeply increasing shear rate from 0.001s^{-1} to 1000s^{-1} . For very low viscous polymer solutions we used Ostwald viscometer.

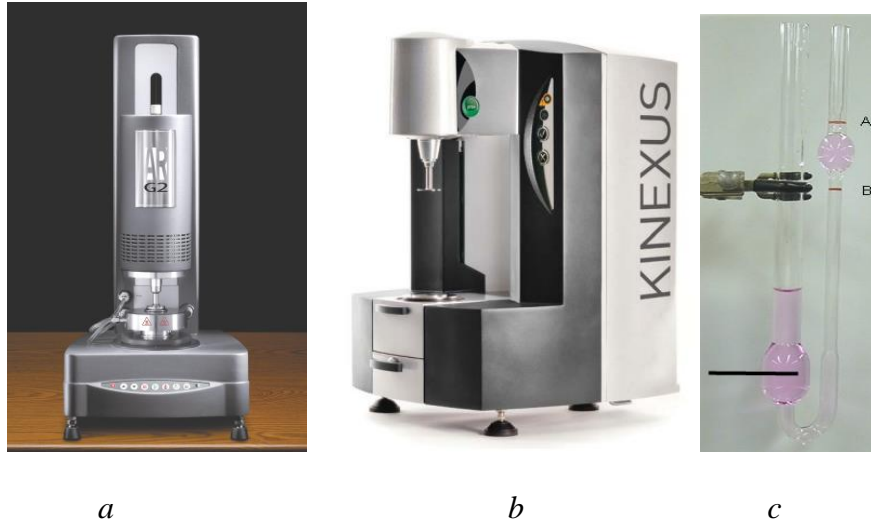


Figure 2-4. Rheometers ARG2(a) and Kinexus(b), and Ostwald viscometer(c)

An example of relative viscosity – $\mu_r = \frac{\mu}{\mu_s}$, where μ and μ_s are respectively the polymer solution and solvent viscosities, – versus shear rate is shown in Figure 2-5. We observe a Newtonian plateau at low shear rates and a shear-thinning regime (pseudoplastic) at high shear rates. These two regions crossover at a characteristic shear rate $\dot{\gamma}^*$. As we will see later when concentration increases: the plateau viscosity increases, the shear-thinning becomes more pronounced and $\dot{\gamma}^*$ is shifted toward lower values.

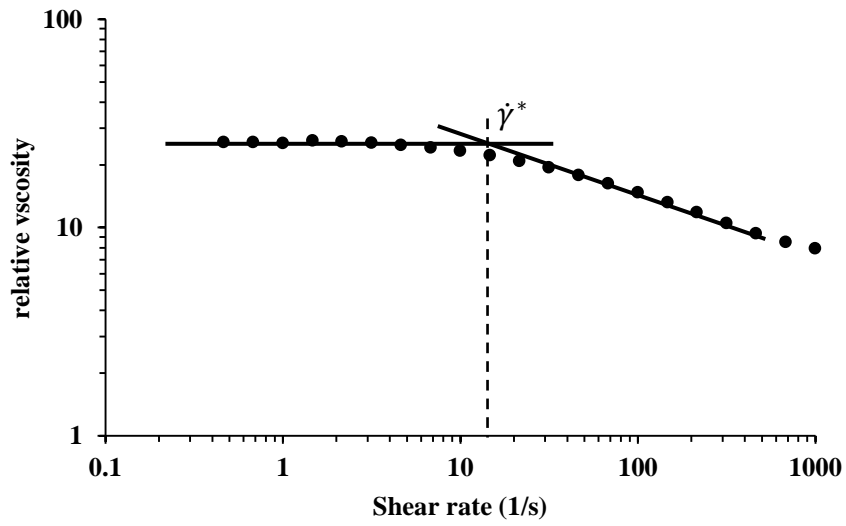


Figure 2-5. Typical plot of relative viscosity versus shear rate

2.4. Experimental setup

The experimental setup is presented in Figure 2-6.

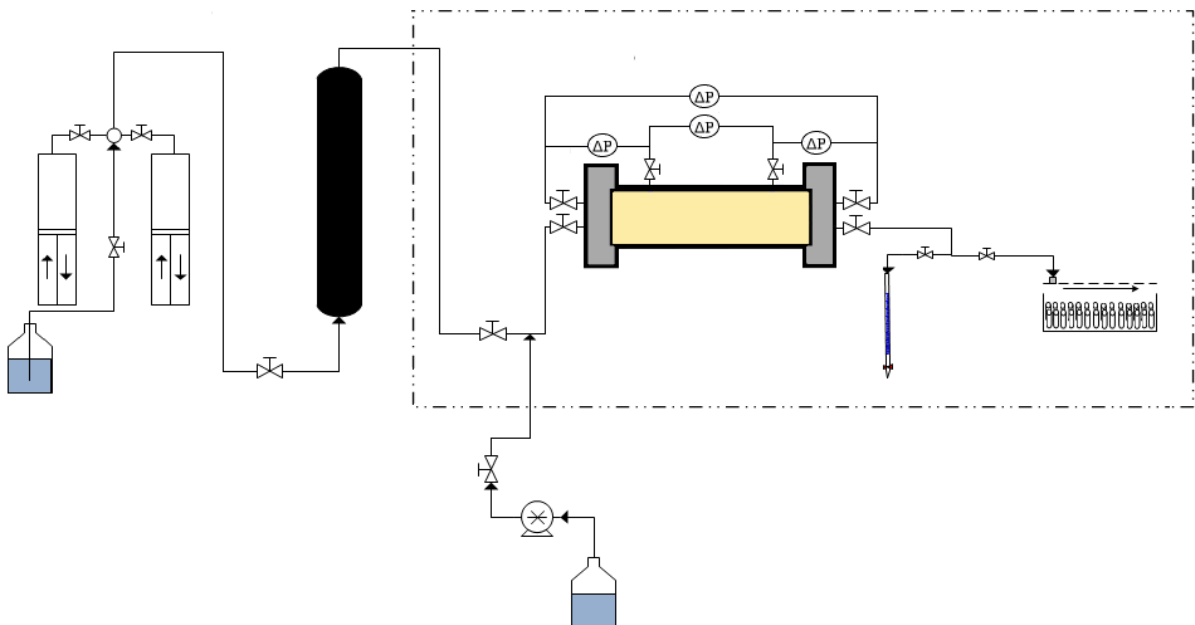




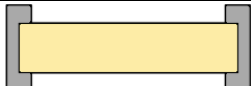

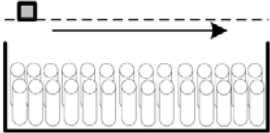




Figure 2-6. Experimental setup

Legend	
	Brine/polymer solution
	DCP50 pump
	Isco pump
	Valve
	Porous medium
	Oil tank
	Fractional collector
	100ml burette
	Oven at $T=25^{\circ}\text{C}$

2.5.Experimental equipment

2.5.1. Pressure transducers

The differential pressure sensor model is Rosemount 3051. The pressure drop is measured at the ends of each sample as well as between intermediate pressure taps.



Figure 2-7. Differential pressure transducer Rosemount 3051

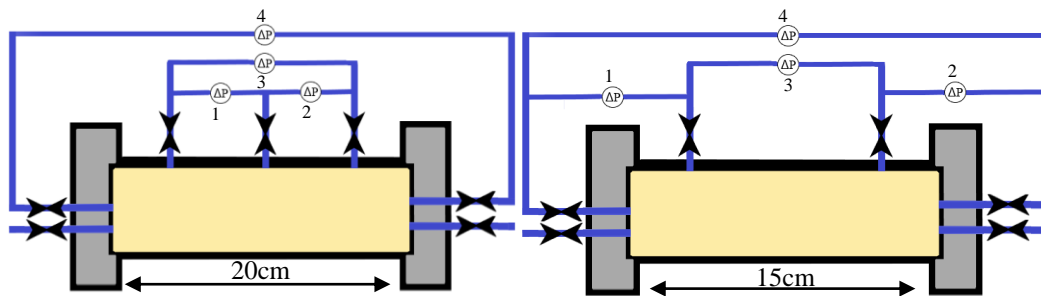


Figure 2-8. Pressure taps location in porous media with different length: 20cm and 15cm

In figure 2-8, we present two different ways of installing the pressure tabs in the interior part of porous media. In the case of long porous media (20cm), we can install three taps and measure the pressure drop as it shows in the scheme. However, in a 15cm core, we do not have enough space for three taps, so we measure pressure drop between external and internal pressure tabs (1 and 2 in Figure 2-8). Our main interest in both cases is pressure drop data from pressure transducer number 3 that it is not affected by end effects.

2.5.2. Pumps

The pumping systems allow a continuous and regular flow at precise and constant injection rate / pressure.



Syringe Pump ISCO 500D	DCP50 Pump
Minimum flow rate: 0.06ml/hr	Minimum flow rate: 0.01ml/hr
Maximum flow rate: 12240ml/hr	Maximum flow rate: 500ml/hr
Maximum working pressure: 258.6bar	Maximum working pressure: 50bar

Figure 2-9. Pumps used in the experiments

Figure 2-9 shows the different pumps used for the experiments. ISCO pump was used for oil injection by pushing the oil from oil tank with water from the bottom, and DCP50 pump for brine and polymer solution injection.

2.5.3. Spectrophotometer

We used a spectrophotometer to measure the concentration of Potassium Iodide (KI) in the effluent that was collected during the dispersion test. The measurements were performed at wavelength 226nm. The absorbance of light in our conditions increases linearly with the concentration of KI until 20ppm. Therefore, we diluted the effluent to have the correct signal from the apparatus.



Figure 2-10. Spectrophotometer UV-3100PC

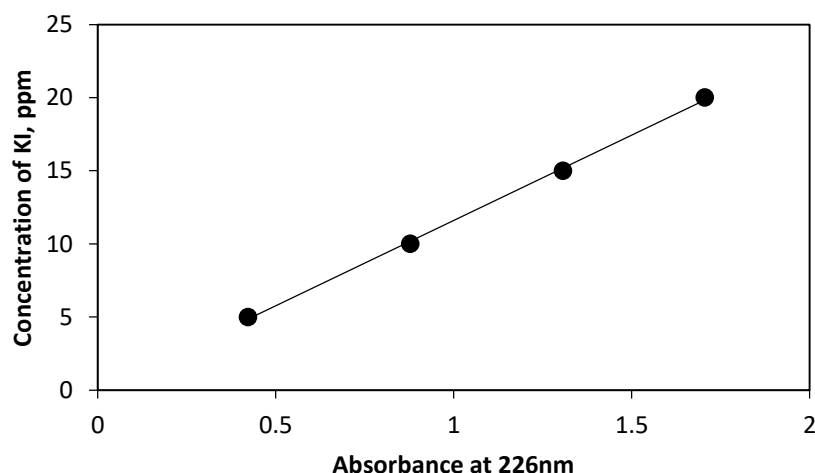


Figure 2-11. Calibration curve of concentration of KI vs Absorbance of light at 226nm

2.5.4. TOC-L/TNM-L

TOC refers to a Total Organic Carbon analyzer, which utilizes a catalytic oxidation combustion technique at high temperature (the temperature rises up to 720 °C), to convert organic carbon into CO₂. The CO₂ generated by oxidation is measured with a Non-dispersive Infra-Red (NDIR) sensor.

The nitrogen content of the sample can also be determined by means of the Shimadzu's TNM-1, the Total Nitrogen Module on basis of a chemi-luminescence reaction., It can accurately measure nitrogen over a broad range: Total Nitrogen (TN) from 100ppb to 4000ppm. A nitrogen-containing sample is combusted to NO and NO₂. The reaction products react with ozone to an excited state of NO₂. When falling back to the ground level, energy is emitted as light. The nitrogen is measured with a chemi-luminescence detector.

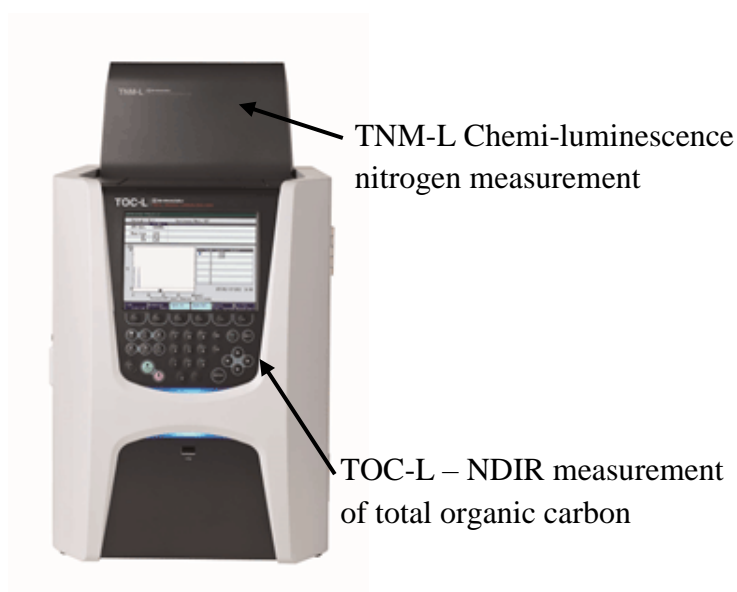


Figure 2-12. TOC-L/TNM-L analyser

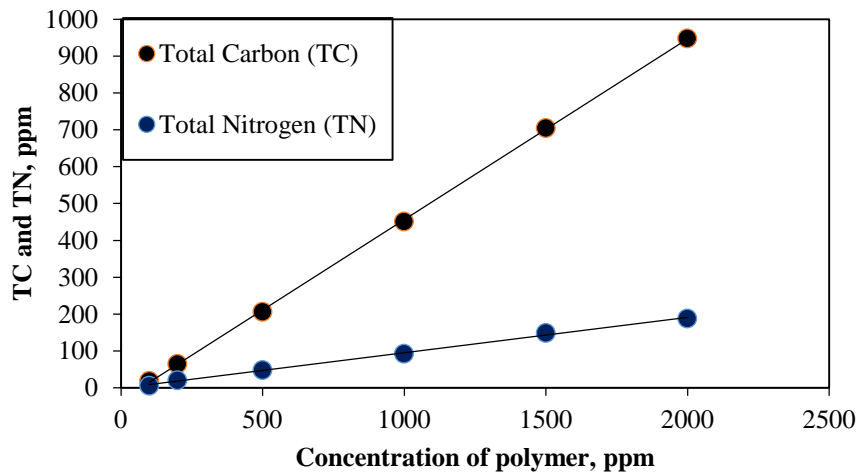


Figure 2-13. Calibration curve

2.6. Experimental procedure

2.6.1. Characterization of porous media

After preparation of porous media (PM) as described before, we start the brine saturation under vacuum (obtained by an Edwards vacuum pump). The saturated medium is weighed and the porosity and pore volume are deduced therefrom.

After saturation of the PM with brine, the dispersion curve is obtained by injection of brine containing Potassium Iodide (KI $C = 250\text{ppm}$), considered as a tracer, at a constant flow rate of 30ml/h . The concentration of Iodide is measured from the effluents in spectrophotometry. It is worth noting that the symmetry of the dispersion curve is an indication of the homogeneity of the core.

Next step is calculating brine permeability. The permeability is determined by measuring ΔP at different flow rates and applying Darcy's law.

2.6.2. Monophasic experimental procedure

After characterization of PM, we can start polymer flooding at a constant flow rate of 10ml/h which corresponds to a front velocity of 2 ft/day . During polymer injection, we record the pressure drop along the core.

The effluent concentration is checked in TOC before stopping the polymer injection to be sure that we have reached 100% of injected polymer concentration or almost reached it. After stopping the polymer flooding we inject the polymer at different flow rates to calculate the mobility reduction (RM).

We measure the concentration of polymer in the effluents, which was collected during polymer flooding, to see the flow of polymer front in PM.

The next step consists of the flush of the PM with brine to remove all the mobile (not retained) polymer. Brine flush is performed at the same flow rate as polymer flooding for 1-2 days. We check the concentration of polymer in the effluents to be sure that all polymer is flushed. Then we inject the brine at different flow rates to calculate the permeability reduction (R_k).

After calculating the permeability reduction, we perform a second polymer flooding to estimate the inaccessible pore volume and quantify the amount of retained polymer. The second polymer flooding is non-reactive since all the retention is completed by the first polymer flooding. Therefore we use the second front of the polymer as a tracer for polymer flooding.

2.6.3. Diphasic experimental procedure

Oil Drainage

We performed the diphasic experiments using the crude oil provided by Shell. The viscosity of oil measured in the Ostwald viscometer at $T=25^{\circ}\text{C}$ is around 13cP.

The crude oil was injected at a flow rate of 50 ml/h by pushing the oil with water from the oil tank using an Isco pump (Figure 2-6). While injecting the oil we record the pressure data along the core and collect the effluent in the burette to measure the recovered water amount. When we reach the irreducible water saturation, that means no water recovery is observed anymore, we stop the oil drainage.

After oil drainage, we measure the pressure drop at a different flow rate to calculate the permeability to oil in presence of irreducible water, $k_{oil}^1(S_{wi})$.

Water displacement

After oil drainage we have 2 options:

- ageing of PM in the oven at $T=40^{\circ}\text{C}$ for at least 4 weeks to alter the wettability;
- water imbibition right away (water-wet).

In both cases, the waterflooding process is the same. We injected brine at a constant flow rate of 50 ml / h and collect the effluents in burettes. When we reach the residual oil saturation, which means no oil is coming out of PM, we stop the water injection. Then we inject the brine at different flow rates to calculate the effective water permeability in presence of residual oil, $k_w^1(S_{or})$.

Following this step, we perform a dispersion test by injecting brine with Potassium Iodide as a tracer. It can be used to calculate the new pore volume available for water flow, and the volume of residual oil.

Two-phase polymer injection

Waterflooding is followed by polymer injection at 10ml/h. The process of polymer flooding is the same as in the monophasic case.

We have studied different injection procedures:

- Tertiary: polymer injection after waterflooding
- Secondary: injection of the polymer after oil drainage or ageing

In the secondary stage experiments, we were not able to quantify the retained amount of polymer because of oil presence in the effluent. So we have decided to work in the tertiary stage only.

Starting this point the experimental procedure is the same as in monophasic experimental procedure.

3 Chapter III – Results and Discussion

In this chapter, we collected all the results obtained from experiments performed in this work and we tried to interpret them on basis of acknowledgements frame given in chapter I. All the experiments were performed following the procedures described in chapter II. Experimental conditions will be precised from one experiment to the other but the flow rate for polymer flooding was constant 10ml/h in every experiment, which corresponds to the frontal velocity of 2ft/day. The velocity used in EOR applications usually around 1ft/day, so we have chosen our flow rate to have a relatively fast experimental process and be in the magnitude of reservoir conditions. All the experiments were performed in an oven at constant temperature 25°C (room temperature). We have decided to keep the flow rate of polymer flooding and the temperature constant and study the other effect of other variables on the retention of polymer.

We start with the characterization of the materials used in this work, brine, polymer solution, and porous media. Then show the results obtained during monophasic and diphasic experiments step by step. At the end we compare the results of monophasic and diphasic experiments and show the trend of retention in our work and try to draw some conclusions about the influence of oil on polymer adsorption process. We organized the results by the impact of one or another parameter on the retention of the polymer to make it easier for the reader.

3.1 Composition of brine

The objective of working with Synthetic Sea Water (SSW) was to mimic the field-case where it is common to use the water from reservoirs as a displacing fluid. Sometimes it is named simplified sea water in the sense that it contains only major compounds of real sea water. The composition of used SSW is given in Table 2-2. To that brine we added Potassium Iodide (KI) as a tracer for dispersion test. When polymer is dissolved at, the sodium azide is also used as a bactericide to protect polymer against biological degradation.

pH	6.8
Conductivity	166 mS/cm
Ionic strength	3.268M

Table 3-1. Characteristics of brine

After its preparation, the pH and conductivity were measured and the ionic strength was calculated. These are displayed in Table 3-1.

3.2 Viscosity of polymer solutions

Polymer solutions were prepared according to the procedure described in Chapter II. After that and before core experiments, their shear viscosities were measured versus shear rate at various concentrations and for each polymer. The measurements were performed using an imposed stress rheometer (ARG2 or KinexusPro) equipped with a cone-plate geometry by applying increasing shear rates, ranging from 0.01 s^{-1} to 1000 s^{-1} at $T=25^\circ\text{C}$. As usual the

polymer solutions are shown total non-Newtonian fluids, with a Newtonian plateau at low shear rates and a pseudoplastic behavior at high shear rates (see Figure 3-1).

3.2.1 Influence of concentration on viscosity

The range of concentration investigated depends on polymer type and was typically from 100ppm to 5000ppm in order to scan both dilute and semi-dilute regimes. In Figure 3-1 we show viscosity versus shear rate $\eta(\dot{\gamma})$ obtained for 5115BPM polymer sample at various concentrations, C_p .

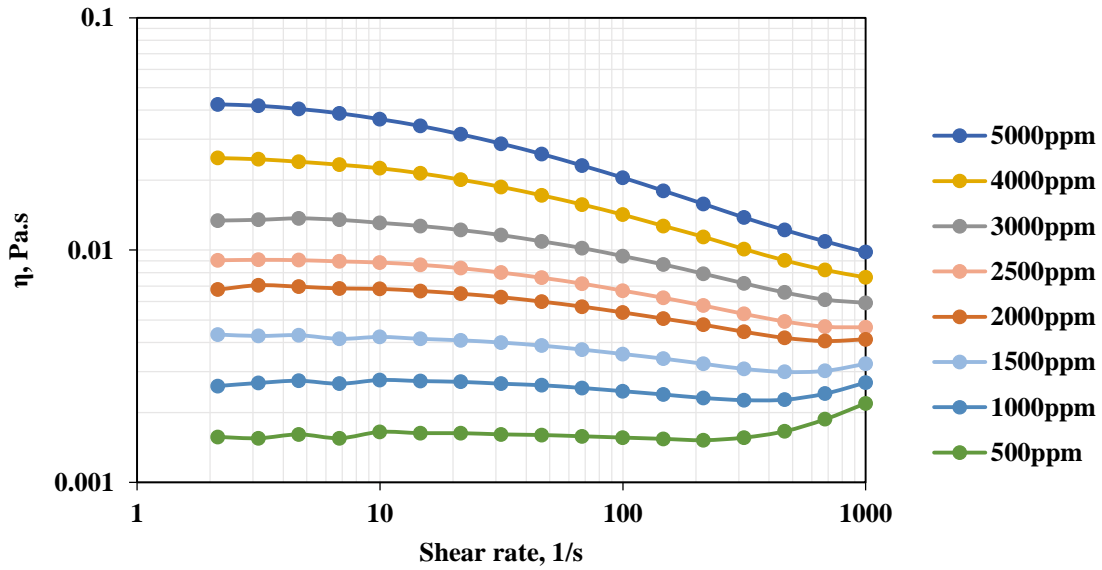


Figure 3-1. Dynamic viscosity of Flopaam 5115 BPM as a function of the shear rate at different concentrations at $T = 25^\circ\text{C}$

The viscosity data obtained for the other polymers are displayed in Appendix.

As expected, whatever the polymer, the plateau viscosity is seen to increase as polymer concentration increases and the shear-thinning behavior is more and more pronounced. Furthermore, the critical shear rate, characterizing the crossover of the two asymptotic regimes (Newtonian and pseudoplastic), is a decreasing function of polymer concentration.

As usually done the viscosity at the Newtonian plateau is represented versus concentration for each polymer in a log-log plot. Figure 3-2 shows these plots for the four considered polymers.

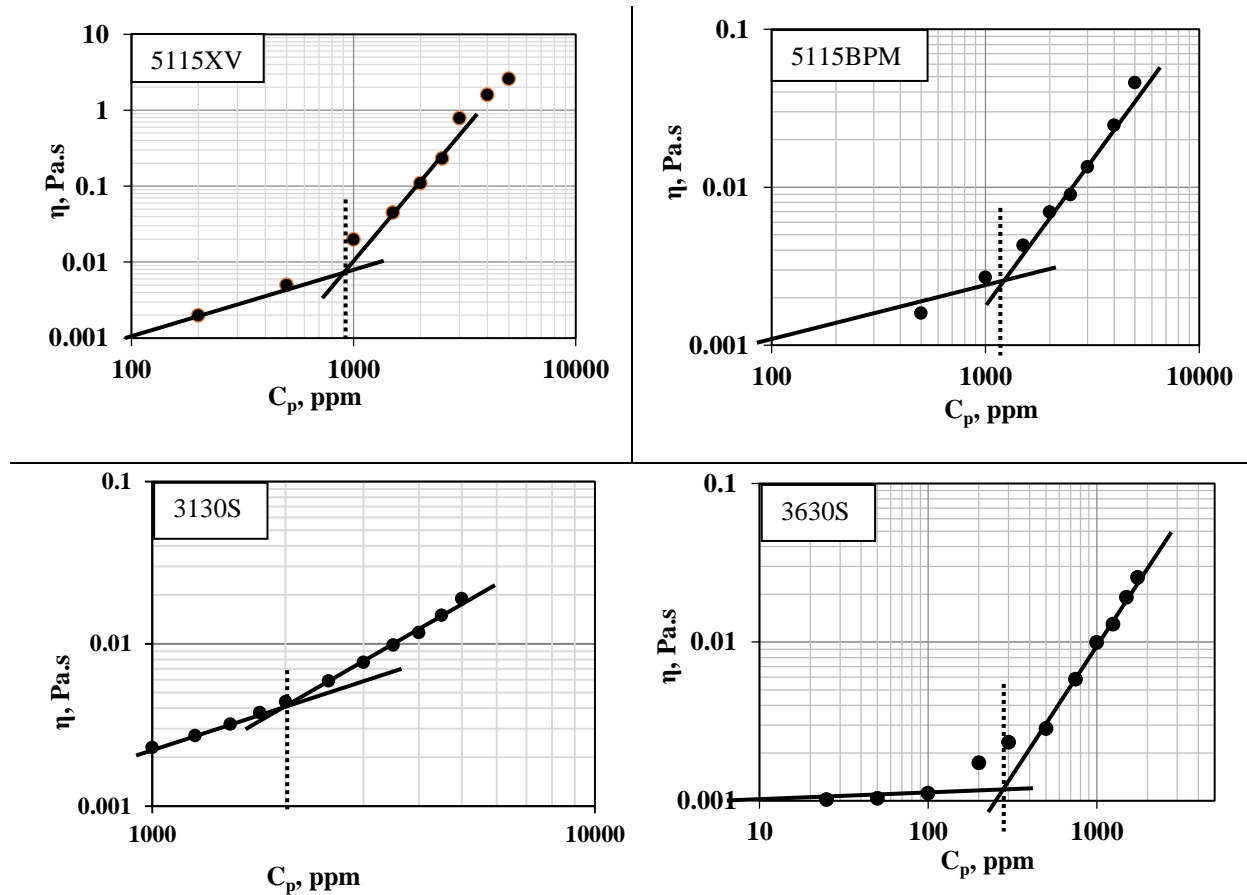


Figure 3-2. Viscosity of polymers at Newtonian plateau as a function of concentration. Solid line: power-law fits to dilute and semi-dilute regimes. Dashed line: the overlap concentrations

As it may be seen, two regimes may be distinguished in investigated concentration range following power-law behavior. At low concentrations, the regime is dilute and η is linear in C_p . At high concentrations, the solution becomes semi-dilute and η is a more rapid function of C_p . The crossover between these regimes corresponds to the unentangled overlap concentration C^* . The overlap concentration hence determined for each polymer is given in table 3-3.

Another way to estimate C^* is to determine first the intrinsic viscosity at zero shear rate $[\eta]_0$. So using viscosity data we plot the relative specific viscosity in the plateau regime, $\frac{\eta_r - 1}{C_p}$, versus concentration, and $[\eta]_0$ is given as the interception with ordinate axis when $C_p \rightarrow 0$ (see Eq. 1-48).

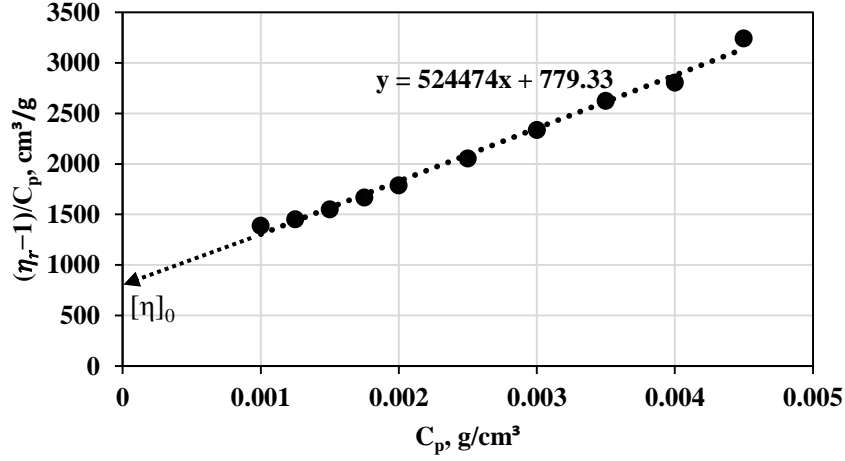


Figure 3-3. Relative specific viscosity, $\frac{\eta_r - 1}{C_p}$, vs concentration of polymer 3130S

The intrinsic viscosities for each polymer are determined that way and presented in table 3-2. The overlap concentration C^* can be estimated since it is theoretically predicted that $C^*[\eta]_0 \approx 0.77$. So, C^* hence determined are given in table 3-2.

	3630S	3130S	5115XV	5115BPM
$[\eta]_0$, cm³/g	2800	780	—	660
$C^* \approx 0.77/[\eta]_0$, ppm	275	987	—	1166
C^* from Figure 3-2, ppm	270	2000	900	1100

Table 3-2. The intrinsic viscosity and overlap concentration of each polymer

The ratio of $[\eta]_0$ for the polymers 3130S and 3630S is $\frac{780}{2800} \approx 0.28$. The ratio of the $[\eta]_0$ using the Mark-Houwink equation (Eq. 1-49), $[\eta]_0 = K' M_w^a$, where K' has the same value for the polymers with the same chemical structure and composition, and a is equal to 0.8 for good solvent. Hence,

$$\frac{[\eta]_0^{3130S}}{[\eta]_0^{3630S}} = \left(\frac{M_w^{3130S}}{M_w^{3630S}} \right)^{0.8} \approx 0.23.$$

It means that experimental and theoretical $[\eta]_0$ values, calculated using Mark-Houwink equation, are of the same magnitude.

When we plotted the relative plateau viscosity versus $C_p[\eta]_0$, known as overlap parameter or Simha parameter, for polymers 3630S and 3130S, we found that all the data lies on a master curve. This was expected since these polymers are of same chemical composition and structure and differs only by their molecular weight. Moreover, data are well fitted by the Huggins model (Eq. 1-47) and the best fit is obtained for a Huggins constant value $k'=0.8$. The Huggins constant value here is higher than expected since for linear polymers in good solvent this value should be in range of 0.3 to 0.5. However, its value is very sensitive to the accuracy of measurement of η at low concentration.

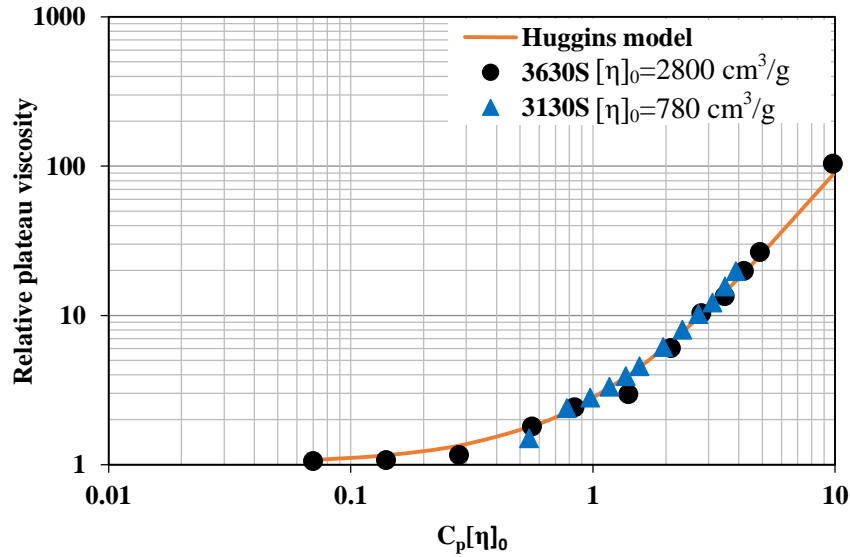


Figure 3-4. Relative plateau viscosity of polymers 3630S and 3130S at various concentrations versus $C_p[\eta]_0$ and fitting Huggins model

Later we will be concerned by solution of different polymers having the same viscosity, so this curve will be used to pre-determine the polymer concentration necessary to get such a viscosity value.

3.3 Characterization of porous media

Porous media (PM) are characterized by measuring their porosity, pore volume (PV), permeability, and checking their homogeneity.

3.3.1 Porosity, pore volume and homogeneity of PM

The porosity and the pore volume are obtained by performing a dispersion test that consists in determining the breakthrough curve after injection of SSW containing KI (250ppm). The dispersion test also provides information on the homogeneity of the PM through the curve symmetry and serves as a reference for the rest of the experiment. The pore volume (PV) is determined by the abscissa value so that areas below and above the curve are equals. The porosity is then calculated by dividing PV by the total volume of the core. When the sample is homogeneous the curve is symmetrical and the PV value corresponds to a C/C_0 of 0.5 when Péclet number, Pe , is low enough. As we can see, it may be stated that Bentheimer samples are homogeneous. It is worth noting that the Pe here is approximately 3.24.

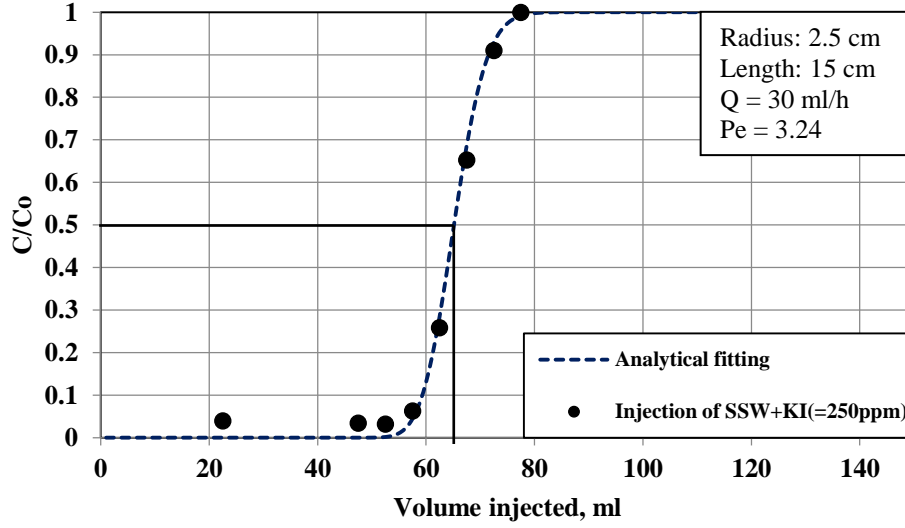


Figure 3-5. Dispersion test carried out on a sample of Bentheimer

We fit the curve using the complementary error function that we discussed in Chapter I which is

$$c(x, t) = \frac{c_0}{2} \left[\operatorname{erfc} \left(\frac{x - \bar{v}t}{2\sqrt{D_x t}} \right) \right] \quad \text{Eq. 3-1}$$

where x is the length of the core, \bar{v} is the Darcy velocity, t is the time and D_x is the dispersion coefficient.

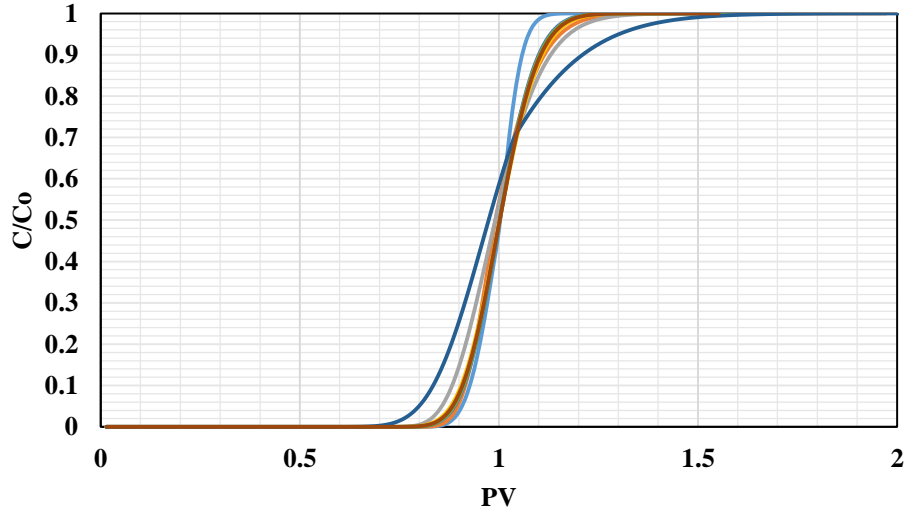


Figure 3-6. The dispersion curves of every Bentheimer sample

In Figure 3-6 we gathered the dispersion curves every Bentheimer used in this work. We would like to remark that few samples (purple curve for example) might be slightly heterogeneous but it is negligibly low.

3.3.2 Permeability

Measuring pressure drops during the injection of brine at different flow rates allows us to calculate the permeability of porous media using Darcy's law. Figure 3-7 shows the raw data of time variation of pressure drop at various injected flow rates for Bentheimer. These pressure drops are measured between pressure taps as indicated in the insert (Figure 3-7).

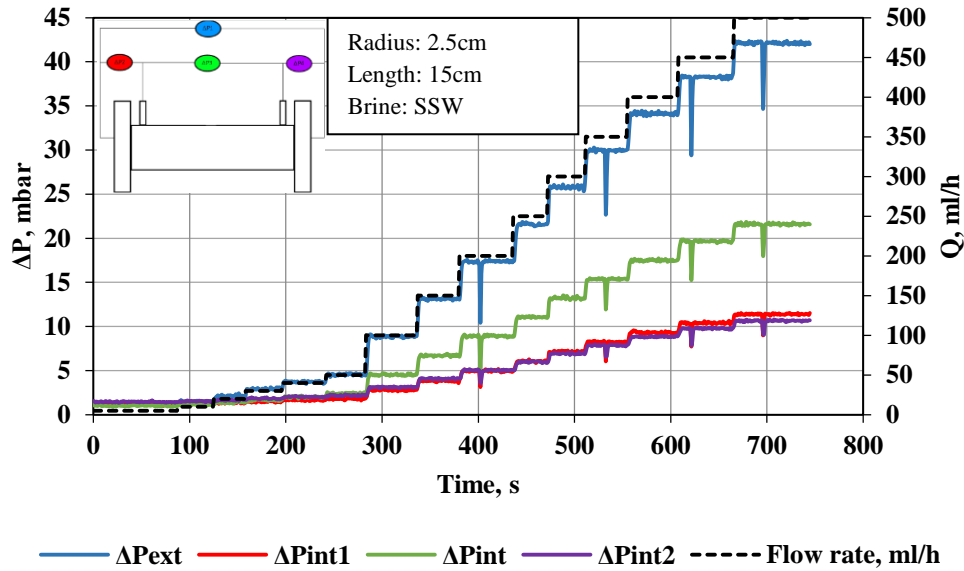


Figure 3-7. Permeability measurement of Bentheimer sample. Evaluation of pressure for different flow rates

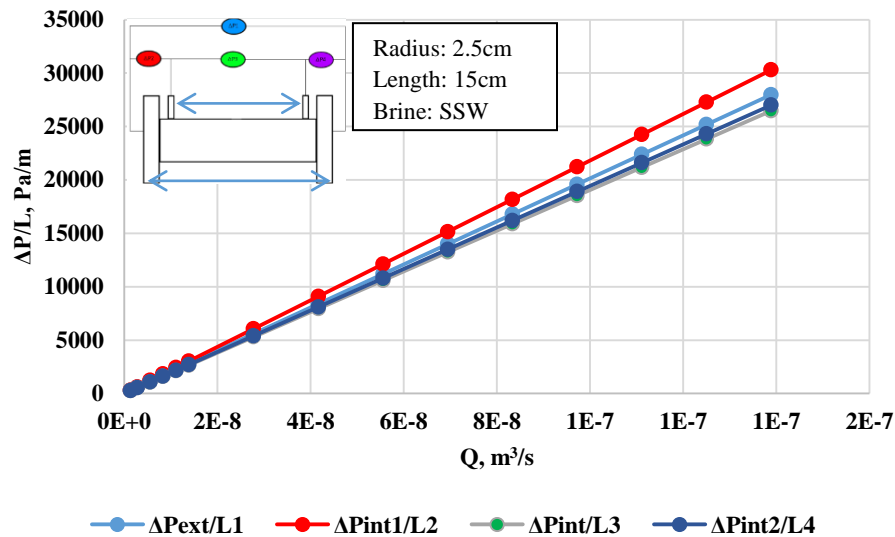


Figure 3-8. Pressure gradients as a function of flow rates for Bentheimer core

The graphical representation of the values of the pressure gradients ($\Delta P/L$) as a function of the flow rate (Q) shows a linear relationship (Figure 3-7) makes it possible to obtain the absolute permeability using Darcy's law knowing the dynamic viscosity of brine. L is the distance between the involved taps.

The four measured pressure gradients are also used to assess the homogeneity of the PM. We note that the permeability at the entrance zone is always slightly higher than in the other zones probably because of the presence of metallic plates at the inlet and outlet of the PM causing the overpressure therein. Therefore, for the rest of the study, we will take the value of the intermediate pressure (green) for the calculation of the permeability.

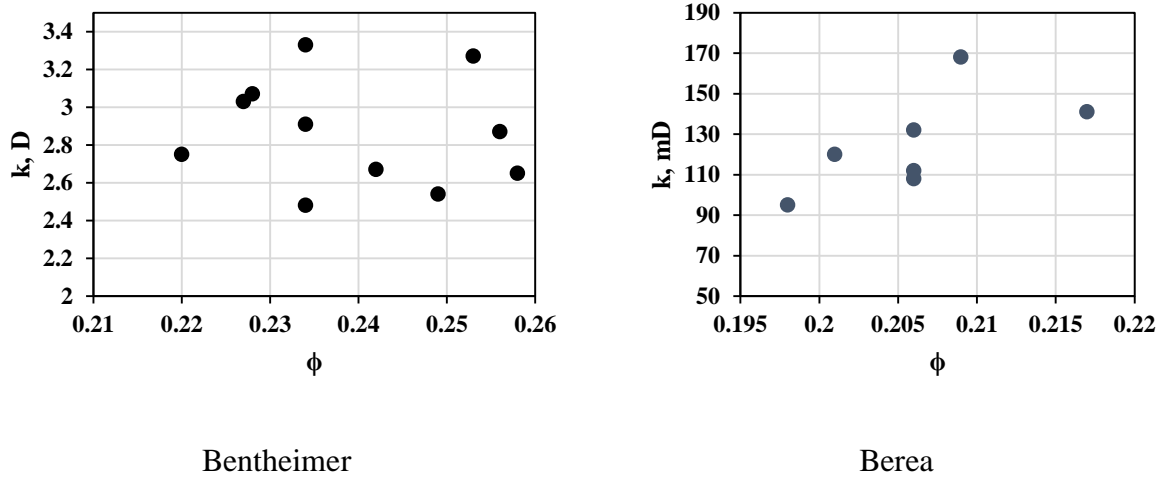


Figure 3-9. Permeability vs porosity of Bentheimer and Berea

All the results of permeability and porosity values obtained for Bentheimer and Berea are gathered in Figure 3-9. The results show that the porosity and permeability vary from one sample to another. Permeability of Bentheimer cores ranges from 2.48D to 3.33D because of using different batches that were ordered separately from Kocurek Industry. Concerning Berea cores, their permeabilities range more widely from 95mD up to 170mD. The porosity of Bentheimer and Berea are, however, similar. In all cases, these results are in agreement with the porosity and permeability value reported in the literature [Peksa et al., 2015]. The repeatability of the experimental results for the characterization of porous media is very satisfactory.

For complete characterization of porous media, we have been provided pore size distribution data from Shell, measured by mercury injection capillary pressure (MICP). The result, which represents the distribution of the pore throat sizes, is shown in Figure 3-10. Most of the pores have a size of approximately 35 microns for the Bentheimer and 15 microns for Berea. However, we see that Berea have a significant part of pores that have very small size.

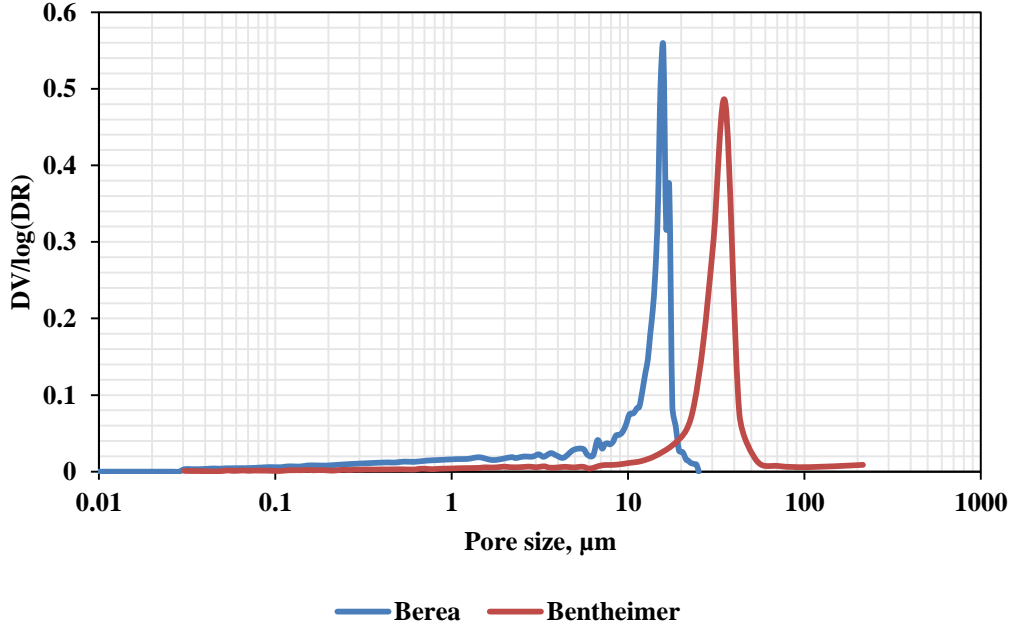


Figure 3-10. Pore size distributions for Bentheimer and Berea sandstones, determined by mercury porosimetry

After characterizing both the PM and polymer solutions, we investigate polymer retention under monophasic conditions before considering the polymer retention under diphasic conditions.

3.4 Monophasic experiments

Here we present results obtained from the single-phase flow of polymer solutions in Bentheimer and Berea. We have studied the retention of the polymer at various concentrations using various polymer types. Besides, we will focus on the impact of such retention on mobility reduction and permeability reduction.

3.4.1 Polymer flooding

So, after saturation with brine and characterization of the PM sample, the polymer solution is injected under a controlled temperature $T = 25^\circ\text{C}$ at an imposed flow rate of 10ml/h (2ft/day) corresponding to an average shear rate of 2.5 s^{-1} , which was calculated using the formula:

$$\dot{\gamma} = 4\beta v \sqrt{\frac{\phi}{8k}} \quad \text{Eq. 3-2}$$

where v is the velocity of the fluid, ϕ and k are the porosity and permeability of the PM, and β is the correction factor that depends on PM structure and was taken here equal to 1.

b) TOC measurement

After dispersion test, we inject a polymer solution of a given concentration at $Q=10\text{ml/h}$ and the injection is continued until we recover the injected polymer concentration at PM outlet.

The effluents are collected using the fraction collector and their polymer concentration is determined by measuring the nitrogen (TN) and carbon (TC) concentration using the beforehand established calibration curves (Figure 3-11).

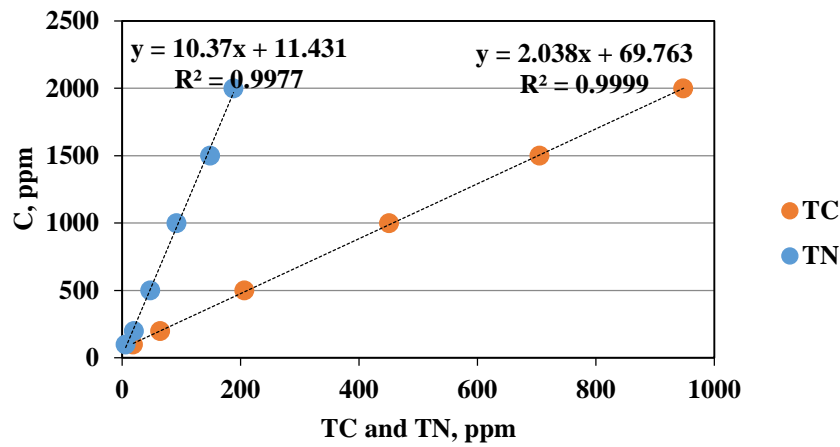


Figure 3-11. Calibration curve giving concentration of polymer 5115BPM versus concentration of carbon and nitrogen

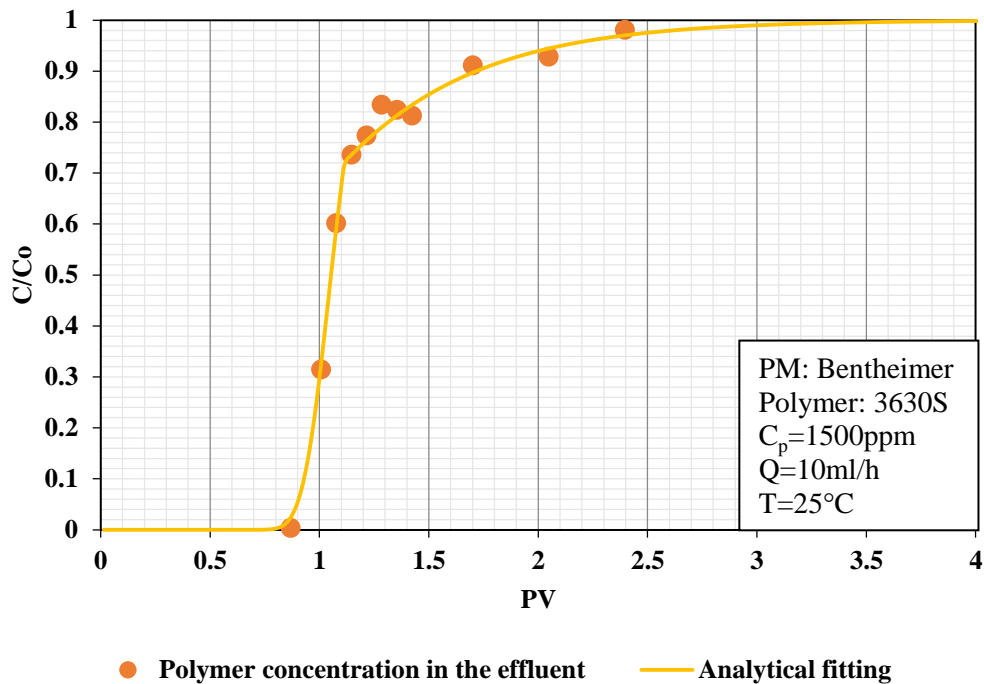


Figure 3-12. The break-through curve of first polymer flooding and its analytical fitting

In Figure 3-12, we present the typical data that obtain during polymer flooding by measuring of concentration of carbon and nitrogen in TOC.

c) Pressure drop

The pressure drop was measured during the injection of fluids by several pressure taps. Here we show the typical data obtained during polymer injection in the case of an experiment

performed for the Bentheimer-3630S system at $C_p=1500\text{ppm}$ and $Q=10\text{ml/h}$ (Figure 3-13). From the slope of the curve (blue), we can see the propagation of the polymer through porous media. When the polymer front reaches the pressure taps in the middle of the PM the pressure starts increasing (green and purple). The pressure drop stabilizes and becomes constant when the polymer front reaches the outlet of the PM. The delay between each curve is due to the distance between the pressure taps. As we can see the red and purple curves stabilized at the same value because these curves show the pressure drop in the inlet and outlet of the PM with the same length between the pressure taps.

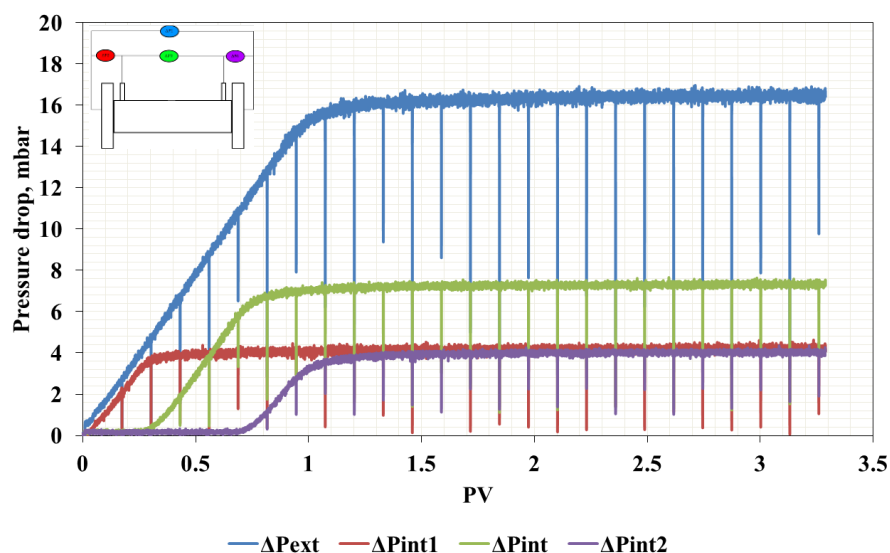


Figure 3-13. The pressure drop data during polymer injection; Bentheimer and 3630S at $C_p=1500\text{ppm}$, $Q=10\text{ml/h}$

3.4.2 Mobility reduction

After polymer flooding we perform the measurement of pressure drop at various flow rate to estimate the mobility reduction (RM).

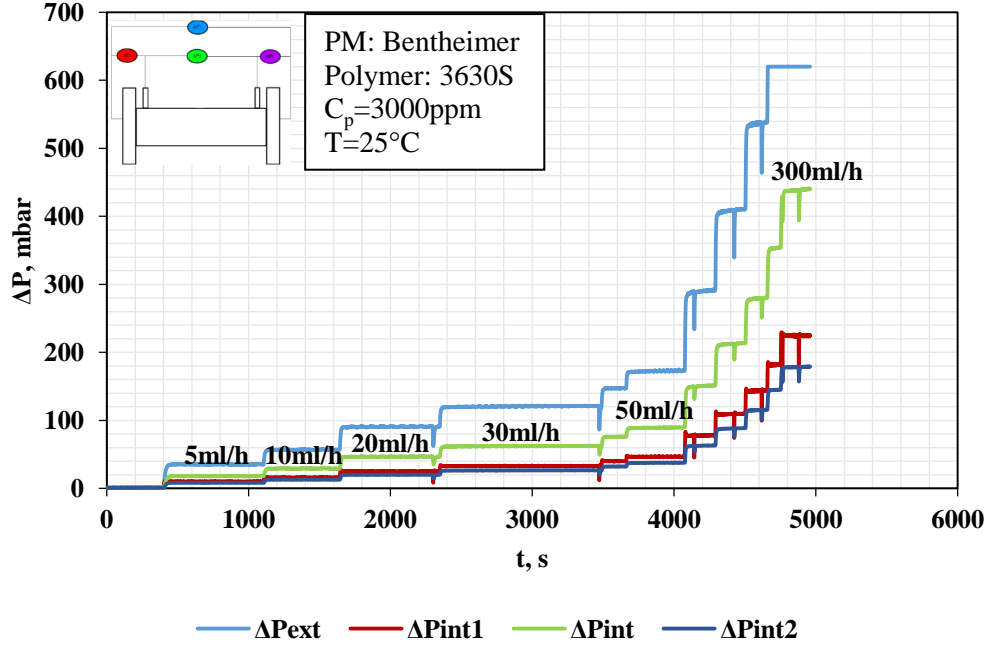


Figure 3-14. Pressure drop during polymer injection at various flow rates in a range of 5 to 300ml/h to estimate the RM

In Figure 3-14, we present the typical pressure data obtained during polymer flooding at various flow rates, in this particular case we injected at flow rates from 5ml/h to 300ml/h. We increased the flow rate when the pressure drop was stabilized. This data further is used to estimate the RM by

$$RM = \frac{k_w/\eta_w}{k_p/\eta_p} = \frac{\Delta P_p}{\Delta P_w} \quad \text{Eq. 3-3}$$

where k , η and ΔP are the permeability, viscosity and pressure drop of respective injected fluid, $\langle w \rangle$ and $\langle p \rangle$ are the water and polymer. Then we can plot this data as a function of shear rate, Figure 3-15.

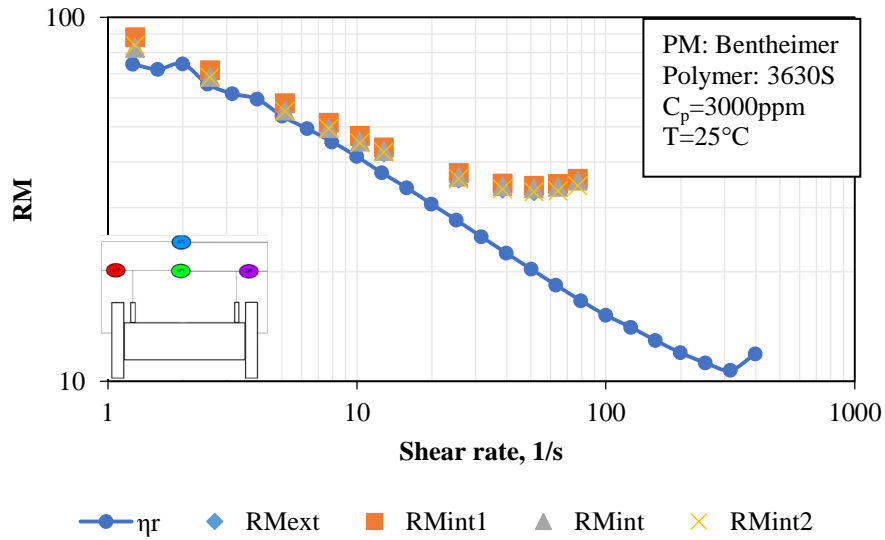


Figure 3-15. Mobility reduction and relative viscosity versus shear rate

We put the RM data in comparison with viscosity of the polymer in the bulk. While η_r presents a plateau followed by a shear-thinning regime only, RM presents a shear-thickening regime at high shear rates (starting at $\dot{\gamma}=33\text{s}^{-1}$), because the flow structure in the PM has an extensional component of velocity rate tensor $\dot{\epsilon}$. When such $\dot{\epsilon}$ become important the elongation of flowing and adsorbed macromolecules comes to play, macromolecules uncoiled and total friction and pressure loss increases.

We have measured the RM value for every experiment. In Figure 3-16, we present the RM value of the Bentheimer-3630S system at $Q=10\text{ml/h}$ and the η_r of 3630S in a bulk solution at $\dot{\gamma}=2.5\text{s}^{-1}$.

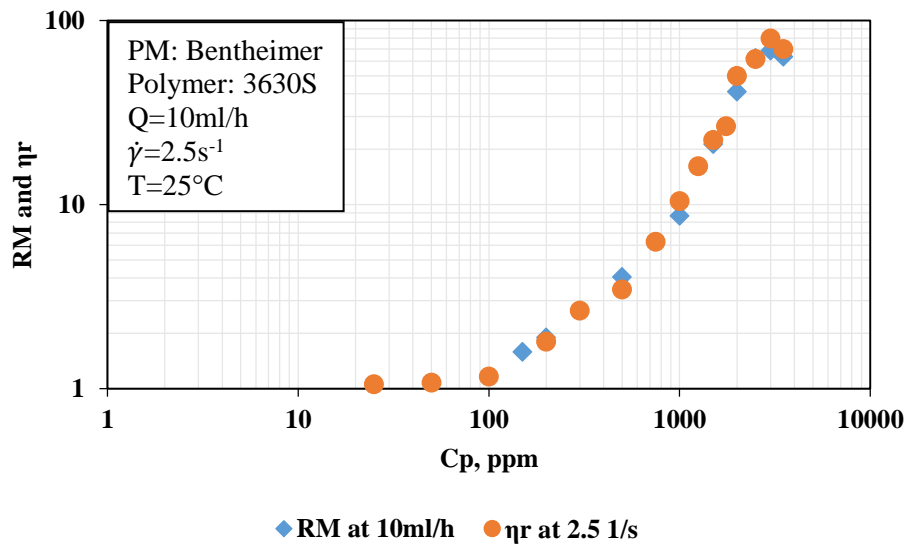


Figure 3-16. The RM value of polymer 3630S in Bentheimer and η_r of 3630S in bulk solution

3.4.3 Brine flush

After finishing the first polymer flooding and measurement of RM we flush the PM with brine to remove all free polymer molecules. We flush the PM with brine at the same flow rate as polymer flooding at $Q=10\text{ml/h}$. While injecting brine we measure and record the pressure drop along the core and collect the effluents by the fraction collector. We inject the brine till we have only brine in the effluent. For that, we perform measurement by TOC and check the concentration and, stop the brine flushing when polymer concentration is null. The data obtained here is similar to the data during the polymer flooding process: pressure drop (Figure 3-17) and TOC measurements. But usually, we measure the last few test tubes with effluents to check that we have only brine in the outlet.

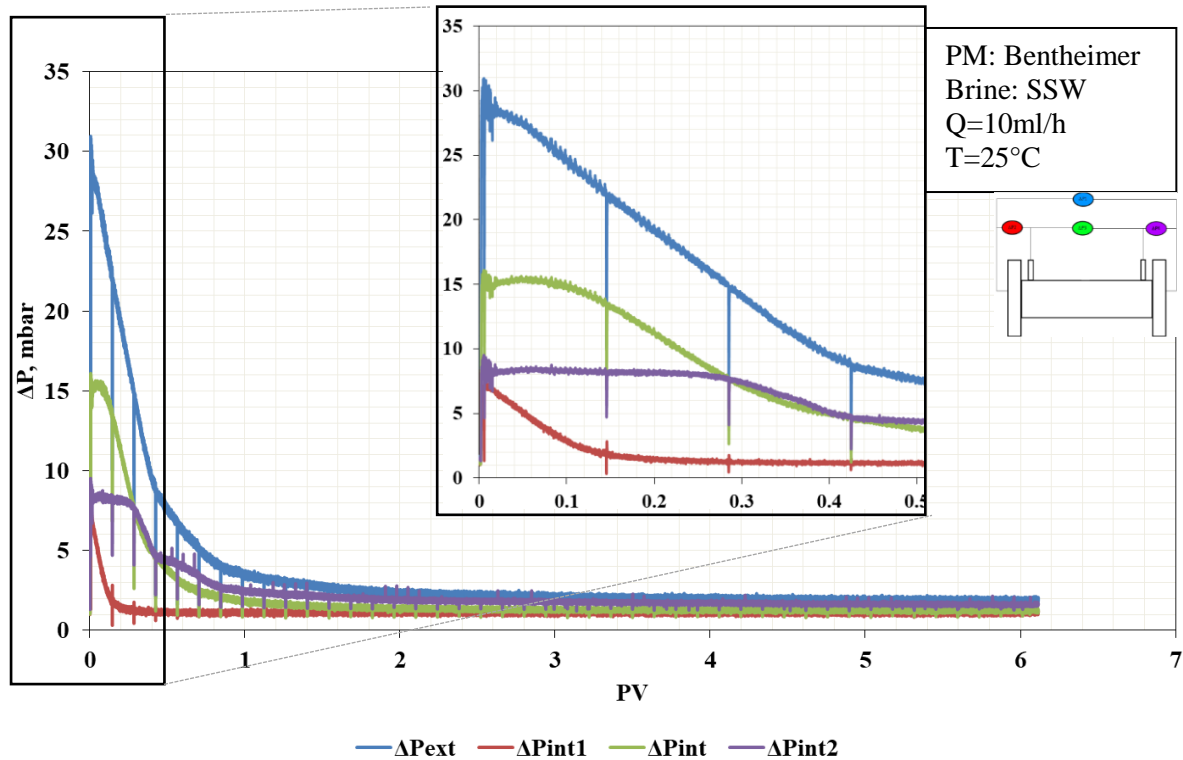


Figure 3-17. Pressure drop data during brine flush, Bentheimer-3630S

3.4.4 Permeability reduction

The brine flush is followed by injection of brine at various flow rate and measuring the pressure drop to estimate the permeability reduction, R_k .

$$R_k = \frac{\Delta P_{w2}}{\Delta P_{w1}} \quad \text{Eq. 3-4}$$

where ΔP_{w1} and ΔP_{w2} are the pressure drop during waterflooding before and after polymer retention respectively. It should be mentioned that only limited data of R_k were accessible due to the lack of equipment precision at low shear rates.

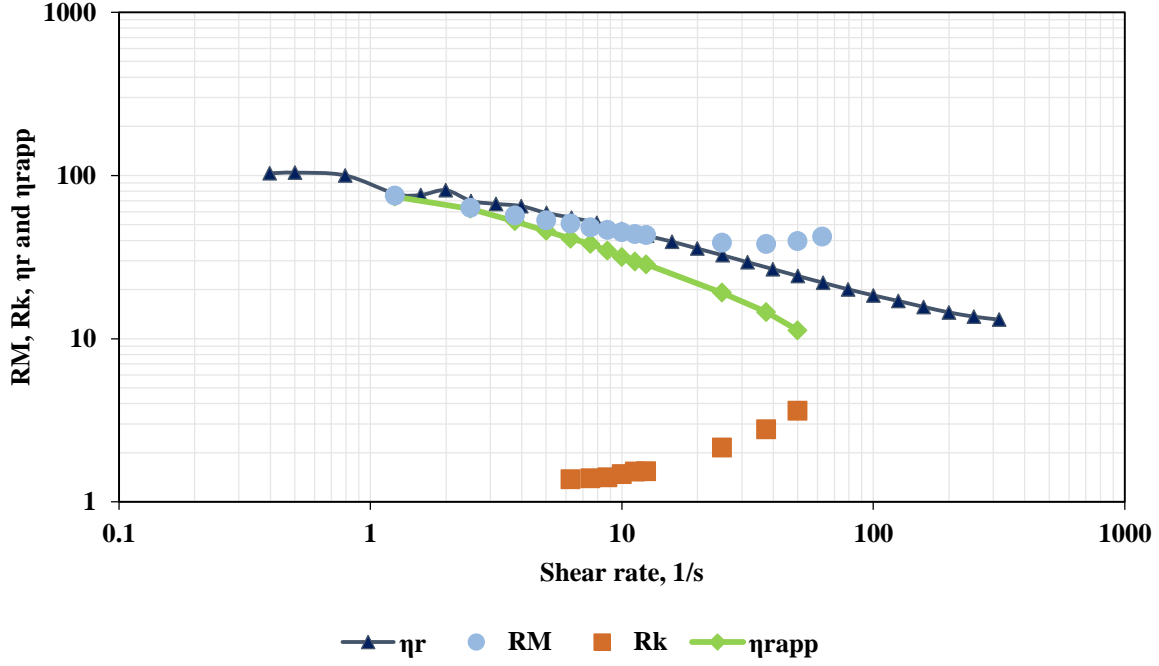


Figure 3-18. Evolution of RM and R_k , relative viscosity, η_r , and relative apparent viscosity, η_{rapp} as a function of shear rate

Figure 3-18 shows the typical result of R_k and RM that we obtained for each experiment together with the relative viscosity, η_r , measured by viscometry. In the non-extensional regime, the relative apparent viscosity that is the ratio RM/R_k is a bit lower than η_r . In literature, this behavior is attributed to depletion in the vicinity of the solid wall where polymer concentration is lower than the concentration in the bulk. This steric exclusion is also reported to happen even when an adsorbed layer exists. In other respects, we used R_k value to estimate the hydrodynamic thickness of adsorbed layer, e_H , using Poiseuille equation and assuming that porous medium is a bundle of capillary tubes of the same radius R_p as we show in Chapter I – §1.2.1. Giving $e_H = R_p(1 - R_k^{-0.25})$ where $R_p = \sqrt{\frac{8k}{\phi}}$. For the case considered in Figure 3-12, for which ϕ and k are respectively 0.24 and 2.67D, and taking $R_k=1.3$ in the plateau zone we obtain $e_H=0.5\mu\text{m}$. Moreover, if we consider that a monolayer of polymer molecules is built on solid surface; such thickness should be comparable to the radius of gyration of macromolecules in the bulk. Since it should be sensitive to the size of the loops of adsorbed chains, so in the present core we found that $e_H/R_G \approx 2.7$ (Table 3-4), where R_G is the gyration radius that is calculated using equation 1-50 (see table 3-3). All the values e_H obtained for each concentration are given in table 3-5.

	3630S	3130S	5115BPM
$R_G, \mu\text{m}$ ($R_G^3 \phi' = [\eta]_0 M_w$ $\phi' = 3.66 \times 10^{24} \text{mol}^{-1}$)	0.244	0.086	0.081

Table 3-3. Gyration radius of each polymer

C_p , ppm	e_H , μm	e_H/R_G
300	0.8	3.3
1500	0.43	1.7
2000	0.95	3.9
2500	0.95	3.9
3000	0.39	1.6
3500	0.49	2

Table 3-4. Effective hydrodynamic thickness of adsorbed layer and the ratio of e_H/R_G of polymer 3630S in Bentheimer; the average $e_H/R_G \approx 2.7$

The fact that e_H is higher than R_G may be due to the modelling of the PM as a bundle of capillaries of the same Radius and does not take into account such a size distribution. Sometimes such apparent discrepancy is attributed to a multilayer of adsorbed polymer and/or to the other sources of polymer retention.

3.4.5 Second polymer flooding

Having characterized PM after polymer retention, we performed a second polymer injection to estimate the IPV and quantify the retained amount of polymer giving a new break-through curve for the non-reactive polymer. The hatched area in Figure 3-19 is used to calculate the final relative amount of retained polymer.

$$\Gamma = \frac{m_{polymer}}{m_{rock}} \quad \text{Eq. 3-5}$$

with

$$m_{polymer} = Area \times Volume \times Concentration \text{ of polymer} \quad \text{Eq. 3-6}$$

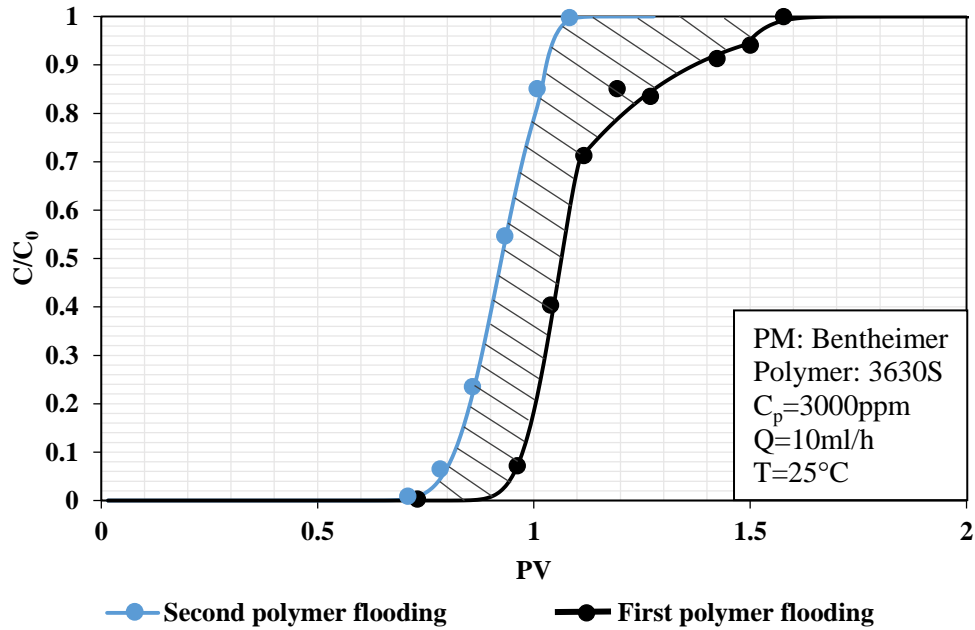


Figure 3-19. Breakthrough curves of first and second polymer flooding

At the beginning we have perfectly parallel curves shifted because of retention of polymer and then the increase of polymer concentration becomes slower and slower. Such a shape may be interpreted as follows: at the beginning, a large solid surface is available for polymer adsorption and the breakthrough curve therein is parallel to the dispersion curve. Later, as adsorption progresses less free surface is now available and adsorption is mitigated by a blocking phenomenon that increases as adsorption increases. So when the surface coverage is significant, a few colliding macromolecules with solid surface do effectively result in its attachment before such a probability goes to zero. In general, when the polymer is polydisperse, small macromolecules desorb and are replaced by macromolecules of high molecular weight that have more attachment energy.

Moreover, the difference between the second polymer flooding and dispersion curve (the hatched area in Figure 3-20) is interpreted as the IPV due to straining. Indeed, both flooding is non-reactive and therefore the shift between the two curves is a result of the different sizes between the polymer chains and the KI ions. So the curves are parallel, but the straining exclusion is, however, present only in the case of second polymer flooding.

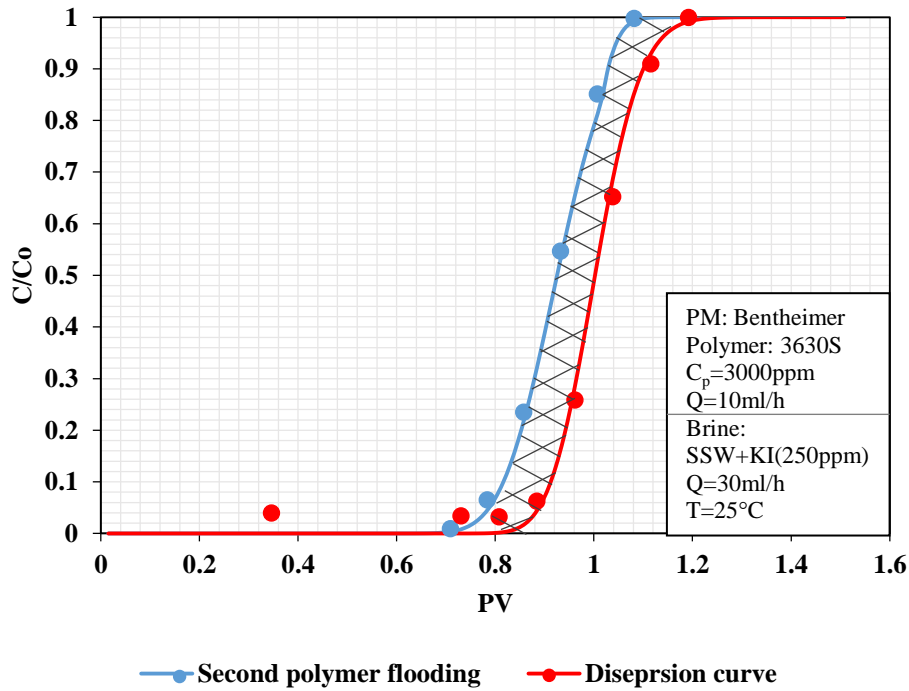


Figure 3-20. Breakthrough curves of second polymer flooding and KI dispersion

All these data presents the typical results for monophasic experiments. Overall, we performed single-phase experiments with four types of polymer and the two types of PM. In these experiments, we investigate the effect of concentration of polymer, the effect of permeability of PM, and the effect of sulfonation degree on adsorption of polymer in PM. However, the influence of flow rate during the step of polymer injection was not considered.

3.4.6 The retention of polymer

Here we discuss the retention data obtained for monophasic experiments with different polymers and PM. We organized this part by the different parameters that we studied to see the trend of retention.

(i) Effect of concentration

The effect of polymer concentration on Γ was observed in experiments performed with polymer 3630S in Bentheimer and polymer 3130S in Berea.

We have investigated the concentration influence for polymer 3630S in Bentheimer in a range of $C_p=150-5000\text{ppm}$ that cover both dilute and semi-dilute regimes. We must recall that from the viscosity measurement of the polymer solution, we had established that the overlap concentration for 3630S is nearly equal to 270ppm. To show the impact of concentration on adsorption of polymer we have plotted in Figure 3-21 the ultimate value of Γ that was reached after injection of 3630S solutions versus the polymer concentration. We note a rapid increase of $\Gamma=f(C_p)$ at low polymer concentration followed by a damped regime where Γ increases more slowly. Indeed, the first regime should correspond to the dilute regime whereas the

second corresponds to the semi-dilute regime. In this figure, the C^* value is indicated by a vertical dashed line.

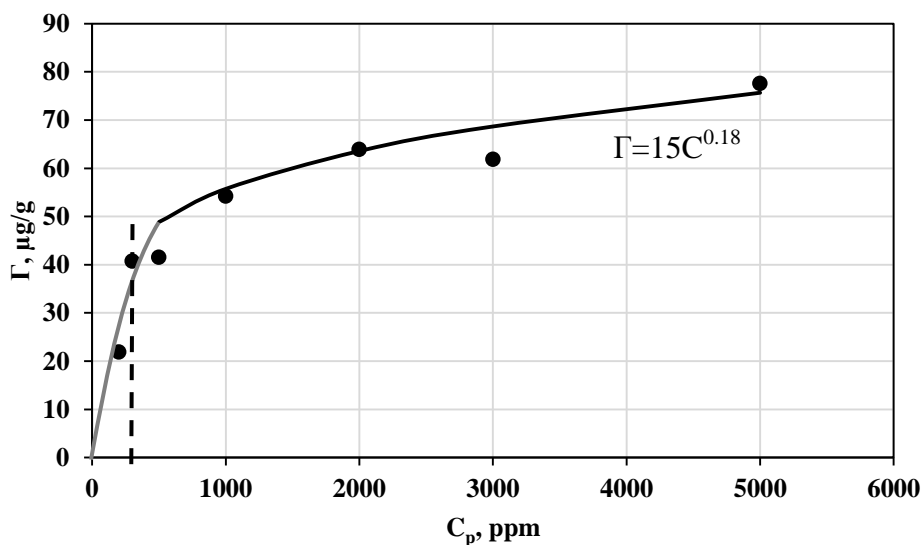
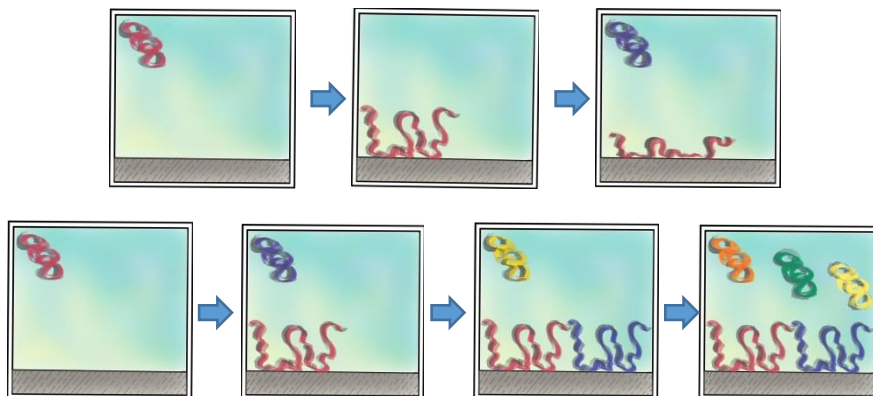


Figure 3-21. Retention of polymer 3630S in Bentheimer versus concentration and Freundlich fitting (black solid line)

In the dilute regime, the polymer chains are located well apart from each other so that when a macromolecule comes in contact with the solid surface it will attach and relax its conformation before a new macromolecule comes to adsorb in its neighbourhood (Figure 3-22a). With increasing concentration but still in the dilute regime, the distance between free moving macromolecules decreases, adsorption goes faster and a newly adsorbed macromolecule has now less time to completely relax before another one come to adsorb aside (Figure 3-22b). As a consequence, the amount of adsorbed polymer per unit surface increases with C_p .

(a) The adsorption mechanism of polymer chains in low concentration dilute regime



(b) The adsorption mechanism if concentration is higher but still in dilute regime

Figure 3-22. Sketch of polymer adsorption mechanism in dilute regime at low and high concentrations

In a semi-dilute regime, however, macromolecules are partly entangled and have only a very short time to relax when they adsorb, and therefore the amount of adsorbed polymer per unit surface increases in the same way as the characteristic size of macromolecule vary with C_p in that regime. This variation is predicted to be very weak as $C_p^{(v-1/2)/(3v-1)}$ (Colby, 2010), where $v=0.6$ for good solvent. This gives a scaling law as $C_p^{0.12}$ that is close to the trend law drawn on the figure as $C_p^{0.18}$.

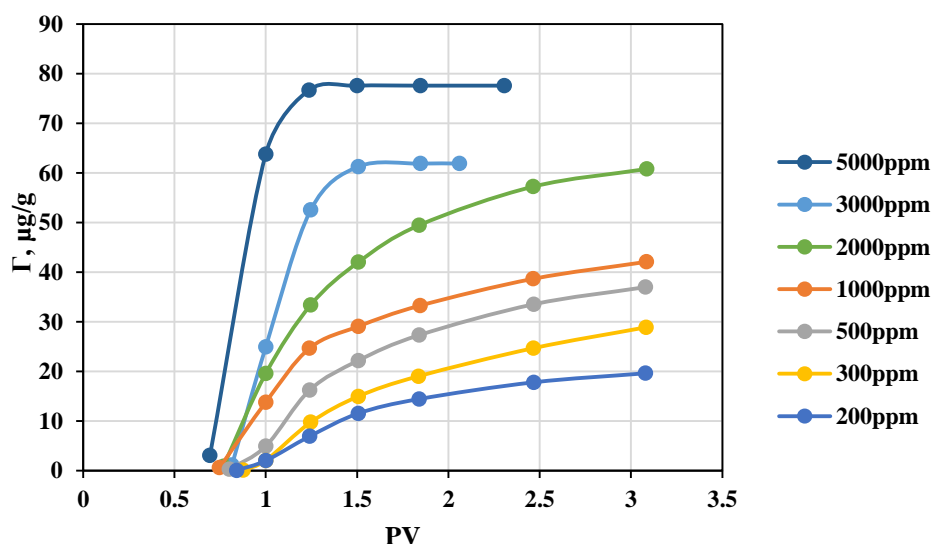


Figure 3-23. Adsorption kinetics of polymer 3630S in Bentheimer at various concentration as a function of injected Pore volume (PV)

In other respects, the polymer retention kinetics may be deduced from calculating the area between first and second polymer fronts over time. This was done for various polymer concentrations. Figure 3-23 shows the obtained results for polymer 3630S that give us an overall view of how fast the retention progresses depending on polymer concentration. As expected, this data shows an initial fast regime, where the polymer adsorbs fast since we are in the free surface conditions (clean bed conditions) when any contact between polymer molecules and solid surface results in adsorption with high probability. When time goes and after the surface coverage becomes significant, the probability of polymer to adsorb is lesser due to the decrease in the number of available adsorption sites. This is known as blocking phenomenon; later adsorption becomes too slow before it levels off when adsorption is over. The initial slope that gives the kinetic rate under clean bed conditions are plotted versus polymer concentration in Figure 3-24.

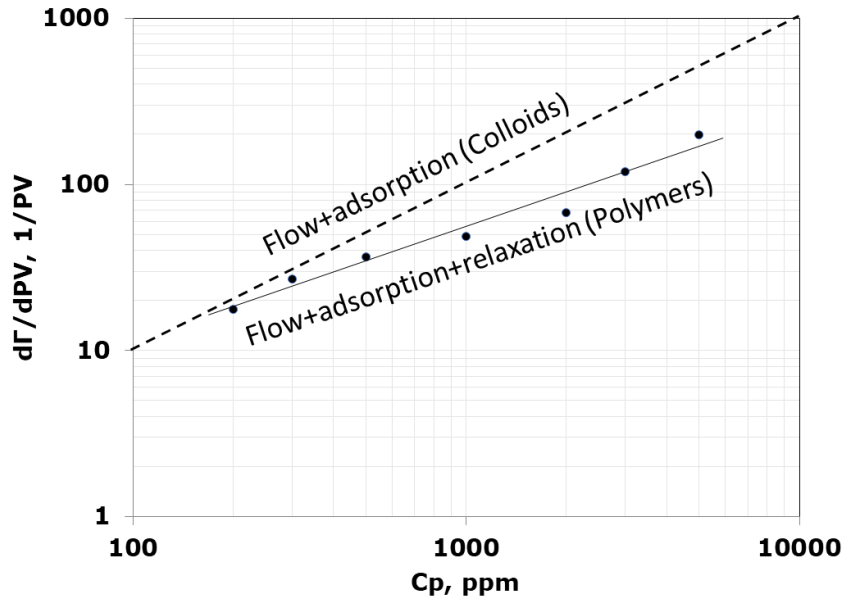


Figure 3-24. Adsorption rate, $d\Gamma/dPV$, versus concentration of polymer 3630S in Bentheimer in log-log scale and the typical adsorption kinetics of colloids(dashed line) versus concentration

From the theory of colloids deposition on a collector ; the flux of colloids toward the collector is predicted to depend on Péclet number Pe and colloids concentration C as the scaling law :

$$J \cong \left(\frac{D}{a}\right) C P_e^{1/3}$$

Where D is colloids diffusivity and a is particle size [Russel et al., 1991].

Adsorption kinetics increases with concentration (Figure 3-24). However, it is shown to follow a power law with an exponent that is slightly lower than unity. When collision efficiency is equal to 1, say that every event of particle/collector collision arises in particle deposition, deposition is then proportional to colloid concentration C . However, in the case of a polymer, the kinetics is shown to follow a power law with an exponent of 0.68 that is lower than unity. Such weaker dependency is because right after adsorption, macromolecules undergo a relaxation of their confirmation process that lengthen the adsorption time as is sketched here below.

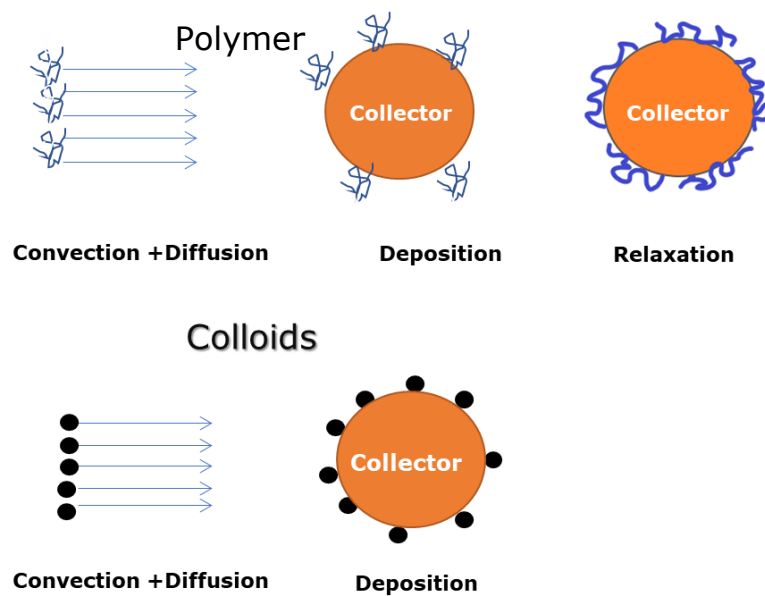


Figure 3-25. The difference between the colloids deposition and polymer adsorption on the surface of the collector

d) Effect of permeability

Berea and 3130S

To see the impact of permeability on retention of polymer first we conducted an experiment with polymer 3630S at a concentration of 300ppm in Berea core under the same flow conditions as before ($Q=10\text{ml/h}$). During this experiment, the polymer concentration in the effluent was null over a long period, and recorded pressure was continuously increasing, i.e. a sign of plugging. Plugging is a consequence of the existence of a population of pore throats which size is less than macromolecules size. Moreover, another contribution to such plugging is, following Zaitoun and Chauveteau (1998), also due to the bridging phenomenon. Bridging occurs at the entrance of small pore necks where the flow has a noticeable elongational component. Then elongated macromolecules may form a bridge at the pore throat entrance as sketched in Figure 3-26. In this sketch, the numbers from 1 to 6 represent the steps from the coil to elongation and at the end bridging between rock surfaces. In our opinion plugging is more likely due to size exclusion rather than to bridging given our experimental conditions. Anyway, and whatever the leading plugging mechanism, the core plug occurs when the fraction of such small pore throats are significant prohibiting polymer percolation through the PM.

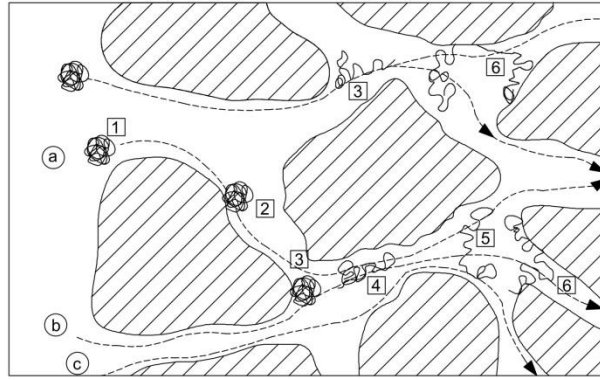


Figure 3-26. Sketch of polymer bridging [Zaitoun and Chauvteau, 1998]

Indeed, the examination of the pore throat size distribution of Berea (see Figure 3-10) shows a long tail of the smallest pore throats and therefore a population of very small pore throats is effectively present. This would be more graphically visible if the distribution is represented in terms of number density rather than by volume density.

After taking note of plugging in the case of the Berea-3630S system, the molecular weight of the polymer was decreased choosing polymer 3130S that have a molecular weight 7 times less. For that polymer, no plugging was observed and Γ was determined as before for polymer concentration ranging from 500 to 7000ppm that covers the same $C_p[\eta]_0$ range as for 3630S polymer in order again to scan both dilute and semi-dilute regimes. Obtained results of Γ over time and final Γ value versus concentration are shown in Figure 3-27 and 3-28 respectively. The trend of adsorption kinetics is the same as in the Bentheimer-3630S system, however, the final Γ value versus C_p is different from the Bentheimer-3630S system.

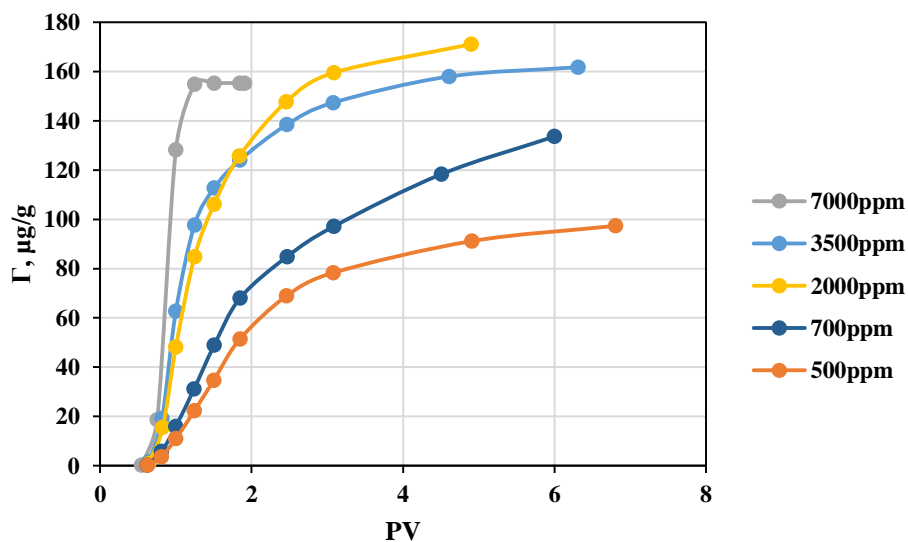


Figure 3-27. Adsorption kinetics of polymer 3130S in Berea at various concentrations

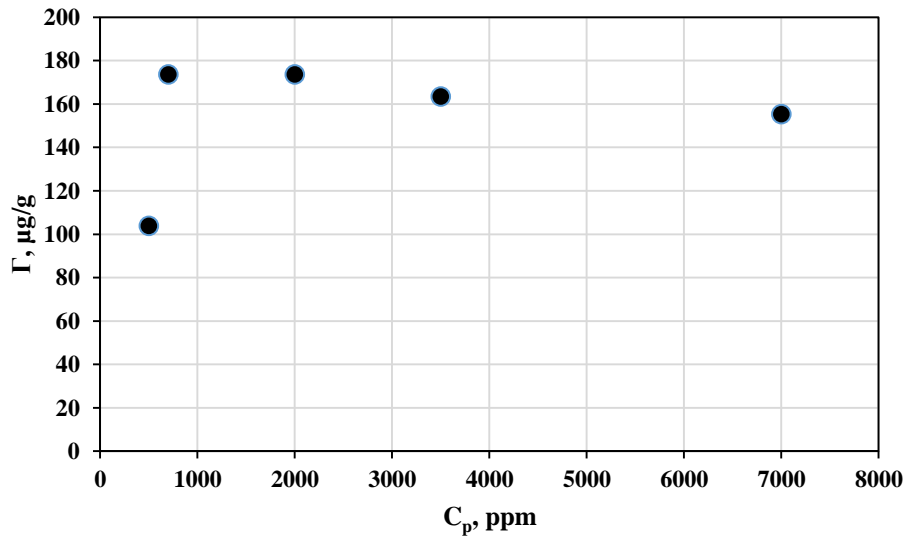


Figure 3-28. Retention of polymer 3130S in Berea at various concentration

We can first see that overall the quantity of retained polymer is significantly high in this case, up to $77\mu\text{g/g}$ in Bentheimer-3630S and up to $165\mu\text{g/g}$ in the Berea-3130S system. Second, in contrast to the Bentheimer-3630S system, retention is almost constant in the semi-dilute regime. In our opinion, the permeability of the PM should play an important role. We must recall that while Bentheimer cores have approximately the same permeability, Berea cores show permeability that varies from one core to the other by a factor of 2. So this may explain why after the expected increase of Γ in the dilute regime, the trend in the semi-dilute regime is somehow contradictory. It is worth noting that the slope of the curve for 7000ppm looks reasonable considering high concentration, but the value seems too low comparing the results obtained at concentrations 2000ppm and 3500ppm.

If we assume the polymer molecules as hard spheres adsorbing on a flat surface of the unit area as is illustrated in Figure 3-29 we can estimate the ratio of adsorbed amounts for polymers 3630S and 3130S. The sphere sizes represent the polymers that differ by molecular weight, hence by size: large spheres are the HPAM 3630S molecules and small ones are HPAM 3130S molecules. Bypassing the surface porosity is the same since it is independent of circle radius.

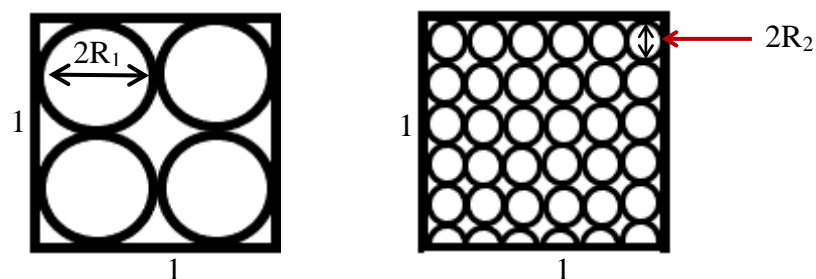


Figure 3-29. Sketch of coverage of the same surface with the polymer molecules of different size

For 3630S polymer, the number of molecules on the surface is equal to $\left(\frac{1}{2R_1}\right)^2$ and the mass of adsorbed polymer would be $\Gamma_1 = \left(\frac{1}{2R_1}\right)^2 * M_1$. Similarly, the adsorbed mass for 3130S polymer is $\Gamma_2 = \left(\frac{1}{2R_2}\right)^2 * M_2$. Then the ratio of adsorbed masses is $\left(\frac{R_1}{R_2}\right)^2 \frac{M_2}{M_1}$. If we recall that the radius of polymer is related to molecular mass as $R \sim M^\nu$ then the previous ratio is

$$\frac{\Gamma_2}{\Gamma_1} = \left(\frac{R_1}{R_2}\right)^2 \frac{M_2}{M_1} = \left(\frac{M_1}{M_2}\right)^{2\nu} \frac{M_2}{M_1} = \left(\frac{M_1}{M_2}\right)^{2\nu-1} = \left(\frac{19}{3}\right)^{0.2} \approx 1.44$$

Of course, the real surface coverage is much less than in the figure and does decreases from the « random sequential adsorption » value of 0.546 in a purely diffusional regime to lower values in the convection dominant regime. Anyways, considering that we are comparing systems Bentheimer-3630S and Berea-3130S the specific surface differs as well. According to the literature, the specific surface of Bentheimer and Berea is $0.45\text{m}^2/\text{g}$ and $0.8\text{-}1\text{m}^2/\text{g}$ respectively. To compare it with the retention value from experiments we need to multiply the value that we calculated above by the ratio of specific surfaces of the sandstones, then we get the value $\frac{\Gamma_2}{\Gamma_1} \times \frac{S_{sp2}}{S_{sp1}} = 3.2$. This value is the same magnitude as the experimental data at high concentrations $C_p[\eta]_0 = 2.8$ and 5.5 (Table 3-5).

$C_p[\eta]_0$	Γ_2/Γ_1
0.55	8
2.8	3
5.5	2.4

Table 3-5. The ratio of retention value for Bentheimer-3630S (1) and Berea-3130S (2) at various $C_p[\eta]_0$

Bentheimer and 3130S

We have chosen 3130S to avoid the injectivity problem in Berea as we said before. Therefore, we performed experiments with the same polymer, HPAM 3130S, in Bentheimer for comparison purposes.

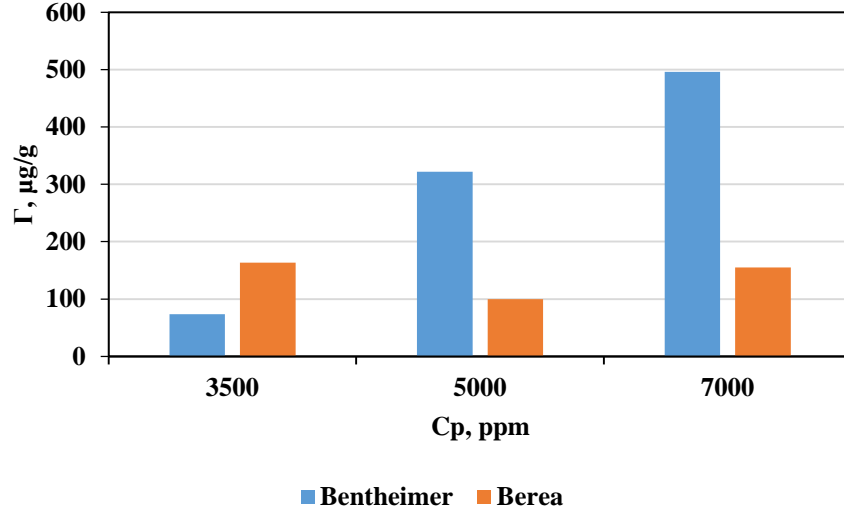


Figure 3-30. Retention of polymer 3130S at various concentration in Bentheimer and Berea

In the case of polymer injection in Bentheimer sandstone, we can see a drastic increase in retention value with concentration, but it is a less marked increase in the case of Berea. It is expected that the retention should increase with decreasing permeability. Because with decreasing permeability usually we observe an increase in the specific surface, hence, increasing adsorption sites per unit mass. We can show it using the simple capillary model as illustrated in Figure 3-30. The specific surface of capillary tubes can be calculated as

$$S_{sp} = 2N\pi R_p L$$

Where N is the number of capillary tubes,

$$N = \frac{A\phi}{\pi R_p^2}$$

then

$$S_{sp} = \frac{2\pi L A \phi}{R_p}$$

with

$$R_p = \sqrt{\frac{8k}{\phi}}$$

That calculation shows that the Berea sandstone should have 5 times more specific surface available for adsorption than Bentheimer.

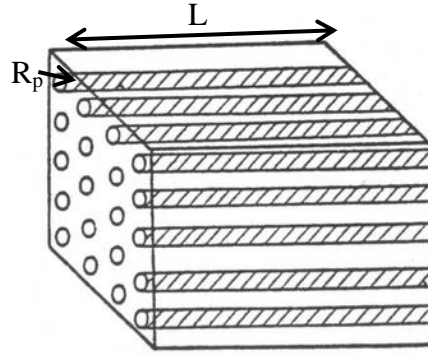


Figure 3-31. Sketch of capillary model with the capillary tubes of radius R_p and length L

We have made a theoretical correction to the retention data for IPV and S_{sp} , which is taken from the literature [Peksa et al., 2015; Churcher et al., 1991] using the equation:

$$\Gamma' = \frac{\Gamma}{1 - IPV} * S_{sp}$$

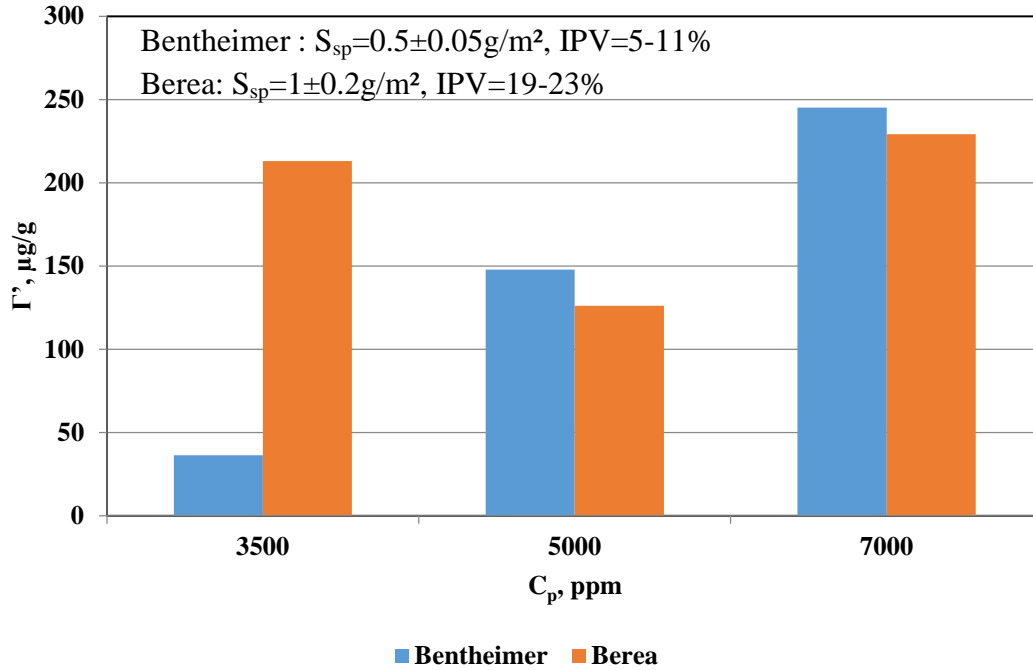


Figure 3-32. Corrected retention data of polymer 3130S in Bentheimer and Berea at concentrations 3500, 5000 and 7000ppm

However, the IPV and S_{sp} in Bentheimer are very small comparing to Berea cores that show the relevance of taking into account both specific surface and IPV when comparing retention in different PM. As we can see from Figure 3-32 the retention quantity for concentrations 5000 and 7000ppm are of the same magnitude, which proves the importance of specific surface and IPV on retention. Another parameter that has changed from one PM to another is the equivalent shear rate value 2.5s^{-1} for Bentheimer and 12.6s^{-1} for Berea. Indeed, the shear rate can change the way how the polymer chains flow through PM. At higher shear rates the polymer chains start disentangling and conforming parallel to the flow. This can explain the

low retention by the conformation of disentangled polymer, which can occupy much more adsorption sites than polymer coils. Hence we observe lower retention of the polymer.

e) Effect of sulfonation degree

In order to investigate the influence of polymer chemistry on the adsorption process, we performed experiments with polymers 5115XV and 5115BPM. To that end, the polymers 5115 have the same chemical composition with 15% of 2-Acrylamido-2-Methylpropane Sulfonic acid (ATBS) but different molecular weights (Table 2-3). The sulfonate group confers to the monomer a high degree of hydrophilicity and anionic character at a wide range of pH. Besides, ATBS is absorbing water readily and also imparts enhanced water absorption and transport characteristics to polymers.

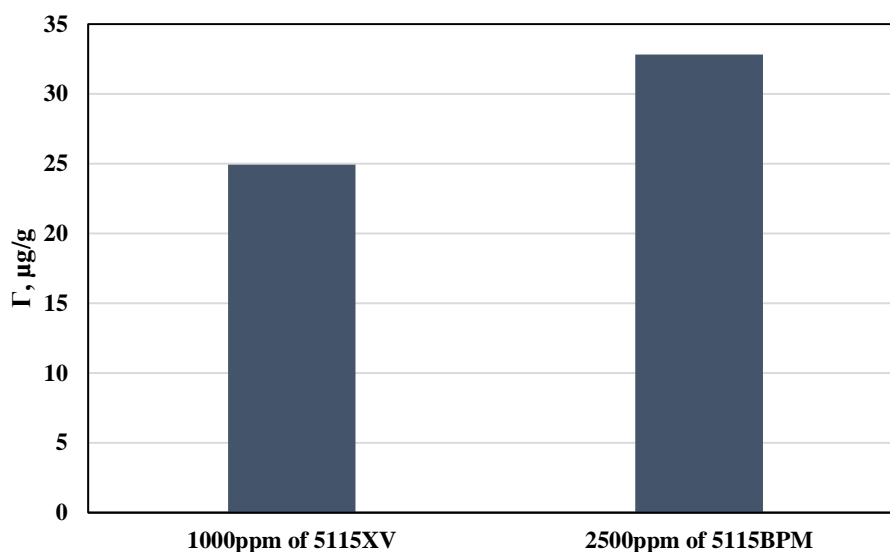


Figure 3-33. Retention of polymers 5115XV and 5115BPM at concentrations 1000ppm and 2500ppm that corresponds to viscosity around 10cP

The experiments with ATBS polymers were performed at fixed concentrations. Concentrations were chosen that way we could compare the single-phase experiments with the coming two-phase ones. For that, we have chosen a viscosity of polymer solutions of 10cP to have a viscosity ratio to oil around 1. Therefore, $C_p=1000\text{ppm}$ for 5115XV and $C_p=2500\text{ppm}$ for 5115BPM was used respectively. The difference in adsorption of polymer is due to the size of polymer macromolecules and consequently the density of adsorption on the pore surface. But overall the adsorption value is much lower than in the case of HPAM (Figure 3-36). It was suggested that the anionic monomers of the polymer chain can adsorb to the silica surface through divalent cations like Ca^{2+} (Figure 3-35). The addition of ATBS enhances the salt tolerance due to the position of the sulfonated group being few atoms away from the polymer backbone, thus shielding acrylic acid monomers from cations and maintaining the acrylic away from the surface (Almubarak et al., 2021). Also in polymer 5115XV, we have a lower content of acrylic acid that can also decrease the adsorption through the mechanism that is presented in Figure 3-35. We need more experiments with these polymers to clarify the retention mechanism.

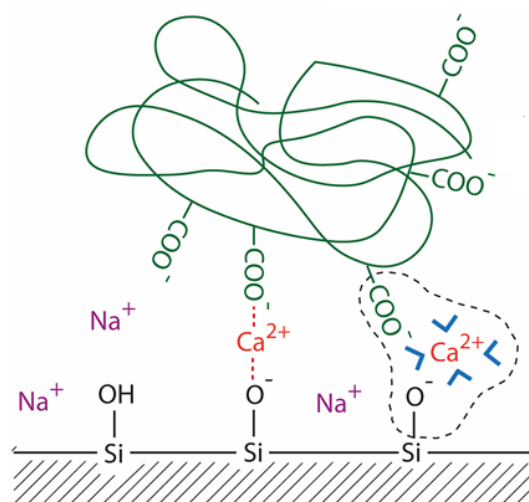


Figure 3-34. Possible calcium mediated adsorption on silica (Mohan et al., 2021)

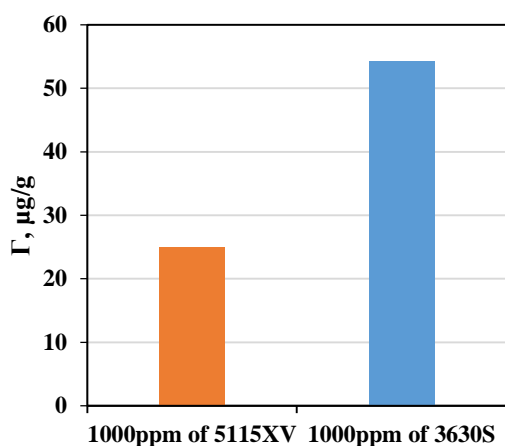


Figure 3-35. Retention of polymer 5115XV and 3630S in Bentheimer at concentration 1000ppm

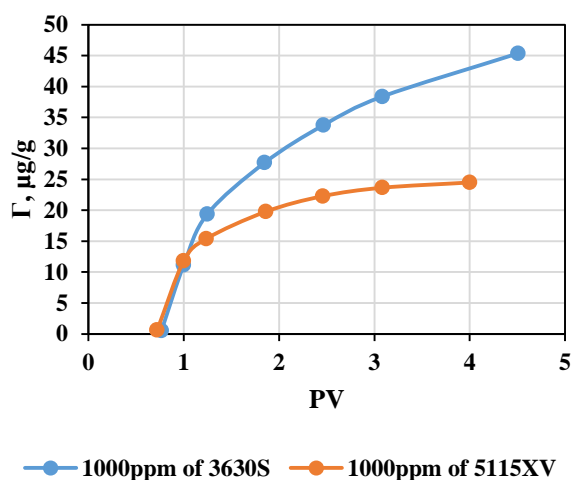


Figure 3-36. Adsorption rate of polymers 5115XV and 3630S in Bentheimer at concentration 1000ppm

The adsorption rate in both cases is equal at the beginning followed by higher values in the case of HPAM (see Figure 3-37). It means that the adsorption to the free skin surface is the same for both polymers, but after ATBS polymer is adsorbing slower. The reason for slower adsorption is maybe because of the difference in energy of adsorption caused by the polymer composition and structure.

To make short conclusions about the part above, we may put forward that:

- The retention depends on concentration strongly with two distinctive regimes: dilute and semi-dilute regimes. In the dilute regime, we observed linear dependence of retention on the concentration of polymer, while in semi-dilute we obtained different

trends for polymers 3630S and 3130S. In the case of HMW polymer 3630S, the retention at the semi-dilute regime fits the Freundlich isotherm, which could be an indicator of heterogeneous adsorption. In the case of LMW polymer 3130S, the retention level at the semi-dilute regime is more or less constant, this is contradictory to the experiments with 3630S. This may be caused by the permeabilities of Berea cores that vary from one core to the other by a factor of 2.

- The retention increased with permeability, which is contradictory to the results in the literature. The increase of permeability decreases the specific surface that should increase the number of adsorption sites hence the increase of retention. However, we have to keep in mind the IPV as well, with increasing permeability the IPV is lower which increases the retention. We assume that the IPV is the main reason why we have higher retention in high permeable cores.
- The retention decreases because of decreasing of the acrylic acid content or/and the presence of ATBS content that can work as a shield and prevent the adsorption to the surface.

3.4.7 Inaccessible pore volume

All the IPV obtained for the Bentheimer-3630S system we collected are gathered in Figure 3-38. As we can see the IPV does not depend on concentration. It depends on PM structure through the distribution of pore throat size and the size of macromolecules of the polymer that is constant in the dilute regime and is only weakly dependent on concentration in the semi-dilute regime. In our experiments, the IPV for the Bentheimer-3630S system is in a typical range of 4 to 11%. It is not far from the values that were reported in the literature. Indeed, Lotsch et al. (1985) reported IPV of 10% for xanthan and 11% for scleroglucan in Bentheimer sandstones and are similar to our finding even if they used polymers of a different type. The characteristics size of 3630S is approaching the size of xanthan's and scleroglucan's semi-rigid macromolecules [Lotsch et al., 1985].

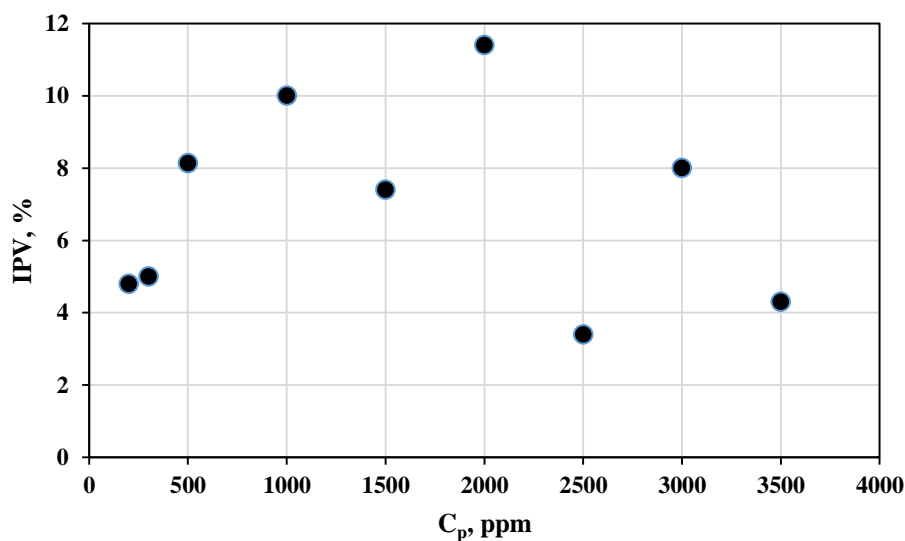


Figure 3-37. Inaccessible pore volume versus polymer concentration for 3630S in Bentheimer

In the case of the Berea-3130S system, the IPV is consistently around 21% (see Figure 3-39), which does not depend on concentration. Shah et al., (1978) and Dawson and Lantzs (1972) reported the IPV value of the same magnitude when they injected Pusher 700 HPAM in Berea sandstone of comparable permeability.

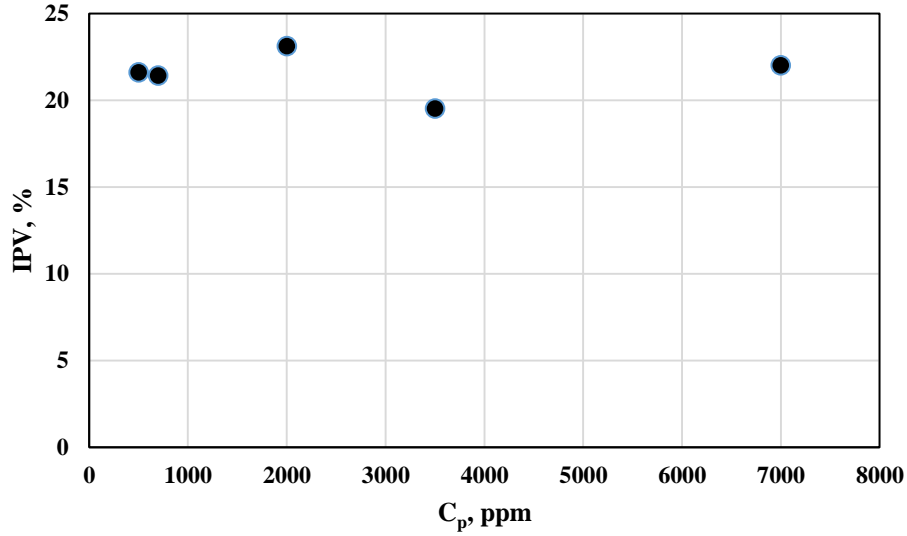


Figure 3-38. Inaccessible pore volume for polymer 3130S in Berea

To go further, if we can assume that the IPV varies as the ratio of the radius of gyration to the radius of the pores, the ratio of IPVs of these two systems is then given by:

$$\frac{IPV_1}{IPV_2} = \frac{R_{G1}/R_{p1}}{R_{G2}/R_{p2}}$$

Where

$$R_p = \sqrt{\frac{8k}{\phi}},$$

and considering that the porosity of Berea and Bentheimer is are of the same magnitude

$$\frac{IPV_1}{IPV_2} = \frac{R_{G1}/\sqrt{k_1}}{R_{G2}/\sqrt{k_2}} = \frac{R_{G1}}{R_{G2}} \sqrt{\frac{k_2}{k_1}},$$

and keeping in mind that $R_G \sim M_w^v$, with $v=0.6$ for good solvent,

$$\frac{IPV_1}{IPV_2} = \left(\frac{M_{w1}}{M_{w2}} \right)^v \sqrt{\frac{k_2}{k_1}} \approx 0.67,$$

where indices 1 and 2 corresponds to the systems Bentheimer-3630S and Berea-3130S respectively. While according to our experimental results the ratio of average IPV of these systems is around 0.42, which is of the same magnitude as the theoretical estimation.

3.5 Diphasic experiments: Water-wet condition

After having performed experiments under monophasic conditions and having discussing retention of our different polymer kinds in Bentheimer and Berea, we move now to diphasic conditions. We focus here as presented in the introduction part on the influence of the presence of oil both on native water-wet Bentheimer and in the case when wettability is altered as well.

To study the impact of the presence of oil and wettability on the retention of polymer we performed experiments in presence of oil in water-wet and aged Bentheimer with polymers 3630S and 5115XV that are of high molecular weight.

Bentheimer sandstone is known to be naturally perfectly water-wet, therefore we considered that this wettability can be maintained after oil drainage. The polymer solution can be injected in the secondary stage, just after oil drainage, or in the tertiary stage after waterflooding. We chose the tertiary stage. As we described in the previous chapter the polymer concentration is determined in the effluent through carbon and/or nitrogen concentration in the aqueous phase. In diphasic experiments, we measured the concentration of nitrogen only, because nitrogen is present only in polymer, while carbon is present in polymer and crude oil too. So the use of TC does not allow a satisfactory measurement accuracy to determine the polymer concentration.

3.5.1 Oil drainage

Before injection, the oil was degassed at $T=40^{\circ}\text{C}$ using a vacuum pump and a magnetic stirrer to avoid the gas formation in a porous medium. The oil drainage was performed under a constant flow rate $Q=50\text{ml/h}$, in a horizontal position, and at $T=25^{\circ}\text{C}$. The effluent was collected in the beaker to measure the amount of recovered water. At the end of oil drainage, the recovered amount of water gives us the amount of remaining water, which corresponds to irreducible water saturation, S_{wi} .

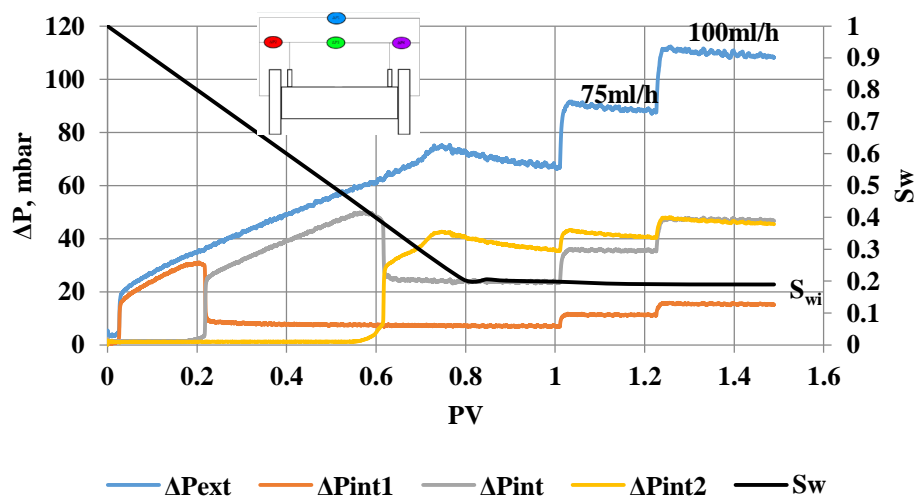


Figure 3-39. Pressure drop and Water saturation versus injected oil volume during the oil drainage and injecting at higher flow rates to estimate the effective permeability to oil

In Figure 3-40, we present the pressure data and S_w obtained during typical oil drainage. We injected oil initially at 50ml/h until reaching a stable value of water saturation that corresponds to S_{wi} and then vary the flow rate to calculate the permeability to oil at irreducible water saturation, $k_o(S_{wi})$, using Darcy's law.

The obtained S_{wi} is 18.9% and 23.6% for experiments 3630S/WW and 5115XV/WW respectively. The permeability of 3630S/WW is higher than 5115XV/WW because of a lower volume of immobile water in 3630S/WW. It is worth mentioning that the permeability to oil for 3630S/WW is higher as well, 3.18D in 3630S/WW and 2.27D in 5115XV/WW. All the data from these experiments are gathered in the table 3-6.

3.5.2 Waterflooding

After oil drainage, we flushed the porous medium with brine at 50ml/h until reaching the residual oil saturation, S_{or} . And then we vary the flow rate to calculate the effective water permeability at residual oil saturation, $k_w(S_{or})$.

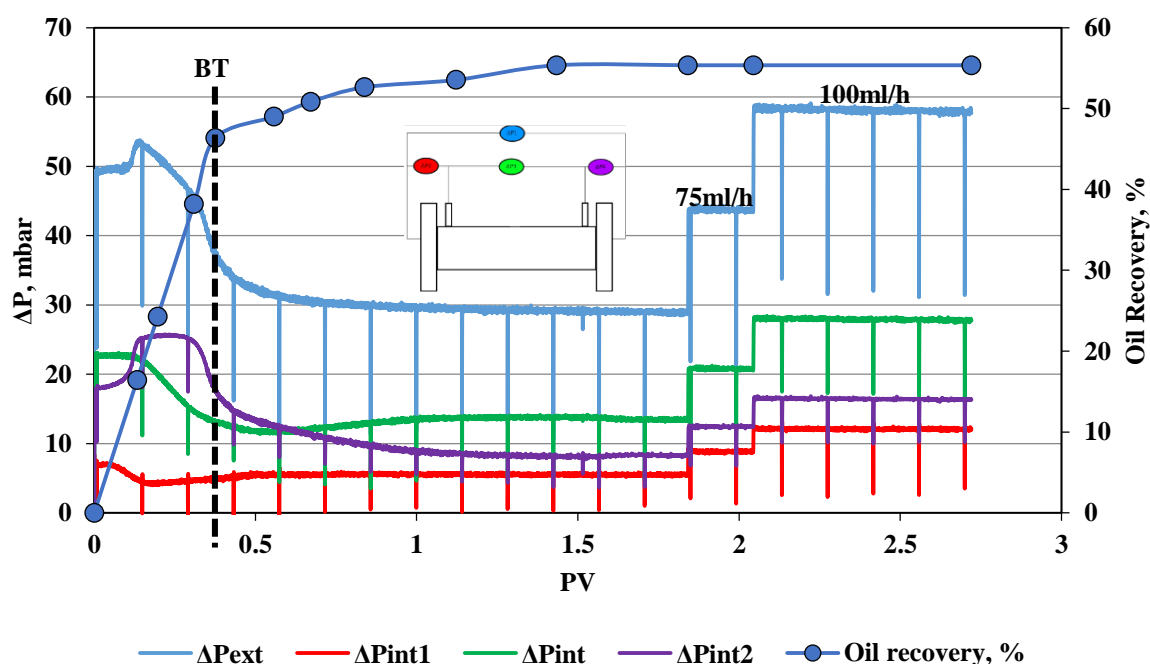


Figure 3-40. Oil recovery and Pressure drop data during water imbibition and at various flow rates to determine the $k_w(S_{or})$

As we can see from Figure 3-40, at 50ml/h we reached a maximum recovery of 54%. Since the oil is of low viscosity we recovered almost all the mobile oil with water. We obtained 55.3% and 51.7% of oil recovery in 3630S/WW and 5115XV/WW respectively. The S_{or} for both cores is almost the same 36.7% and 36.1%. Also, the water permeability at S_{or} , $k_w(S_{or})$, is of the same order, 0.397D and 0.313D for 3630S/WW and 5115XV/WW respectively.

3.5.3 Dispersion test in diphasic

After waterflooding, we injected the brine with KI to get a dispersion curve and calculate again the pore volume occupied by residual oil. The brine with KI was injected at 30ml/h and the effluent was collected to measure the concentration of Iodide by the spectrophotometer.

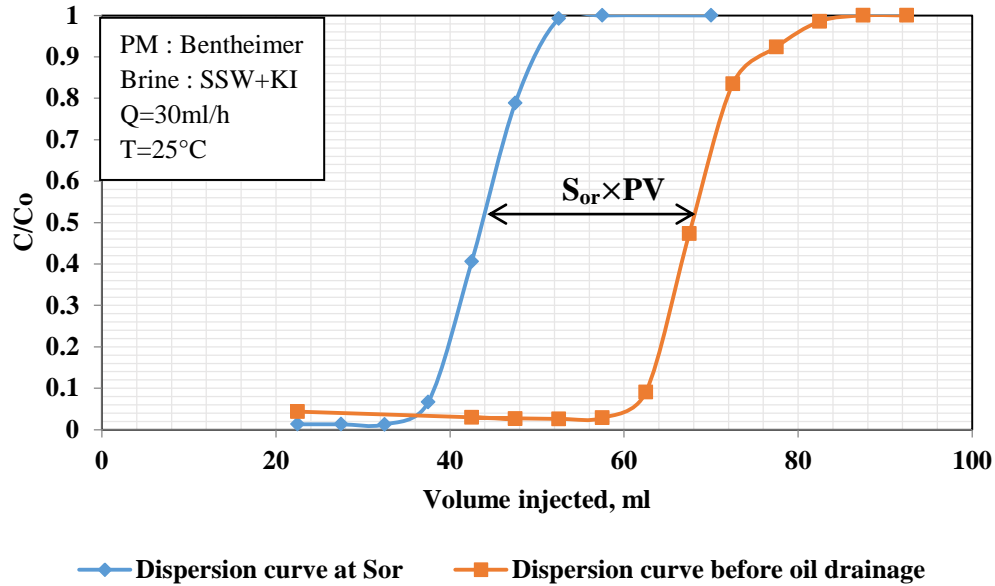


Figure 3-41. Dispersion curve before oil drainage and at S_{or} versus injected volume of brine in Bentheimer

In Figure 3-42, we present two dispersion curves, first the dispersion test we performed before oil drainage in single-phase flow, second after water imbibition in presence of residual oil. Therefore the difference between these curves gives us the volume of residual oil. Besides, we can check the change in the homogeneity of PM if we put them together after correction by the S_{or} , as in Figure 3-43. Here we can see that the PM became slightly more heterogeneous after oil drainage in this case.

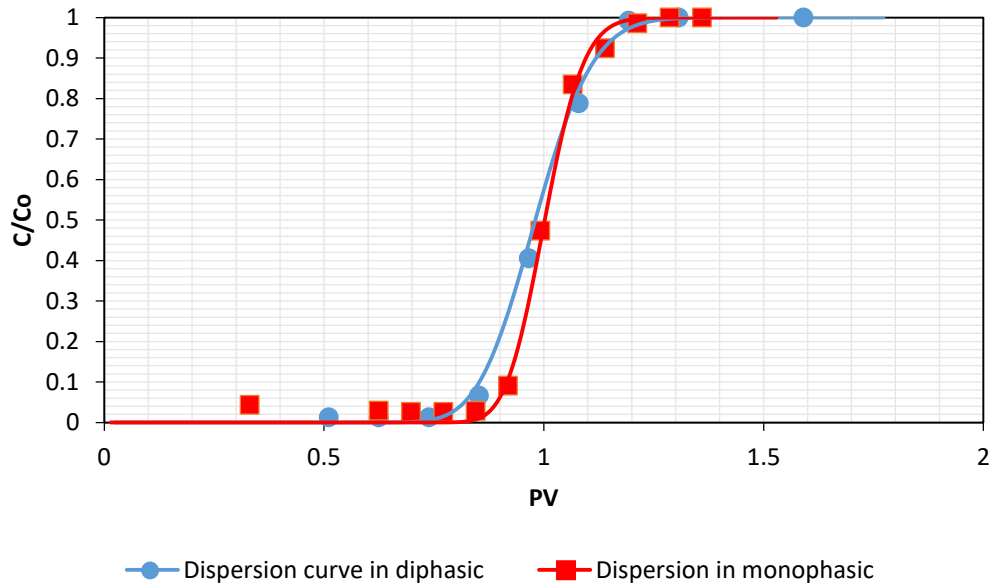


Figure 3-42. Dispersion curve in monophasic, before oil drainage, and in diphasic versus PV in Bentheimer

3.5.4 Polymer flooding

We have chosen the concentration of polymer to have a viscosity ratio around 1, corresponding to a polymer the concentration of 1000ppm for both polymers (3630S and 5115XV). Polymer injection at these conditions did not produce any additional oil.

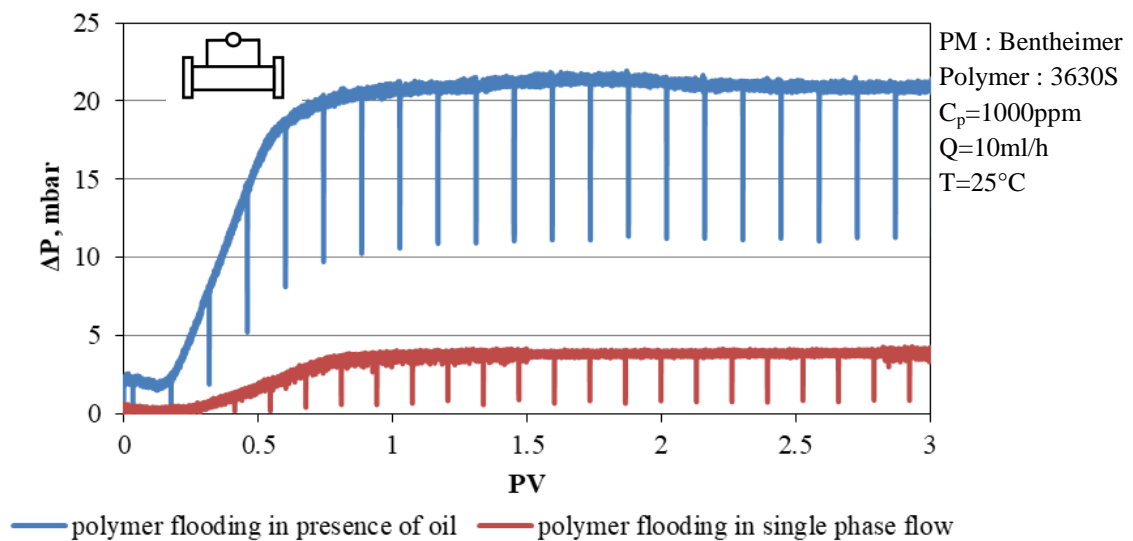


Figure 3-43. Intermediate pressure drop data during first polymer flooding in presence of oil and without oil

In Figure 3-44, we illustrate the intermediate pressure drop data that were recorded during the first polymer flooding in monophasic and diphasic experiments with polymer 3630S at concentration 1000ppm and flow rate 10ml/h. The ratio of pressure drop at S_{or} and in the monophasic state is the relative water permeability, which is $k_{rw} = \frac{k_w(S_{or})}{k}$ at that Q . The

pressure drop ratio at polymer flooding is ~ 0.18 giving $k_{rw}=0.15$. It is worth noting that the slope of the curve is different because the pore space available for polymer flow is of course less than that available for water.

In Figure 3-45, we calculated the normalized pressure drop for polymer flooding in monophasic and diphasic experiments and plotted it versus PV, where PV for the diphasic experiment was corrected for S_{or} taking into account only the accessible pore volume for the aqueous phase. As it is illustrated there the slopes of curves coincide entirely showing that the polymer flow behavior in a diphasic experiment is the same as in monophasic, and observed higher pressure drop is only because of the presence of oil.

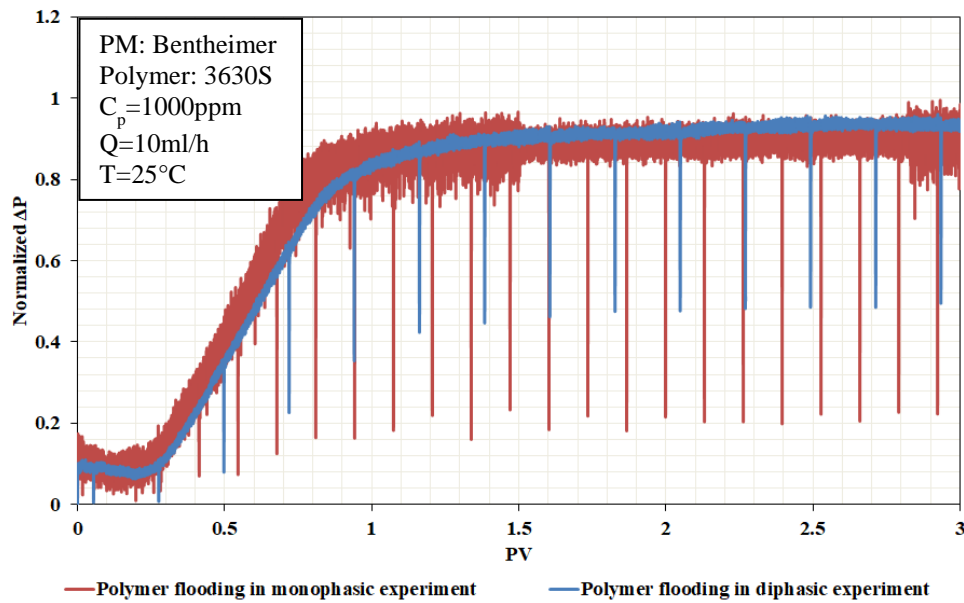


Figure 3-44. Normalized pressure drop data for monophasic and diphasic polymer flooding at 10ml/h; The data for diphasic is corrected to S_{or}

3.5.5 Mobility reduction

As in the monophasic experiments we injected the polymer at various flow rates to calculate the RM for each experiment.

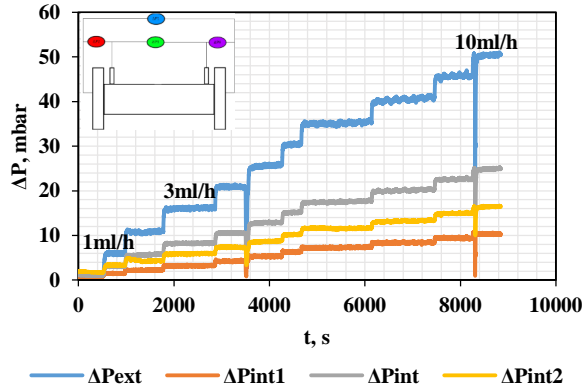


Figure 3-45. Pressure drop data during polymer flooding at various flow rates to estimate the RM in Bentheimer

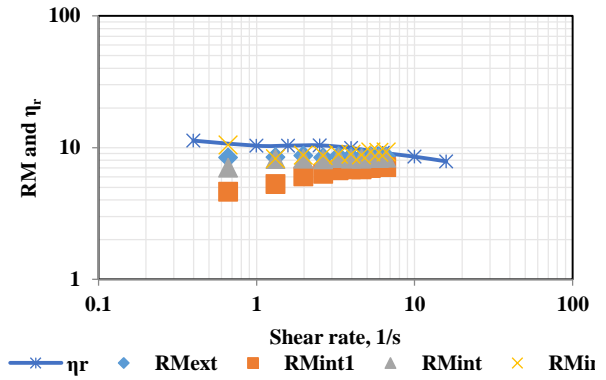


Figure 3-46. RM values of 3630S in Bentheimer and η_r in a bulk solution at $C_p=1000\text{ppm}$

In Figure 3-46, we give the pressure data obtained during polymer injection at various flow rates to calculate RM. In diphasic experiments, we measured the RM at low flow rates up to 10ml/h only to maintain constant the S_{or} . As we can see from the RM versus shear rate plot for polymer 3630S in comparison with the bulk relative viscosity, the Newtonian plateau only present there because of the low shear rate and the RM value is the magnitude as the η_r .

3.5.6 Brine flush and permeability reduction

After first polymer flooding and calculating the RM we flush the PM by brine and remove all free polymer molecules. During brine flush as in monophasic experiments, we record the pressure drop along the core and collect the effluent by the fraction collector. The effluent is then analyzed to check the presence of polymer by TOC, and when the effluents become polymer-free, we stop the brine flush and inject the brine at various flow rates to determine R_k . Unfortunately, because we were injecting brine at low shear rates the pressure drop data is not precise. Therefore the R_k value for diphasic experiments is not reliable.

3.5.7 Second polymer injection

As in monophasic experiments, we inject the polymer a second time after brine flush. During the second polymer flooding, we measure the pressure drop and collect the effluent by the fraction collector. The collected effluent is used to measure the concentration of polymer by determining its Nitrogen content.

As we have done previously in monophasic conditions, the break-through curves of second polymer flooding and first polymer flooding are used to calculate the retained amount of polymer, Γ , and dispersion curve and the break-through curve of second polymer flooding to calculate the IPV. We have to mention here that the dispersion curve is the one that we performed after water imbibition in presence of residual oil (Figure 3-42 and 3-43).

3.5.8 Retention of polymer

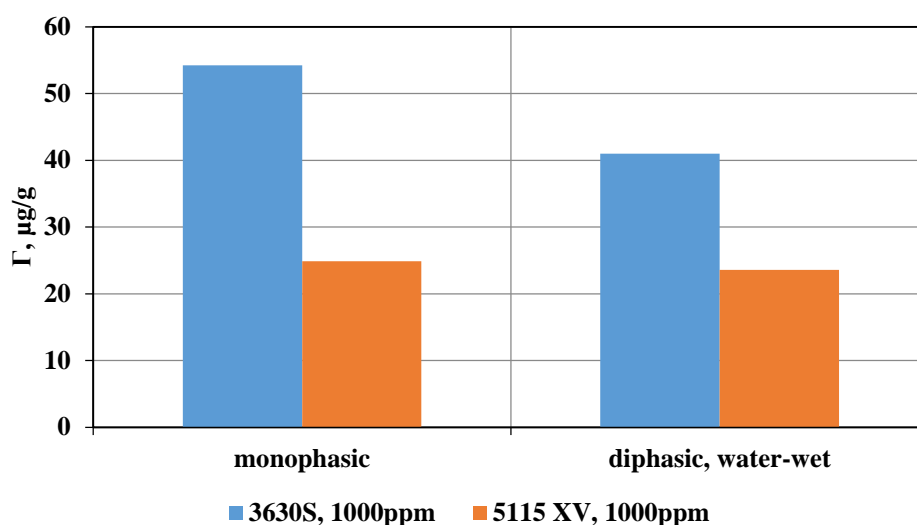


Figure 3-47. The retained polymer of monophasic and diphasic experiments with polymers 3630S and 5115XV in Bentheimer

The retention amounts for the two polymers are shown in Figure 3-48 in comparison with those obtained in monophasic experiments at the same C_p . This figure calls for some comments:

First, we observe that retained polymer quantity is lower in diphasic condition than in monophasic for both polymers. It may be expected that in presence of oil that occupies a part of the pore space prevents polymer adsorption. However, this pore volume occupied by oil cannot be considered inaccessible. As the porous media are water-wet, oil droplets are mainly located in the center of the pores, and in some areas, the polymer is still able to flow and adsorb onto the pore surface, and retained polymer quantity is only slightly reduced. Indeed, considering that retained 3630S polymer is $54\mu\text{g/g}$ in monophasic conditions and if we correct the data by taking to account the S_{or} is equal to 36%, the “theoretical” retained polymer should be equal to $33\mu\text{g/g}$ if we consider that the pore volume occupied by oil is not accessible to the polymer. However, the measured experimental value is significantly greater and is equal to $41\mu\text{g/g}$ confirming that the polymer is adsorbed in some areas where oil is present (Figure 3-49).

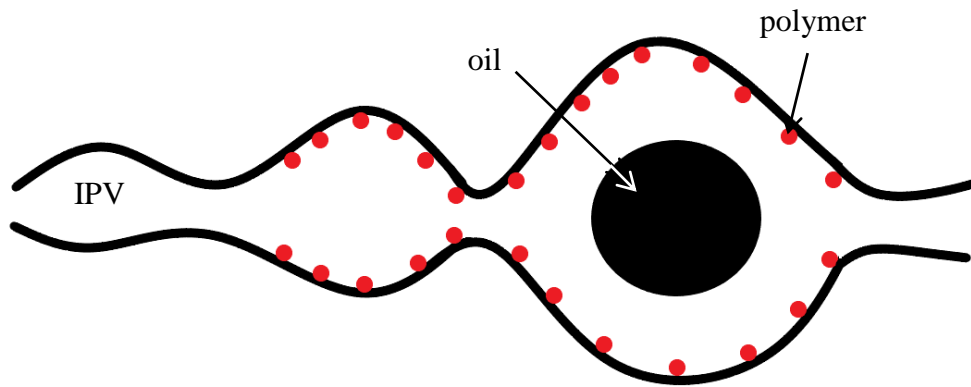


Figure 3-48. Sketch of adsorption of polymer in pores with oil droplet in the center

Second, when we consider the polymer 5115XV, the trend of retained polymer is similar to the one observed for polymer 3630S as adsorption in the monophasic state is higher than in diphasic conditions. However, the quantity of retained polymer in the diphasic condition when corrected for S_{or} as above is higher compared to results from monophasic experiments. A possible explanation of this finding is that the polymer is more retained in areas where oil is present. Indeed, according to Broseta et al. (1995), there are two opposite effects on retention of polymer in presence of oil: (i) the IPV that decreases the retained amount of polymer and (ii) the adsorption to the oil surface that increases the retention. We do not have information on the composition of the oil, but there is a possibility that the ATBS group in polymer 5115 adsorbs on the oil-water interface (Figure 3-50).

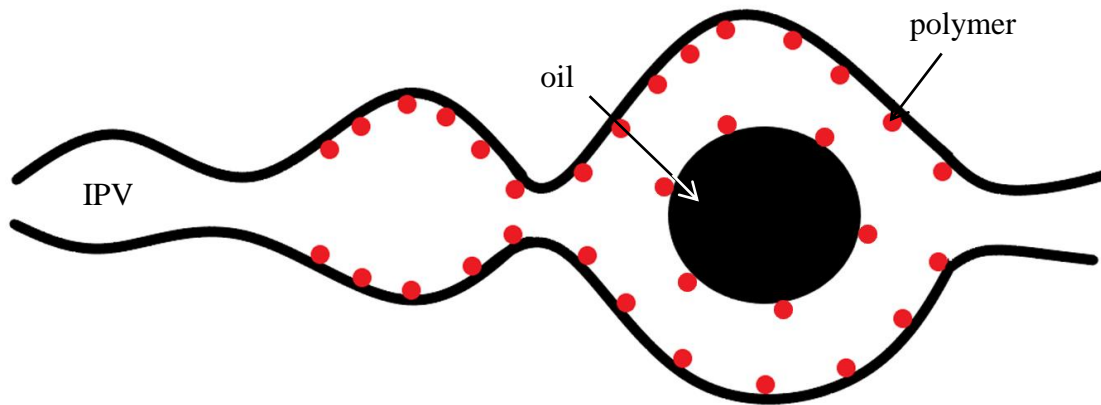


Figure 3-49. Sketch of possible adsorption of polymer on to the oil-water interface

3.5.9 IPV

The IPV for these experiments were obtained using the dispersion curve at S_{or} and second polymer flooding. It is worth noting that IPV is lower than in monophasic cases (2.5% in diphasic and 9% in monophasic, see Figure 3-51).

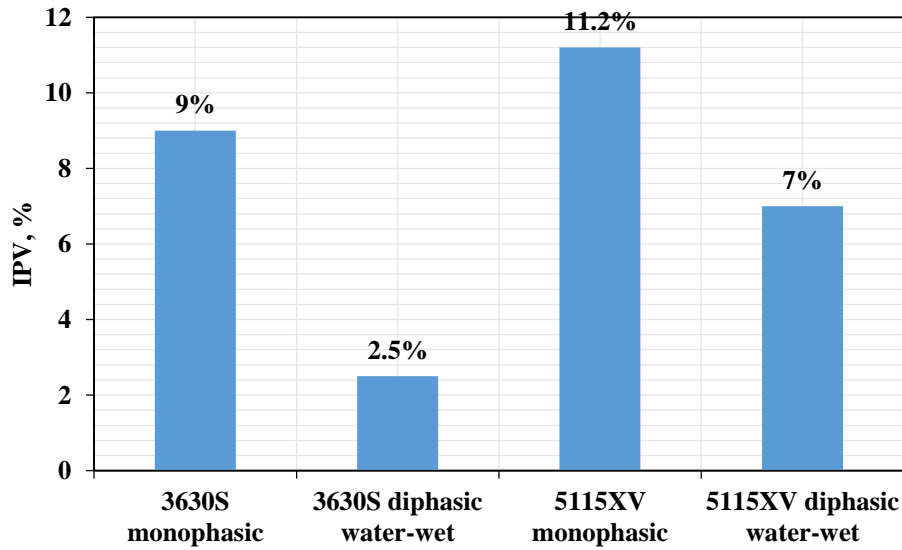


Figure 3-50. IPV of monophasic and diphasic (water-wet) experiments with 3630S and 5115XV

All the data we commented before are gathered in Table 3-6.

	3630S/WW	5115XV/WW
k, D	2.61	2.26
S_{wi} , %	18.9	23.6
$k_o(S_{wi})$, D	3.18	2.27
Oil recovery, %	55.3	51.7
S_{or} , %	36.7	36.1
$k_w(S_{or})$, D	0.397	0.313
Polymer type	3630S	5115XV
Γ , $\mu\text{g/g}$	41.2	23.6
RM	9	35
IPV, %	2.5	7

Table 3-6. The experimental data obtained for experiments with polymers 3630S and 5115XV in Bentheimer in presence of oil

3.6 Diphasic experiments: Altered wettability porous media

Ageing of the cores with crude oil is known to alter its initial wettability changing it from water-wet to oil-wet or intermediate-wet. The process that considers interactions between crude oil compounds and solid surfaces is complex. The change of wettability depends strongly on solid/fluid interactions, namely oil and brine composition, and on pressure, temperature, and ageing time.

The wettability has an impact on the distribution of immiscible fluids in porous media and the flow of these fluids. In general, it is assumed that reservoir rocks are water-wet before the slow migration of hydrocarbons by density difference. If the medium is water-wet, water coats the pore surface and saturates the small pores, while the oil is in the center of the large

pores in the form of drops (see Figure 3-52). The oil-wet porous media show the opposite distribution of fluids. The oil saturates the smallest pores and will cover the surface of the large pores.

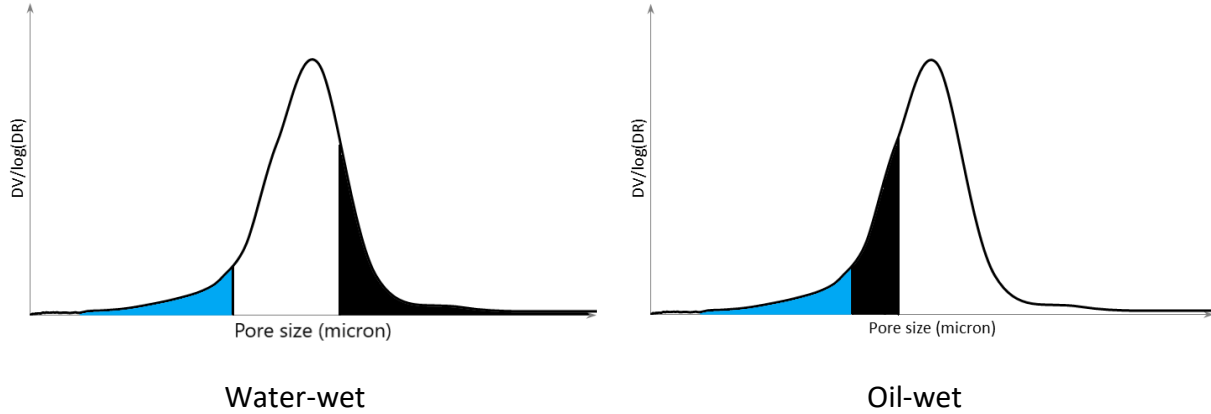


Figure 3-51. The pore repartition of S_{or} (black) and S_{wi} (blue) in water-wet and oil-wet porous media

The procedures preceding the ageing process is the same as in diphasic experiments in water-wet porous media.

3.6.1 Permeability to oil after ageing

In our experiments, we used a degassed crude oil and leave the core after oil drainage in an oven at $T=40^{\circ}\text{C}$ for at least 30 days. The core is oil flushed after the ageing period and permeability to oil is measured and compared to its initial value before ageing. Figure 3-53 shows an example of a measurement of permeability to oil after ageing ($k_o^2(S_{wi})$).

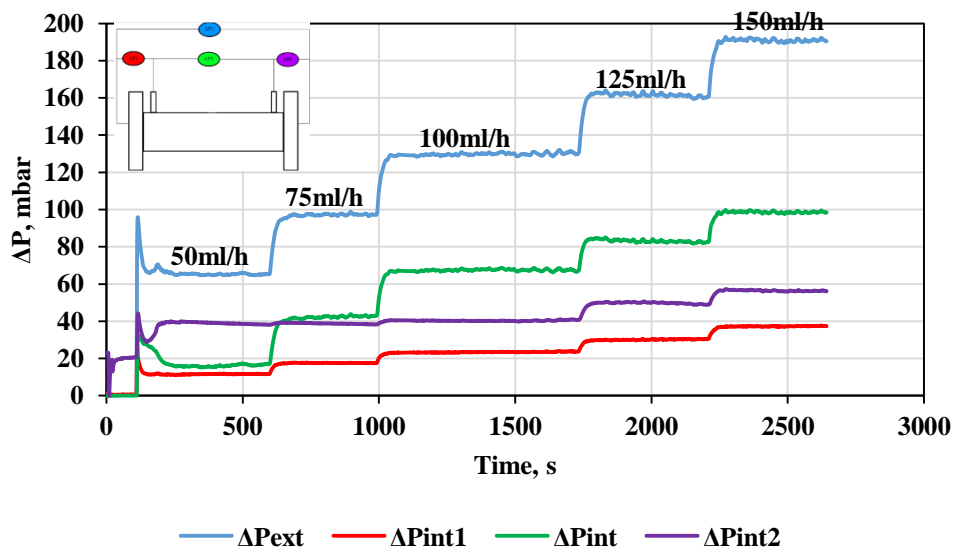


Figure 3-52. Injection of oil at various flow rates after ageing to estimate the $k_o^2(S_{wi})$ in Bentheimer

First of all, we did not notice any water production after ageing process, S_{wi} is constant, but $k_o^2(S_{wi})$ is always lower than $k_o^1(S_{wi})$ (Table 3-7). This result indicates that a change of wettability occurred during the ageing process due to a change of the fluid location in the pore volume. Oil is located on the pore surface or closer to the surface reducing its permeability to oil. This change of permeability to oil is an indication of a change of wettability but does not allow determining how much such a wettability had changed and other techniques are needed for that for example by performing Amott tests. For the rest of the text, we will consider an altered wettability that corresponds probably more to an intermediate-wet than completely oil-wet.

	Before ageing, $k_o^1(S_{wi})$, D	Ageing at 40°C, days	After ageing, $k_o^2(S_{wi})$, D
3630S/IW	2.34	40	2.14
5115XV/IW	2.82	33	1.99

Table 3-7. Permeability to oil before and after ageing in Bentheimer

3.6.2 Waterflooding

After ageing and measurement of permeability to oil, we flushed the porous media with brine at 50ml/h until reaching the residual oil saturation, S_{or} . And then we vary the flow rate to calculate the effective water permeability at residual oil saturation, $k_w(S_{or})$ (Figure 3-54).

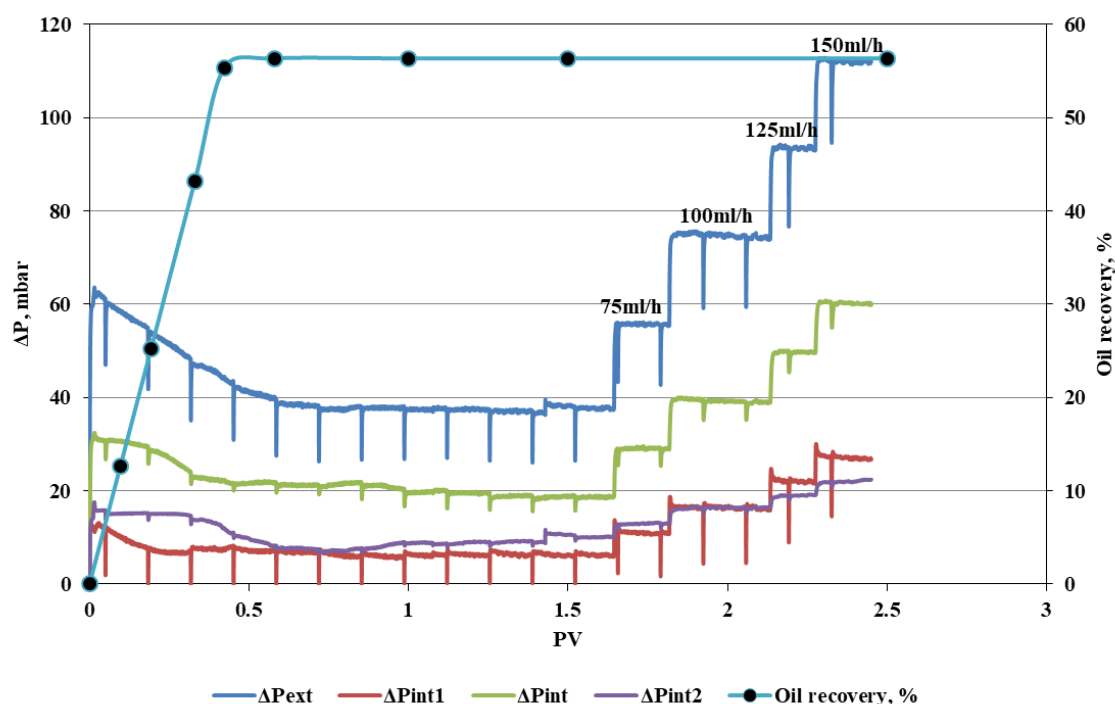


Figure 3-53. Pressure drop during waterflooding and at various flow rates to calculate the water permeability at S_{or} , $k_w(S_{or})$, and oil recovery data

The oil recovery for both experiments 3630S/IW and 5115XV/IW are of the same order of magnitude 56.3% and 57.1% respectively. Besides the oil recovery, the S_{or} and water

permeability at S_{or} are of the same magnitude as well. This is not surprising because the original PM have similar characteristics.

To see the impact of wettability on the recovery of oil we put together the data of recovery over time for both experiments in Figure 3-55. If we consider results corresponding to 3630S/WW (water-wet) and 3630S/IW (aged core) we can make the following remarks:

first of all, the breakthrough of water occurs early in water-wet PM than in the aged core, say at 0.37PV in water-wet and 0.42PV in the aged core. And since the break-through occurs early for water-wet core the recovery is respectively lower, 46%, and slowly increasing till 55% (see Figure 3-55). While in the aged core, however, we see that almost maximum recovery is reached right after breakthrough, 56%. In the end, we obtained more or less the same S_{or} despite having different wettabilities. Concerning their water permeability at residual oil saturation ($k_w(S_{or})$), which is 0.397D and 0.275D for water-wet and aged core respectively, so it is understandable to have an early breakthrough in water-wet because it has higher permeability and the same amount of residual oil as in aged core. However, there is discrepancy in results concerning the recovery of oil, since the permeability to oil in water-wet PM (3.18D) is much higher than in aged core (2.14D) it should cause the recovery to reach the maximum value at the breakthrough because oil should move much more freely in the water-wet core. However, we see the opposite picture in Figure 3-55, reaching maximum recovery at a breakthrough in aged core and having additional recovery after breakthrough in the water-wet core.

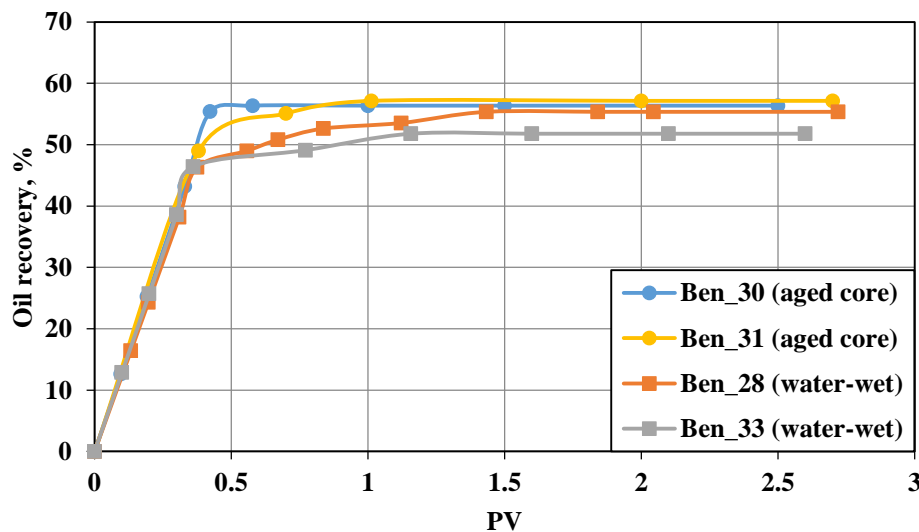


Figure 3-54. Oil recovery in water-wet and altered wettability cores experiments.

3.6.3 Polymer flooding

We injected the polymers 3630S and 5115XV as in water-wet experiments at the same conditions. The pressure drop data during polymer flooding is presented in Figure 3-56 in comparison with data obtained in monophasic and diphasic water-wet experiments.

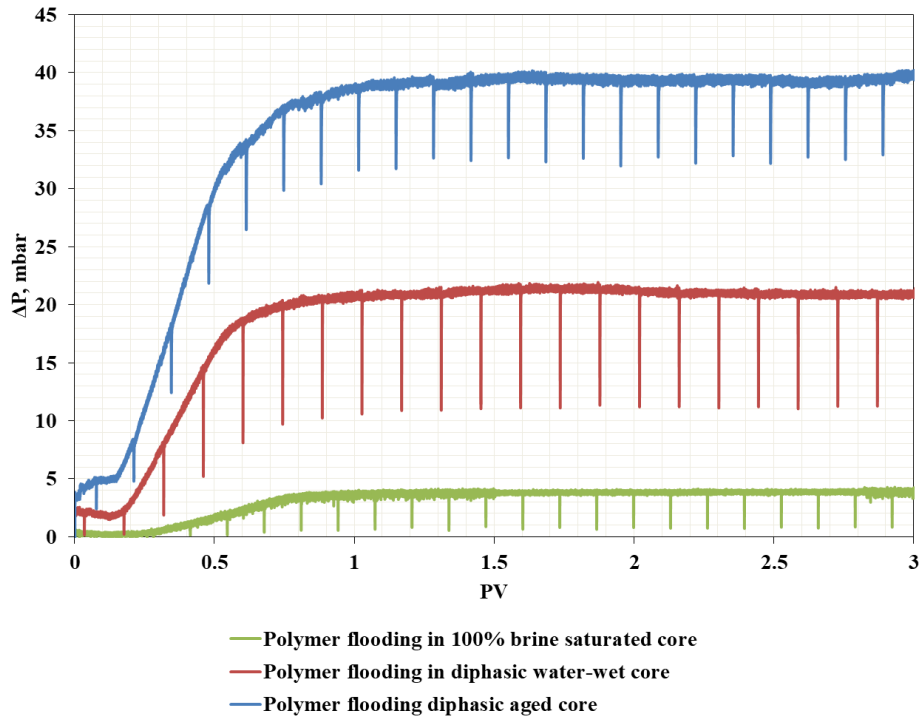


Figure 3-55. Pressure drop data during flooding polymer 3630S at $C_p=1000\text{ppm}$ in 100% brine-saturated core, water-wet and aged diphasic cores

As we can see from that figure, we obtained higher pressure in the aged core than in the water-wet core, because of the difference in water permeability $k_w(S_{or})$. The ratio of pressure drop during polymer flooding in single-phase and diphasic experiments is around 0.09. It is of the same order as the relative water permeability, $k_{rw} = \frac{k_w(S_{or})}{k} = 0.11$. In Figure 3-56, we present the same data but with normalized pressure data and PV corrected for S_{or} . Data for diphasic experiments are very close, with a slightly different slope at the beginning. This difference is caused by the retention; in the case of the aged core, we have a lower level of retention than in the water-wet core and the monophasic experiment.

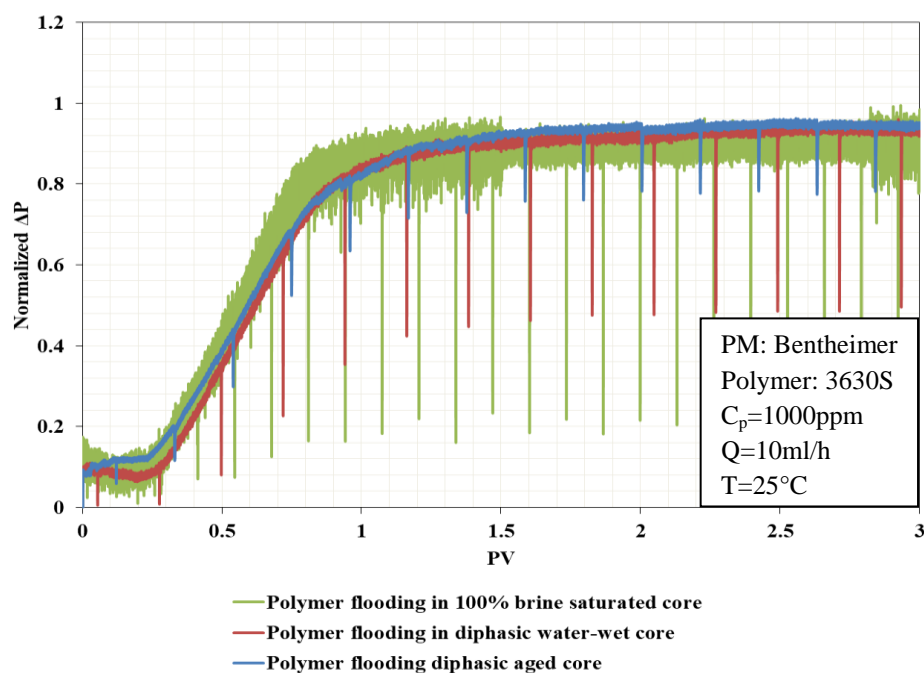


Figure 3-56. Normalized pressure drop during polymer flooding in 100% brine saturated core, diphasic water-wet core and diphasic aged core

3.6.4 Retention of polymer

In the aged core, we had 2 experiments with polymers 3630S and 5115XV at the same conditions as in previous experiments except for this time we had an ageing process after oil drainage, which is supposed to change the wettability of the PM.

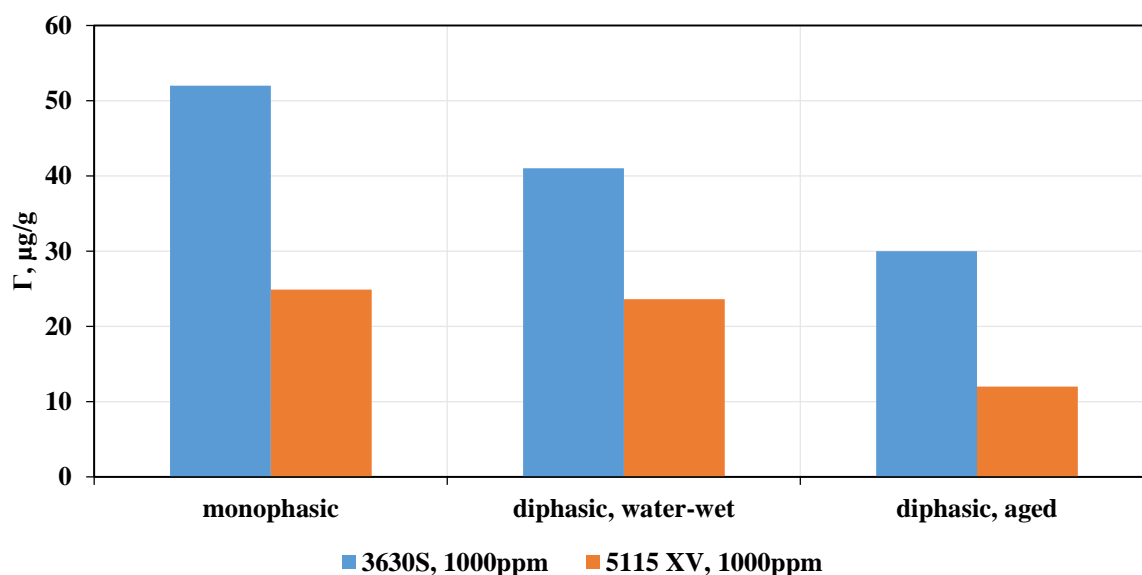


Figure 3-57. The retention of polymers 3630S and 5115XV in Bentheimer at monophasic and diphasic cases

In Figure 3-58, we collected the retention results obtained from monophasic, diphasic water-wet, and aged PM experiments for the two involved polymers. The comparison of results of

altered wettability cores with the water-wet experiments clearly shows decreasing in retention in aged PM whatever the polymer. To interpret the cause of this trend we would like to remind the repartition of oil and water phases in PM that is water-wet or oil-wet (Figure 3-59).

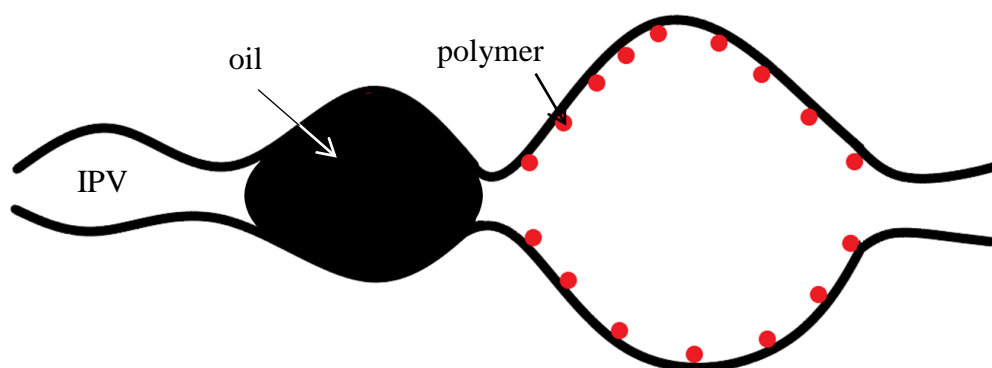


Figure 3-58. The adsorption of polymer and oil location in oil-wet core

Using the pore size distribution curve and assuming that PM is a bundle of capillary tubes, we can identify the location of each phase in this model (see Figure 3-59). In both cases, the irreducible water saturation is in the smallest pores where water is trapped and immobile. However, the residual oil is located in big pores in case of water-wet PM and smaller pores in oil-wet case. We characterized our aged core as somewhere between those two extreme wettabilities – intermediate wettability, where some pores have changed the wettability during ageing and some are still completely water-wet. It is difficult to point out the phase distribution in this case because residual oil can be located everywhere, in small pores where the wettability might be altered and might also be left in some large ones like in the water-wet case.

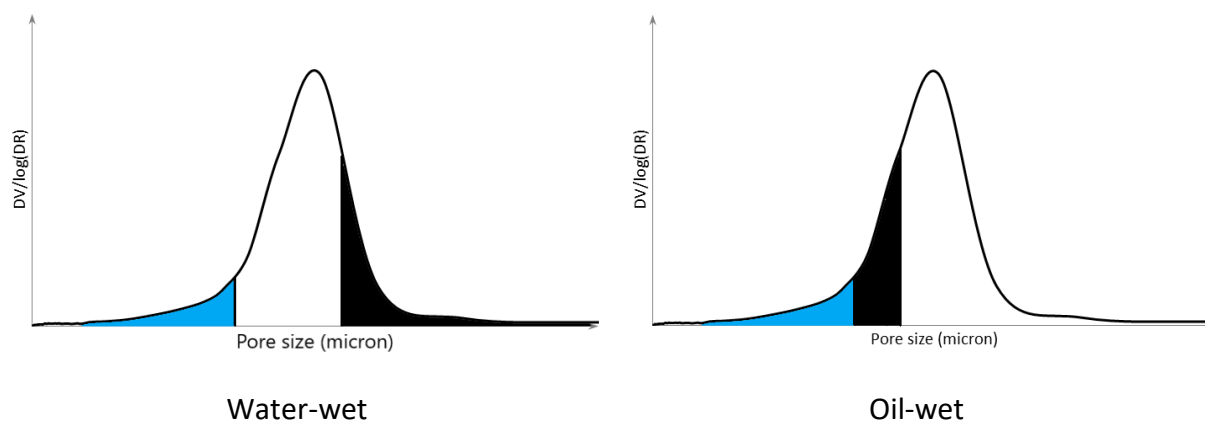


Figure 3-59. The pore repartition of S_{or} (black) and S_{wi} (blue) in water-wet and oil-wet porous media

The specific surface area in small pores is much higher than in large pores, consequently, we would expect more retention in small pores than in large ones. Therefore, we have higher adsorption in water-wet PM because in this case, the small pores are available for polymer flow while the residual oil is located in large pores (Figure 3-60). When we perform ageing we relocate some oil droplets from large pores to intermediate and small pores causing less

adsorption there, which decreases the total retention value. The pores where is the oil droplets are relocated now are inaccessible for adsorption of polymer chains because the ageing process changed the chemistry of the surface next to the oil droplets making it hydrophobic and oil droplets are closer to the surface or covering the surface and blocking polymer flow there.

The retained amounts in aged cores are approximately half of the amount obtained in monophasic experiments. Moreover, we would expect to have the same trend at every concentration. It will allow us to extrapolate the data obtained from monophasic experiments to the diphasic. The trend of decreasing retention with wettability change from water-wet to oil-wet was reported by Lakatos et al. (1981). They found null retention in oil-wet PM, 6.5µg/g in intermediate-wet, and 19µg/g in the natural sandstone. Even though we have no information on the experimental conditions we can see the trend of retention with changing wettability.

	3630S/IW	5115XV/IW
k, D	2.43	2.6
S_{wi} , %	23.6	24.3
$k_o^1(S_{wi})$, D	2.34	2.82
Ageing at 40°C, days	40	33
$k_o^2(S_{wi})$, D	2.14	1.99
Oil recovery, %	56.3	57.1
S_{or} , %	36.1	33.1
$k_w(S_{or})$, D	0.275	0.291
Polymer type	3630S	5115XV
Γ , µg/g	29.7	12
RM	—	29
IPV, %	—	5

Table 3-8. The experimental results obtained in altered wettability Bentheimer cores with polymers 3630S and 5115XV

In Table 3-8, we collected all the experimental results obtained during experiments in aged diphasic Bentheimer cores with polymers 3630S and 5115XV at $C_p=1000\text{ppm}$. The characteristics of these two cores are very close before and after ageing, therefore comparing retention levels is very reliable. We would like to mention also that the experimental procedure after polymer flooding in experiment 3630S/IW went wrong because of equipment malfunction, so we did not obtain the RM and IPV data for that experiment.

Chapter IV: Conclusions and perspectives

This thesis aimed to make new contributions to the study of polymer retention in natural sandstones during monophasic and diphasic flows especially when the porous medium is not water wet. The experimental results in literature dealing with retention in presence of oil are scarce. The few experimental results that were reported in the literature gives some contradictory results: according to Broseta et al. (1995), the retention is the same in the presence of oil and 100% brine saturated porous media, while Wever et al. (2018) found that the retention decreases up to 3-4 times in presence of oil than without oil in high permeable porous media. Even if experimental conditions were different this means that this phenomenon needs more study at various conditions with different types of polymers, oil, and porous media.

All the experiments were performed with natural sandstones of different permeabilities, polymers of different types, molecular weight and concentration. Coreflooding were performed in monophasic and diphasic conditions during which the pressure drop along the core and the polymer concentration in the effluent were measured continuously. All the data obtained in the experiments were presented and commented in Chapter III. First, we started with monophasic experiments when the porous media is fully saturated by brine. In this case, we have studied the impact of several parameters on the retention of polymer: the molecular weight of the polymer using High Molecular Weight (HMW) and Low Molecular weight (LMW) polymers, concentration of polymer, polymer type (HPAM and sulfonated), and the permeability of porous media. Our conclusions are given below

- The strongest impact on retention level we found to be the molecular weight of the polymer, the retention decreased up to 2 to 10 times when molecular weight increased 7 times. The retention level was quantified in the systems Bentheimer-HMW and Berea-LMW. In the latter case, we performed experiments only for 3 concentrations but enough to see the trend. In high permeable porous media, the main retention process is adsorption. It can be interpreted simply by the fact that for the same available surface we can adsorb more small size molecules (LMW) than large ones (HMW). In the literature, the same trend was observed but the authors explained it by the IPV differences. In our experiments, we observed slightly lower IPV in the case of LMW polymer, but not significant enough to increase the adsorption up to 10 times.
- We observed that the concentration effect has two different regimes, drastic and linear increasing of retention when concentration corresponds to the dilute regime, and a much slower increase of retention in the semi-dilute regime. The retention level in dilute-regime was explained as a competition between the relaxation time of adsorbed polymer molecules and the distance between the individual molecules. Since the distance between the molecules strongly depends on the concentration we observe the drastic increase of retention with concentration.
- The permeability effect on retention was a bit contradictory. According to the literature, the retention should increase with decreasing the permeability according to

specific surface trend. However, our data showed the opposite effect, increasing retention with permeability. When the permeability was increased 20 times the retention increased up to 3 times. We estimated the theoretical value of specific surface area using the capillary tube bundle model and we found that Berea (low permeable sandstone) has 5 times more S_{sp} than Bentheimer (high permeable sandstone), which means we should have higher adsorption in Berea than in Bentheimer. But we have to keep in mind that at the same time by changing permeability IPV will change and by keeping the flow rate at the same value, the experienced shear rate change too. For the same flow rate value the shear rate in Berea is 6 times higher than in Bentheimer due to pore size and a high shear rate can cause the disentangling of polymer chains and consequently decreasing the retention. Also, Berea has a higher IPV that decreases the retention value.

- We performed experiments with polymer 5115XV and 5115BPM to study the effect of sulfonation degree on the retention of polymer. The retention level is 2 times lower in sulfonated polymer than in HPAM at the same conditions. The sulfonated polymer has lower acrylic acid content that can decrease the adsorption through mediation of divalent cations or/and the presence of ATBS groups that can shield the polymer from adsorption to the surface.

To see the impact of the presence of oil and wettability on retention we performed 4 experiments in water-wet and altered wettability cores with polymers 3630S (HMW) and 5115XV, the same molecular weight as 3630S but the presence of sulfonate groups.

- The retention in presence of oil in the water-wet core decreases because of the increase of IPV through the S_{or} contribution. If we correct the retention value of HMW for S_{or} we obtained $33\mu\text{g/g}$ which is slightly lower than the actual experimental data, which is $41\mu\text{g/g}$. We can explain that by the fact that in water-wet core the residual oil is located in large pores and the small pores have much more specific surface area, therefore we have higher retention than expected value $33\mu\text{g/g}$. The experiment with polymer 5115XV didn't show a significant change in presence of oil comparing to the monophasic experiment. We assumed that it was caused by the adsorption on the oil-water interface that was proposed before by Broseta et al. (1995), which can balance the decrease of retention because of IPV.
- The change of wettability from water-wet to intermediate wettability further decreased the retention level for both polymers. It was explained by the change of location of residual oil in the core, in some large pores the oil droplets moved closer to the surface making the surface inaccessible for adsorption, other oil droplets moved to small pores and decreased overall specific surface area. All these processes can lead to decreasing in retention level for both polymers and fits our experimental data.

In perspective, the experimental study can be continued by performing more experiments with sulfonated polymers 5115XV and 5115BPM to test the mechanic of adsorption that we proposed in detail. Also can be used different polymers that have a lower or higher level of ATBS groups to have a complete picture. We need more experiments in the presence of oil and at different wettabilities. And ideally, the Amott test needed to check the wettability.

Affiliation

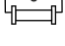

DPI, P.O. Box 902, 5600 AX Eindhoven, the Netherlands.

Acknowledgment

This research forms part of the research programme of DPI, project #808.

Nomenclature

A = cross-section of the flow, m^2
 a = size of monomer or lattice parameter, m
 C = concentration of the fluid in the effluent, ppm, g/cm^3
 C^* = overlap concentration, ppm, g/cm^3
 C_0 = concentration of injected fluid, ppm, g/cm^3
 C_b = concentration in a bulk solution, ppm, g/cm^3
 C_e = entanglement concentration, ppm, g/cm^3
 C_p = concentration of polymer, ppm, g/cm^3
 C_s = monomer fraction per unit area on the surface
 D = adsorption region or extrapolation region, m
 D_d = diffusion coefficient, m^2/s
 D_H = hydraulic diameter of the pipe, m
 D_L = longitudinal dispersion coefficient, m^2/s
 d_p = diameter of the spheres, m
 D_T = transverse dispersion coefficient, m^2/s
 D_x = total dispersion in the x direction, m^2/s
 e_H = effective hydrodynamic thickness of adsorbed layer, m
 F = diffusion flux, mol/m^2s
 f_g = characteristic shape factor of the medium
 g = acceleration of gravity, m/s^2
 I = identity tensor
 J_D = convective flux, $kg/(m^2s)$
 J_D = dispersive flux, $kg/(m^2s)$
 J = sum of the convective and dispersive flux components, $kg/(m^2s)$
 K = permeability tensor
 k = permeability, $\mu m^2, D$
 k' = Huggins coefficient
 K' = Mark-Houwink constant
 Kc = reaction rate, mol/s
 k_o = permeability to oil, m^2, D
 k_p = permeability to polymer, m^2, D
 k_{ro} = relative permeability to oil
 k_{rw} = relative water permeability
 k_w = water permeability, m^2, D
 k_o^1 = permeability to oil before ageing, bar, D
 k_o^2 = permeability to oil after ageing, bar, D
 L = length of the core, m
 L_g = length of the real path travelled between two points, m
 L_s = rectilinear length, m
 M_s = mass of the sphere, g
 M_w = molecular weight of polymer, $g/mol, Da$

N = number of monomers in polymer
 \tilde{n} = number of spheres
 n_t = number of capillary tubes
 n_ξ = number of monomers per correlation blob
 P_c = capillary pressure, bar, Pa
 P = pressure, Pa
 Pe = Péclet number
 ΔP = pressure drop, bar, Pa
 $\Delta P/L$ = pressure gradient, Pa/m
 ΔP_{b1} = pressure drop during waterflooding before polymer retention, bar, Pa
 ΔP_{b2} = pressure drop during waterflooding after polymer retention, bar, Pa
 ΔP_{ext} = pressure drop between the inlet and outlet of PM , bar, Pa
 ΔP_{int} = pressure drop in intermediate part of PM , bar, Pa
 Q = flow rate, ml/h
 r = radius of particles (or spheres), m
 Re = Reynolds number
 R_k = permeability reduction
 RM = mobility reduction
 R_p = radius of pores, m
 S_o = oil saturation
 S_{or} = residual oil saturation
 S_{sp} = specific surface area, m²/g
 S_{sphere} = area of the sphere, m²
 S_w = water saturation
 S_{wi} = irreducible water saturation
 T = temperature, °C
 t = time, s
 v = velocity, m/s
 v_w = water velocity, m/s
 v_o = oil velocity, m/s
 V = volume, ml
 V_o = volume of oil, ml
 V_p = volume of pores, ml
 V_T = total volume of porous medium, ml
 V_w = volume of water, ml
 z = distance from the wall, m

Greek symbols

α_L = longitudinal dispersivity, m
 α_T = transverse dispersivity, m
 β = correction factor
 $\dot{\gamma}^*$ = characteristic shear rate, s⁻¹
 $\dot{\gamma}$ = shear rate, s⁻¹

Γ = mass of retained polymer per unit mass of rock, $\mu\text{g/g}$
 Γ = retained amount of polymer, $\mu\text{g/g}$
 $[\eta]$ = intrinsic viscosity, cm^3/g
 $[\eta]_0$ = zero-shear-rate intrinsic viscosity, cm^3/g
 η = dynamic viscosity, cP, Pa.s
 η_p = polymer viscosity, cP, Pa.s
 η_r = relative viscosity
 η_s = solvent viscosity, cP, Pa.s
 η_w = water viscosity, cP, Pa.s
 η_o = oil viscosity, cP, Pa.s
 ξ = size of polymer blobs or correlation length, m
 ξ_b = correlation length in bulk solution, m
 ρ = density, kg/m^3
 σ = interfacial tension, dyne/cm, mN/m
 σ_{os} = interfacial tension between oil phase and the solid surface, dyne/cm, mN/m
 σ_{ow} = interfacial tension between water phase and the solid surface, dyne/cm, mN/m
 σ_{ws} = interfacial tension between water phase and the solid surface, dyne/cm, mN/m
 ϕ = porosity
 Ψ = kinematic viscosity, m^2/s
 θ = contact angle, $^\circ$

Bibliography

- Almubarak, T., Li, L., Ng, J.H., Nasr-El-Din, H., AlKhaldi, M., 2020. New insights into hydraulic fracturing fluids used for high-temperature wells. *Petroleum*.
- Anderson, W.G., 1986a. Wettability Literature Survey- Part 1: Rock/Oil/Brine Interactions and the Effects of Core Handling on Wettability. *Journal of Petroleum Technology* 38, 1,125-1,144.
- Anderson, W., 1986b. Wettability Literature Survey- Part 2: Wettability Measurement. *Journal of Petroleum Technology* 38, 1,246-1,262.
- Anderson, W.G., 1987c. Wettability Literature Survey- Part 4: Effects of Wettability on Capillary Pressure. *Journal of Petroleum Technology* 39, 1,283-1,300.
- Anderson, W.G., 1987d. Wettability Literature Survey-Part 6: The Effects of Wettability on Waterflooding. *Journal of Petroleum Technology* 39, 1,605-1,622.
- Bear, J., 1988. Dynamics of fluids in porous media, Dover books on physics and chemistry. Elsevier, New York.
- Besnard, K., 2004. Modélisation du transport réactif dans les milieux poreux hétérogènes: application aux processus d'adsorption cinétique non linéaire, Mémoire du CAREN. Géosciences Rennes, Rennes, France.
- Bessaies Bey, H., Fusier, J., Harisson, S., Destarac, M., Jouenne, S., Passade-Boupat, N., Lequeux, F., d'Espinose de Lacaillerie, J.-B., Sanson, N., 2018. Impact of Polyacrylamide Adsorption on Flow through Porous Siliceous Materials: State of the Art, Discussion and Industrial Concern. *Journal of Colloid and Interface Science* 531.
- Bird, R.B., Armstrong, C.R., Hassager, O., 1977. Dynamics of polymeric liquids. Wiley, New York.
- Bohdanecký, M., Kovar, J., 1982. Viscosity of Polymer Solutions. Elsevier Scientific Publishing Company.
- Bousseau, C., Liu, Y., Buckley, J.S., 1995. 1995: Wetting Alteration of Silicate Surfaces by Brine and Crude Oil 10.
- Broseta, D., Medjahed, F., Lecourtier, J., Robin, M., 1995. Polymer Adsorption/Retention in Porous Media: Effects of Core Wettability and Residual Oil. *SPE Advanced Technology Series* 3, 103–112.
- Buckley, J.S., Liu, Y., Monsterleet, S., 1998. Mechanisms of Wetting Alteration by Crude Oils. *SPE Journal* 3, 54–61.
- Carman, P.C., 1937. Fluid flow through granular beds. *Chemical Engineering Research and Design* 75, 32–48.
- Chauveteau, G., Kohler, N., 1974. Polymer Flooding: The Essential Elements for Laboratory Evaluation. Presented at the SPE Improved Oil Recovery Symposium, OnePetro.
- Chiappa, L., Mennella, A., Lockhart, T.P., Burrafato, G., 1999. Polymer adsorption at the brine/rock interface: the role of electrostatic interactions and wettability. *Journal of Petroleum Science and Engineering* 24, 113–122.
- Chiara, R., 2009. Développement d'un code de calcul multiphasique multiconstituants. Université de Strasbourg.
- Chilingar, G.V., 1964. Relationship Between Porosity, Permeability, and Grain-Size Distribution of Sands and Sandstones, in: van Straaten, L.M.J.U. (Ed.), *Developments in Sedimentology, Deltaic and Shallow Marine Deposits*. Elsevier, pp. 71–75.
- Clennell, M.B., 1997. Tortuosity: a guide through the maze. Geological Society, London, Special Publications 122, 299–344.
- Cohen, Y., Christ, F.R., 1986. Polymer Retention and Adsorption in the Flow of Polymer Solutions Through Porous Media. *SPE Res Eng* 1, 113–118.
- Colby, R.H., 2010. Structure and linear viscoelasticity of flexible polymer solutions: comparison of polyelectrolyte and neutral polymer solutions. *Rheol Acta* 49, 425–442.

- Corey, A.T., 1994. Mechanics of immiscible fluids in porous media, 3rd ed. ed. Water Resources Publications, Highlands Ranch, Colo.
- Cossé, R., 1988. Techniques d'exploitation pétrolière. Le Gisement, Publications de l'Institut français du pétrole. Editions Technip, Paris.
- Cuiec, L., 1984. Rock/Crude-Oil Interactions and Wettability: An Attempt To Understand Their Interrelation. Presented at the SPE Annual Technical Conference and Exhibition, Society of Petroleum Engineers.
- Dabbous, M.K., 1976. Displacement of polymers in waterflooded porous media and its effects on a subsequent micellar flood.
- Daoud, M., Cotton, J.P., Farnoux, B., Jannink, G., Sarma, G., Benoit, H., Duplessix, C., Picot, C., 1975. Solutions of Flexible Polymers. Neutron Experiments and Interpretation 8, 15.
- Dawson, R., Lantz, R.B., 1972. Inaccessible Pore Volume in Polymer Flooding. SPE J. 12, 448–452.
- de Gennes, P.G., 1987. Polymers at an interface; a simplified view. Advances in Colloid and Interface Science 27, 189–209.
- de Gennes, P.G., 1979. Scaling concepts in polymer physics. Cornell University Press, Ithaca, N.Y.
- Dobrynin, A., Rubinstein, M., 2005. Theory of polyelectrolytes in solutions and at surfaces. Progress in Polymer Science 30, 1049–1118.
- Dobrynin, A.V., Colby, R.H., Rubinstein, M., 1995. Scaling Theory of Polyelectrolyte Solutions. Macromolecules 28, 1859–1871.
- Dominguez, J.G., Willhite, G.P., 1977. Retention and Flow Characteristics of Polymer Solutions in Porous Media. SPE J. 17, 111–121.
- Dullien, F.A.L., 1979. Porous media: fluid transport and pore structure. Academic Press, New York.
- Edwards, M., 1973. Dynamics of fluids in porous media By J. Bear. Pp xvii + 764. American Elsevier Publishing Company, Inc., New York.
- Epstein, N., 1989. On tortuosity and the tortuosity factor in flow and diffusion through porous media. Chemical Engineering Science 44, 777–779.
- Ergun, S., 1952. Fluid Flow Through Packed Columns.
- Ferreira, V.H.S., Moreno, R.B.Z.L., 2020. Polyacrylamide Adsorption and Readsorption in Sandstone Porous Media. SPE J. 25, 497–514.
- Fick, A., 1855. Ueber diffusion. J.A. Barth.
- Fleer, G.J., 2010. Polymers at interfaces and in colloidal dispersions. Advances in Colloid and Interface Science 159, 99–116.
- Glover, P.W.J., 2010. Formation Evaluation MSc Course Notes.
- Graessley, W.W., 2008. Polymeric liquids and networks: dynamics and rheology. Garland Science, London.
- Graessley, W.W., 2003. Polymeric Liquids & Networks: Structure and Properties. Garland Science.
- Graessley, W.W., 1980. Polymer chain dimensions and the dependence of viscoelastic properties on concentration, molecular weight and solvent power. Polymer 21, 258–262.
- Graveling, G.J., Vala Ragnarsdottir, K., Allen, G.C., Eastman, J., Brady, P.V., Balsley, S.D., Skuse, D.R., 1997. Controls on polyacrylamide adsorption to quartz, kaolinite, and feldspar. Geochimica et Cosmochimica Acta 61, 3515–3523.
- Green, D.W., Willhite, G.P., 1998. Enhanced Oil Recovery. Henry L. Doherty Memorial Fund of AIME, Society of Petroleum Engineers.
- Gregory, J., Barany, S., 2011. Adsorption and flocculation by polymers and polymer mixtures. Advances in Colloid and Interface Science 169, 1–12.
- Harris, D.C., 2007. Quantitative chemical analysis, 7th ed, 3rd printing. ed. W. H. Freeman, New York.

- Herzig, J.P., Leclerc, D.M., Goff, P.Le., 1970. Flow of Suspensions through Porous Media—Application to Deep Filtration. *Ind. Eng. Chem.* 62, 8–35.
- Huang, Y., Sorbie, K.S., 1993. Scleroglucan Behavior in Flow Through Porous Media: Comparison of Adsorption and In-Situ Rheology With Xanthan. Presented at the SPE International Symposium on Oilfield Chemistry, OnePetro.
- Hughes, D.S., Cottrell, C.W., Teeuw, D., Tollas, J.M., 1990. Appraisal of the use of polymer injection to suppress aquifer influx and to improve volumetric sweep in a viscous oil reservoir—. SPE (Society of Petroleum Engineers) Reservoir Engineering.
- Juárez Morejón, J.L., Bertin, H., Omari, A., Hamon, G., Cottin, C., Morel, D., Romero, C., Bourdarot, G., 2018. A New Approach to Polymer Flooding: Effects of Early Polymer Injection and Wettability on Final Oil Recovery. *SPE Journal* 24.
- Klein, E., Reuschlé, T., 2003. A Model for the Mechanical Behaviour of Bentheim Sandstone in the Brittle Regime. *Pure appl. geophys.* 160, 833–849.
- Kozeny, J., 1927. Über kapillare Leitung des Wassers im Boden.
- Kulicke, W.-M., Kniewske, R., 1984. The shear viscosity dependence on concentration, molecular weight, and shear rate of polystyrene solutions. *Rheol Acta* 23, 75–83.
- Lakatos, I., Lakatos-Szabó, J., Tóth, J., 1981. Factors Influencing Polyacrylamide Adsorption in Porous Media and Their Effect on Flow Behavior, in: Shah, D.O. (Ed.), *Surface Phenomena in Enhanced Oil Recovery*. Springer US, Boston, MA, pp. 821–842.
- Lecourtier, J., Chauveteau, G., 1985. Adsorption des polyacrylamides et du xanthane sur des surfaces minérales. Presented at the Colloque européen sur l'amélioration de la récupération du pétrole. 3, pp. 187–198.
- Lecourtier, J., Lee, L.T., Chauveteau, G., 1990. Adsorption of polyacrylamides on siliceous minerals. *Colloids and Surfaces* 47, 219–231.
- Lee, L.T., Somasundaran, P., 1989. Adsorption of polyacrylamide on oxide minerals. *Langmuir* 5, 854–860.
- Leontaritis, K.J., Mansoori, G.A., 1987. Asphaltene Flocculation During Oil Production and Processing: A Thermodynamic Colloidal Model. Presented at the SPE International Symposium on Oilfield Chemistry, Society of Petroleum Engineers.
- Ligoure, C., Leibler, L., 1990. Thermodynamics and kinetics of grafting end-functionalized polymers to an interface. *J. Phys. France* 51, 1313–1328.
- Liu, Q., Dong, M., Asghari, K., Tu, Y., 2007. Wettability alteration by magnesium ion binding in heavy oil/brine/chemical/sand systems — Analysis of electrostatic forces. *Journal of Petroleum Science and Engineering* 59, 147–156.
- Lotsch, T., Muller, T., Pusch, G., 1985. The Effect of Inaccessible Pore Volume on Polymer Coreflood Experiments.
- MacWilliams, D.C., Rogers, J.H., West, T.J., 1973. Water-Soluble Polymers in Petroleum Recovery, in: Bikales, N.M. (Ed.), *Water-Soluble Polymers*, Polymer Science and Technology. Springer US, Boston, MA, pp. 105–126.
- Marker, J.M., 1973. Dependence of Polymer Retention on Flow Rate. *J Pet Technol* 25, 1307–1308.
- Marques, C., Joanny, J.F., Leibler, L., 1988. Adsorption of block copolymers in selective solvents. *Macromolecules* 21, 1051–1059.
- Meybodi, H.E., Kharrat, R., Araghi, M.N., 2011. Experimental studying of pore morphology and wettability effects on microscopic and macroscopic displacement efficiency of polymer flooding. *Journal of Petroleum Science and Engineering* 2, 347–363.
- Moldrup, P., Olesen, T., Komatsu, T., Schjønning, P., Rolston, D.E., 2001. Tortuosity, Diffusivity, and Permeability in the Soil Liquid and Gaseous Phases. *Soil Sci. Soc. Am. J.* 65, 613–623.
- Monicard, R., Houpeurt, A., 1975. Cours de production. 1: Caractéristiques des roches réservoirs, Publications de l'Institut Français du Pétrole. Soc. des Editions Technip, Paris.

- Morejon, J.L.J., 2017. Récupération assistée du pétrole par injection de polymères hydrosolubles : nouvelle approche.
- Morrow, N.R., 1990. Wettability and Its Effect on Oil Recovery. *Journal of Petroleum Technology* 42, 1,476-1,484.
- Mungan, N., 1969. Rheology and Adsorption of Aqueous Polymer Solutions. *Journal of Canadian Petroleum Technology* 8, 45–50.
- Nelson, P.H., 1994. Permeability-porosity relationships in sedimentary rocks. *Log Analyst* 35, 38–62.
- Nierlich, M., Boue, F., Lapp, A., Oberthür, R., 1985. Characteristic lengths and the structure of salt free polyelectrolyte solutions. A small angle neutron scattering study. *Colloid & Polymer Sci* 263, 955–964.
- Nooruddin, H.A., Hossain, M.E., 2011. Modified Kozeny–Carmen correlation for enhanced hydraulic flow unit characterization. *Journal of Petroleum Science and Engineering* 80, 107–115.
- Ogata, A., Banks, R.B., 1961. A Solution of the Differential Equation of Longitudinal Dispersion in Porous Media. U.S. Government Printing Office.
- Onogi, S., Masuda, T., Miyanaga, N., Kimura, Y., 1967. Dependence of viscosity of concentrated polymer solutions upon molecular weight and concentration. *Journal of Polymer Science Part A-2: Polymer Physics* 5, 899–913.
- Pefferkorn, E., Nabzar, L., Carroy, A., 1985. Adsorption of polyacrylamide to Na kaolinite: Correlation between clay structure and surface properties. *Journal of Colloid and Interface Science* 106, 94–103.
- Perkins, T.K., Johnston, O.C., 1963. A Review of Diffusion and Dispersion in Porous Media. *Society of Petroleum Engineers Journal* 3, 70–84.
- Rege, S.D., Fogler, H.S., 1988. A network model for deep bed filtration of solid particles and emulsion drops. *AIChE Journal* 34, 1761–1772.
- Rouquerol, J., Avnir, D., Fairbridge, C.W., Everett, D.H., Haynes, J.M., Pernicone, N., Ramsay, J.D.F., Sing, K.S.W., Unger, K.K., 1994. Recommendations for the characterization of porous solids (Technical Report). *Pure and Applied Chemistry* 66, 1739–1758.
- Rubinstein, M., Colby, R.H., 2003. *Polymer Physics*. OUP Oxford.
- Ruedrich, J., Siegesmund, S., 2007. Salt and ice crystallisation in porous sandstones. *Environ Geol* 52, 225–249.
- Runkel, R.L., 1996. Solution of the advection-dispersion equation: Continuous load of finite duration. *Journal of Environmental Engineering*.
- Runkel, R.L., Bencala, K.E., 1995. Transport of reacting solutes in rivers and streams, in: Singh, V.P. (Ed.), *Environmental Hydrology, Water Science and Technology Library*. Springer Netherlands, Dordrecht, pp. 137–164.
- Russel, W.B., Saville, D.A., Schowalter, W.R., 1991. *Colloidal Dispersions*. Cambridge University Press.
- Sahimi, M., 1993. Flow phenomena in rocks: from continuum models to fractals, percolation, cellular automata, and simulated annealing. *Rev. Mod. Phys.* 65, 1393–1534.
- Saraji, S., Goual, L., Piri, M., 2010. Adsorption of Asphaltenes in Porous Media under Flow Conditions. *Energy Fuels* 24, 6009–6017.
- Scheidegger, A.E., 1974. *The physics of flow through porous media*, 3d ed. ed. University of Toronto Press, Toronto.
- Scheidegger, A.E., 1960. *The physics of flow through porous media*. University of Toronto Pr., Canada.
- Semenov, A.N., Khokhlov, A.R., 1988. Statistical physics of liquid-crystalline polymers. *Sov. Phys. Usp.* 31, 988.
- Serra, O., 1985. *Sedimentary environments from wireline logs*. Schlumberger Ltd., Houston, Tex.

- Sheng, J., 2011. Modern chemical enhanced oil recovery: theory and practice. Gulf Professional Pub, Amsterdam ; Boston, MA.
- Skauge, A., 2013. Low Salinity Flooding - A Critical Review. Presented at the IOR 2013 - 17th European Symposium on Improved Oil Recovery, European Association of Geoscientists & Engineers.
- Skauge, A., Fosse, B., 1994. A Study of Adhesion, Interfacial Tensions, and Contact Angles for a Brine, Quartz Crude Oil System. Presented at the International Symposium on Reservoir Wettability and Its Effect on Oil Recovery.
- Smith, F.W., 1970. The Behavior of Partially Hydrolyzed Polyacrylamide Solutions in Porous Media. *Journal of Petroleum Technology* 22, 148–156.
- Sorbie, K., Johnson, P., Hubbard, S., Temple, J., 1989. Non-equilibrium effects in the adsorption of polyacrylamide onto sandstone; Experimental and modelling study.
- Sorbie, K.S., 2013. Polymer-improved oil recovery. Springer Science & Business Media.
- Sorbie, K.S., 1991. Polymer-Improved Oil Recovery. Springer Netherlands, Dordrecht.
- Szabo, M.T., 1975. Some Aspects of Polymer Retention in Porous Media Using a C14-Tagged Hydrolyzed Polyacrylamide. *SPE J.* 15, 323–337.
- Tiab, D., Donaldson, E.C., 2012. Petrophysics: Theory and Practice of Measuring Reservoir Rock and Fluid Transport Properties. Gulf Professional Publishing.
- Tien, C., Payatakes, A.C., 1979. Advances in deep bed filtration. *AIChE Journal* 25, 737–759.
- Todd, A.C., Somerville, J.E., Scott, G., 1984. The Application of Depth of Formation Damage Measurements in Predicting Water Injectivity Decline. Presented at the SPE Formation Damage Control Symposium, OnePetro.
- Tye, F.L., 1983. Tortuosity. *Journal of Power Sources* 9, 89–100.
- Valat, M., Bertin, H., Robin, M., 1993. Two-phase flow in porous media: influence of pH on wettability.
- Wever, D.A., Bartlema, H., ten Berge, A.B., Al-Mjeni, R., Glasbergen, G., 2018. The Effect of the Presence of Oil on Polymer Retention in Porous Media from Clastic Reservoirs in the Sultanate of Oman. Presented at the SPE EOR Conference at Oil and Gas West Asia, OnePetro.
- Whitaker, S., 1986. Flow in porous media I: A theoretical derivation of Darcy's law. *Transp Porous Med* 1, 3–25.
- Willhite, G., Dominguez, J.G., 1977. Mechanisms of polymer retention in porous media.
- Zaitoun, A., Chauveteau, G., 1998. Effect of Pore Structure and Residual Oil on Polymer Bridging Adsorption, in: All Days. Presented at the SPE/DOE Improved Oil Recovery Symposium, SPE, Tulsa, Oklahoma, p. SPE-39674-MS.
- Zaitoun, A., Kohler, N., 1987. The Role of Adsorption in Polymer Propagation Through Reservoir Rocks. Presented at the SPE International Symposium on Oilfield Chemistry, OnePetro.
- Zhang, G., Seright, R., 2014. Effect of Concentration on HPAM Retention in Porous Media.
- Zheng, C.G., Gall, B.L., Gao, H.W., Miller, A.E., Bryant, R.S., 2000. Effects of Polymer Adsorption and Flow Behavior on Two-Phase Flow in Porous Media. *SPE Res Eval & Eng* 3, 216–223.

Appendix A

Viscosity of polymers

The shear viscosity of each polymer solution was measured using a controlled shear stress rheometer ARG2 (TA Instruments, France) or Kinexus (Malverne, France). We measured viscosity at temperature $T=25^{\circ}\text{C}$ using a 2° cone/plate geometry by steeply increasing shear rate from 0.001s^{-1} to 1000s^{-1} .

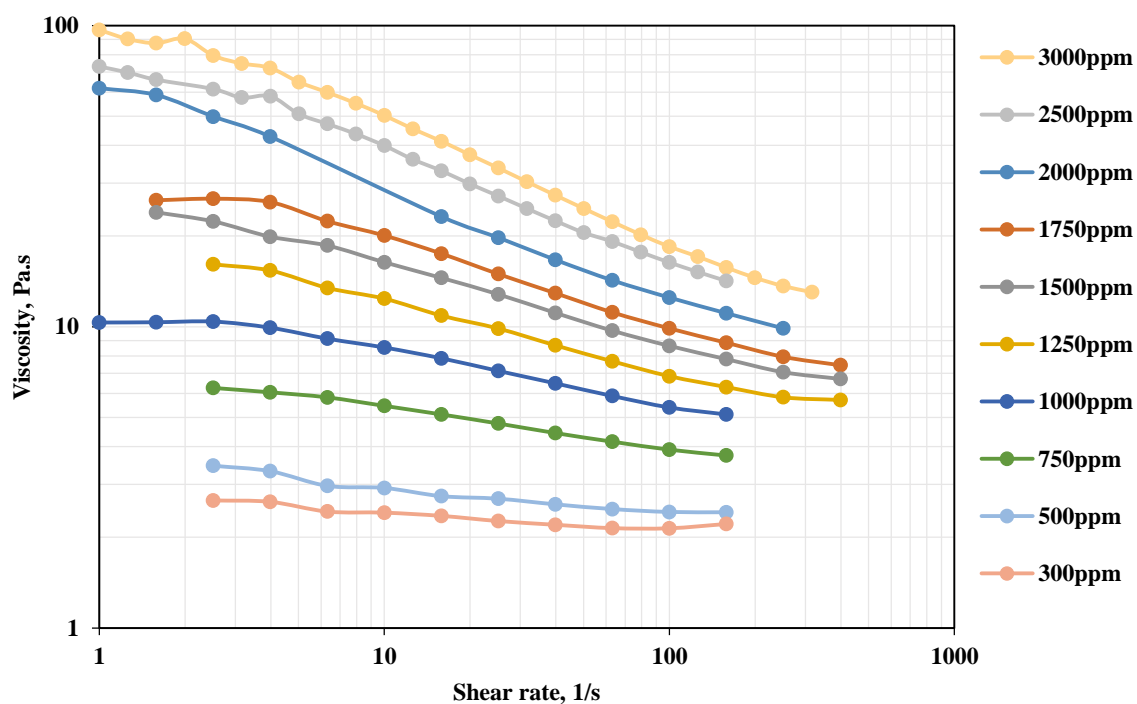


Figure 7-1. Dynamic viscosity of Flopaam 3630S as a function of the shear rate at different concentrations at $T = 25^{\circ}\text{C}$

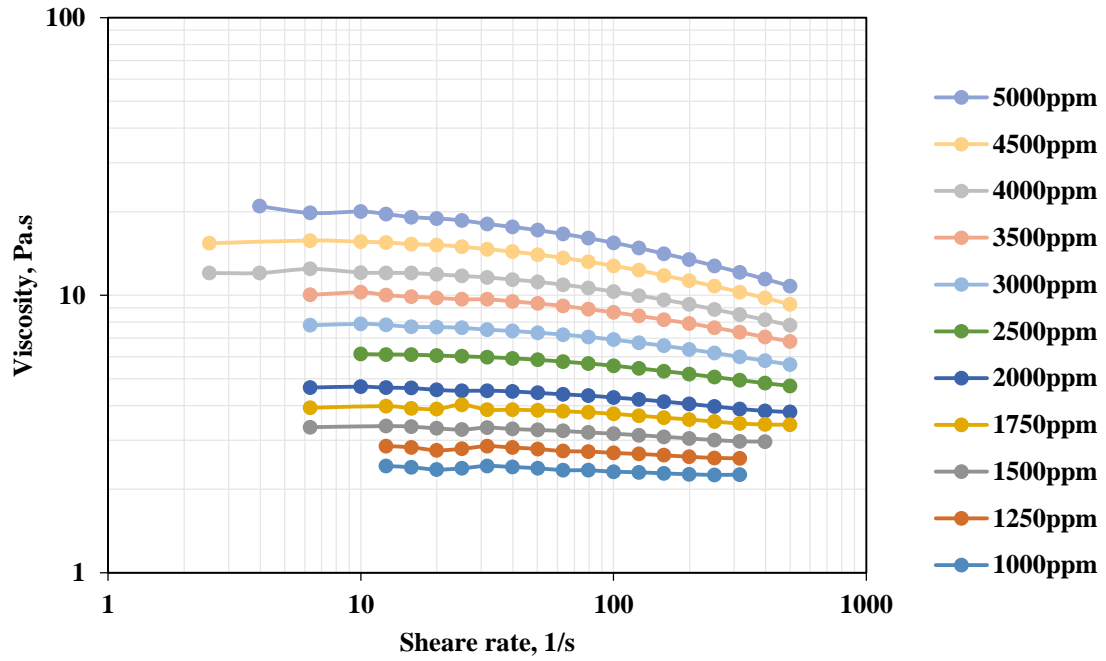


Figure 7-2. Dynamic viscosity of Flopaam 3130S as a function of the shear rate at different concentrations at T = 25°C

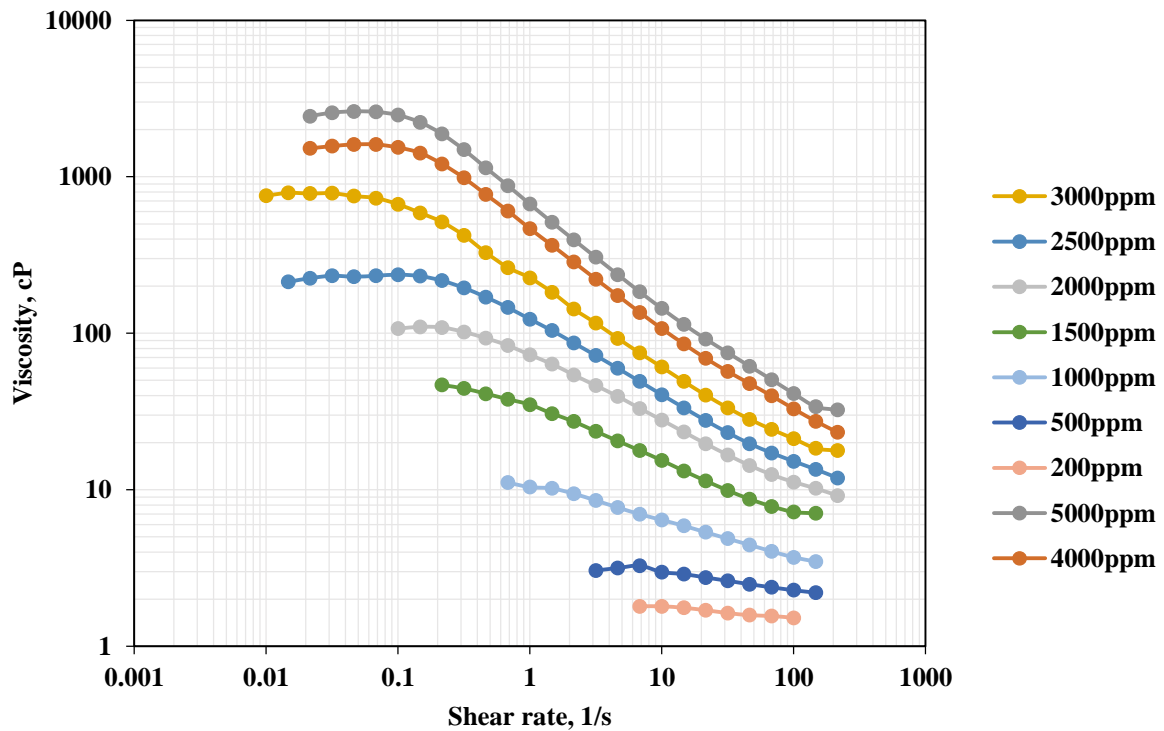


Figure 7-3. Dynamic viscosity of Flopaam 5115XV as a function of the shear rate at different concentrations at T = 25°C

Appendix B

Experimental data on polymer front and dispersion test

3630S in Bentheimer

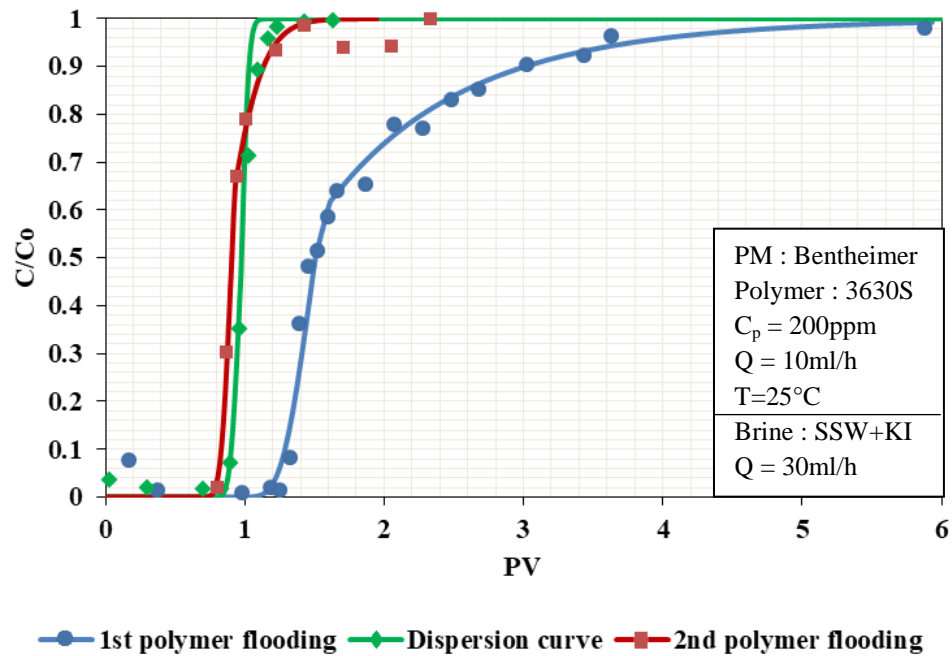


Figure 8-1. Breakthrough curves of first and second polymer flooding at $C_p=200\text{ppm}$ of 3630S in Bentheimer and KI dispersion

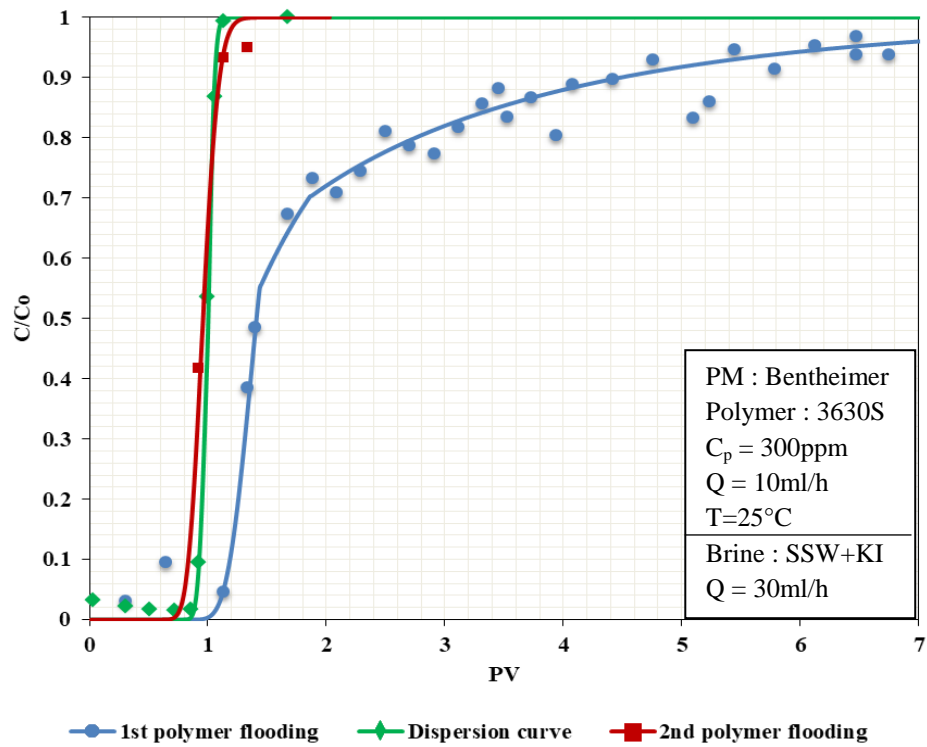


Figure 8-2. Breakthrough curves of first and second polymer flooding at $C_p=300\text{ppm}$ of 3630S in Bentheimer and KI dispersion

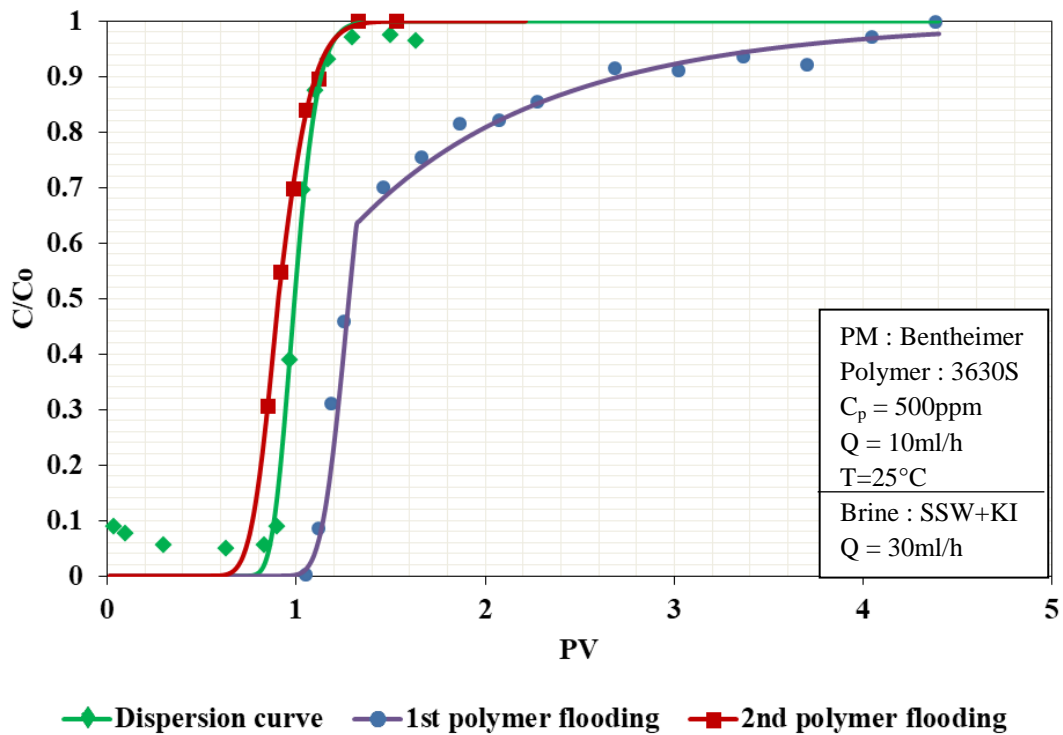


Figure 8-3. Breakthrough curves of first and second polymer flooding at $C_p=500\text{ppm}$ of 3630S in Bentheimer and KI dispersion

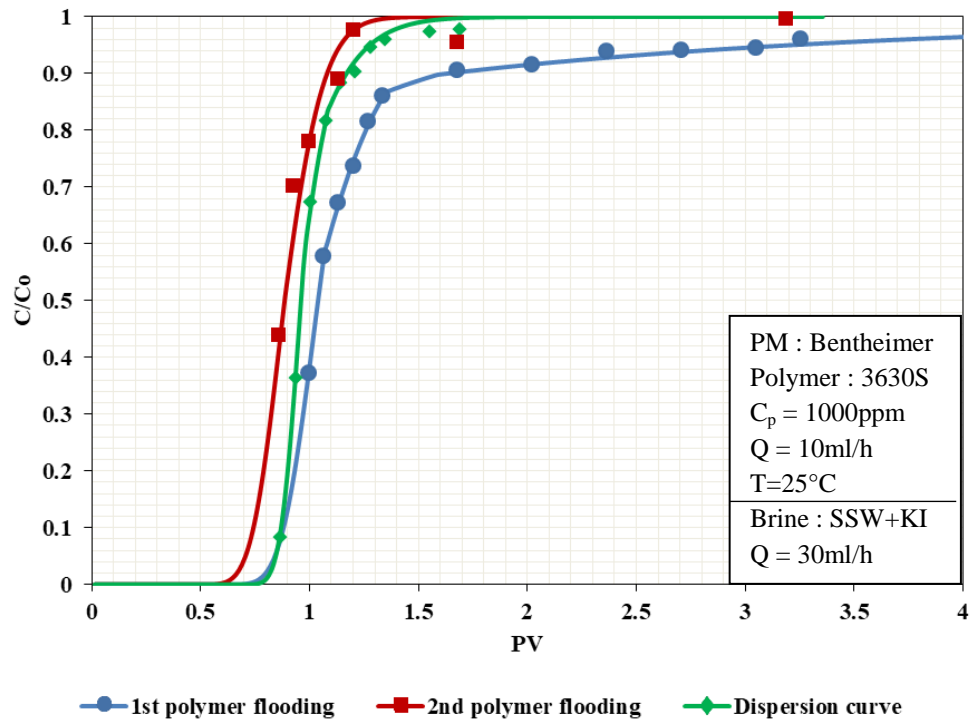


Figure 8-4. Breakthrough curves of first and second polymer flooding at $C_p=1000\text{ppm}$ of 3630S in Bentheimer and KI dispersion

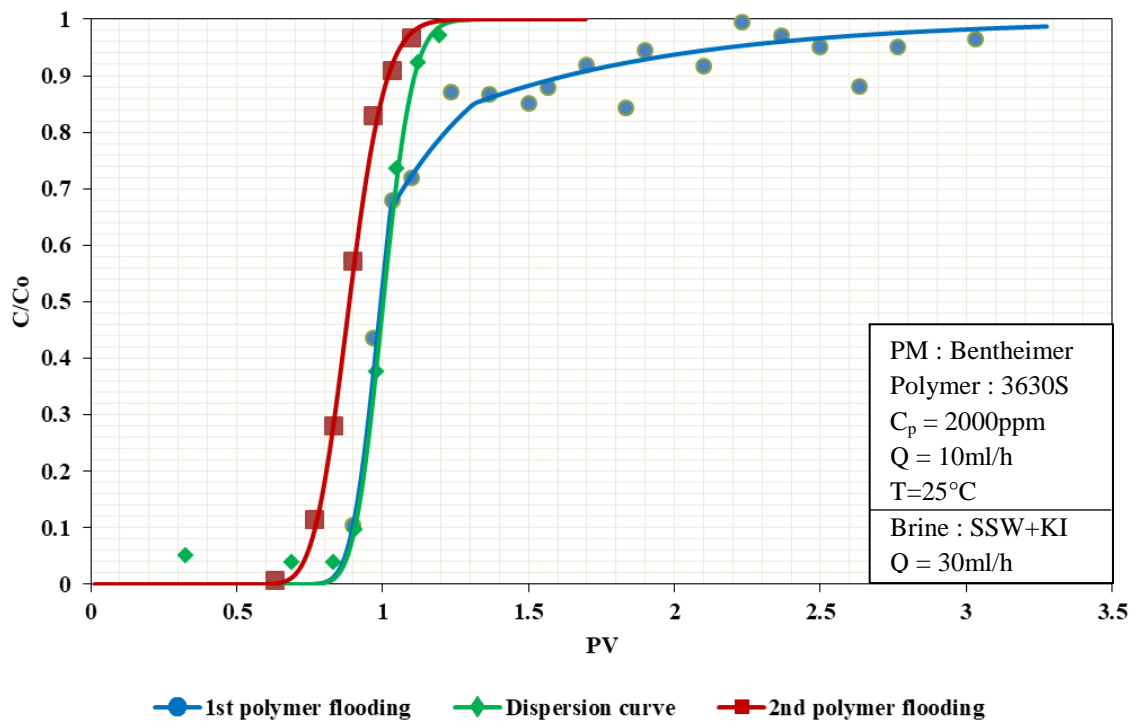


Figure 8-5. Breakthrough curves of first and second polymer flooding at $C_p=2000\text{ppm}$ of 3630S in Bentheimer and KI dispersion

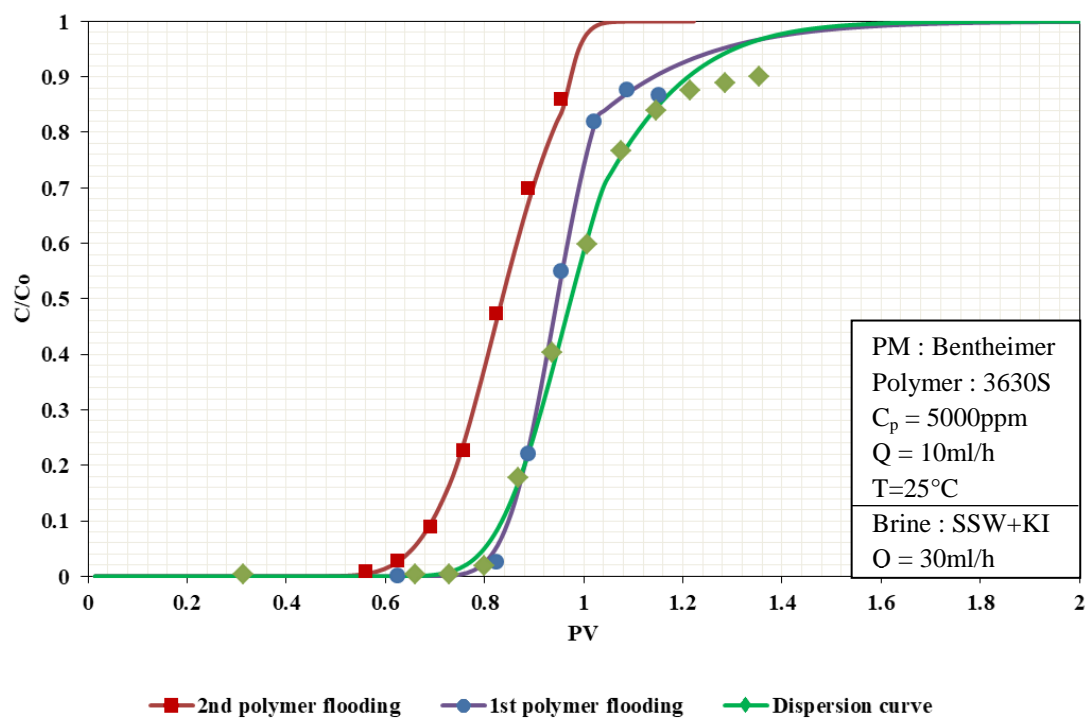


Figure 8-6. Breakthrough curves of first and second polymer flooding at $C_p=5000\text{ppm}$ of 3630S in Bentheimer and KI dispersion

3130S in Berea

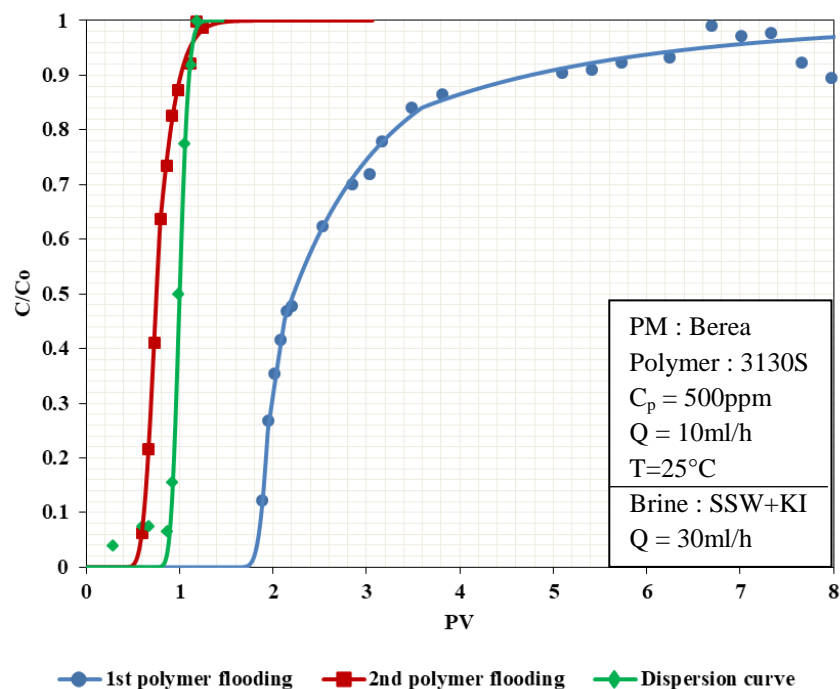


Figure 8-7. Breakthrough curves of first and second polymer flooding at $C_p=500\text{ppm}$ of 3130S in Berea and KI dispersion

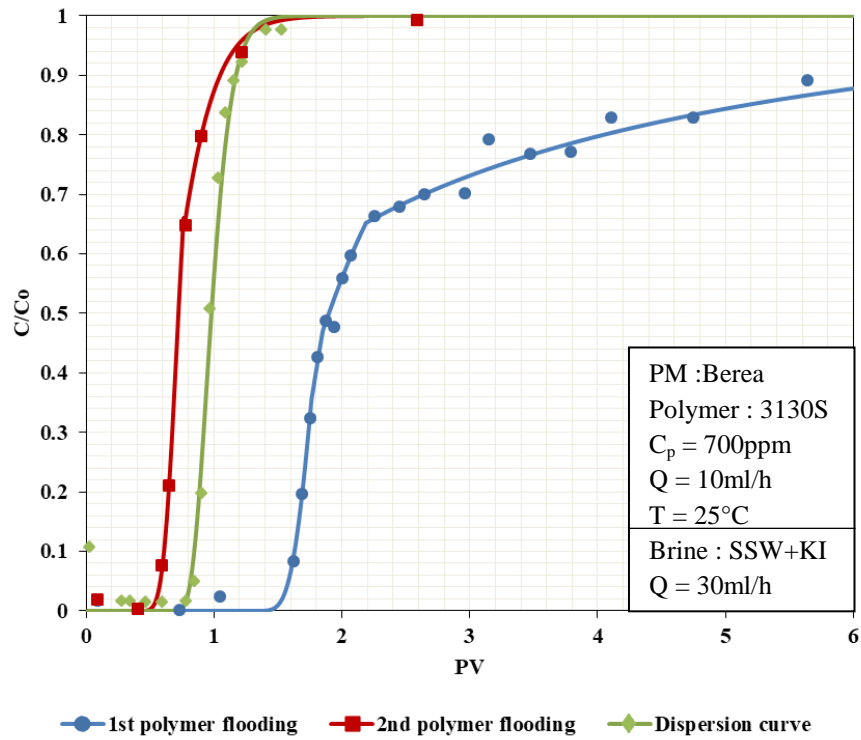


Figure 8-8. Breakthrough curves of first and second polymer flooding at $C_p=700\text{ppm}$ of 3130S in Berea and KI dispersion

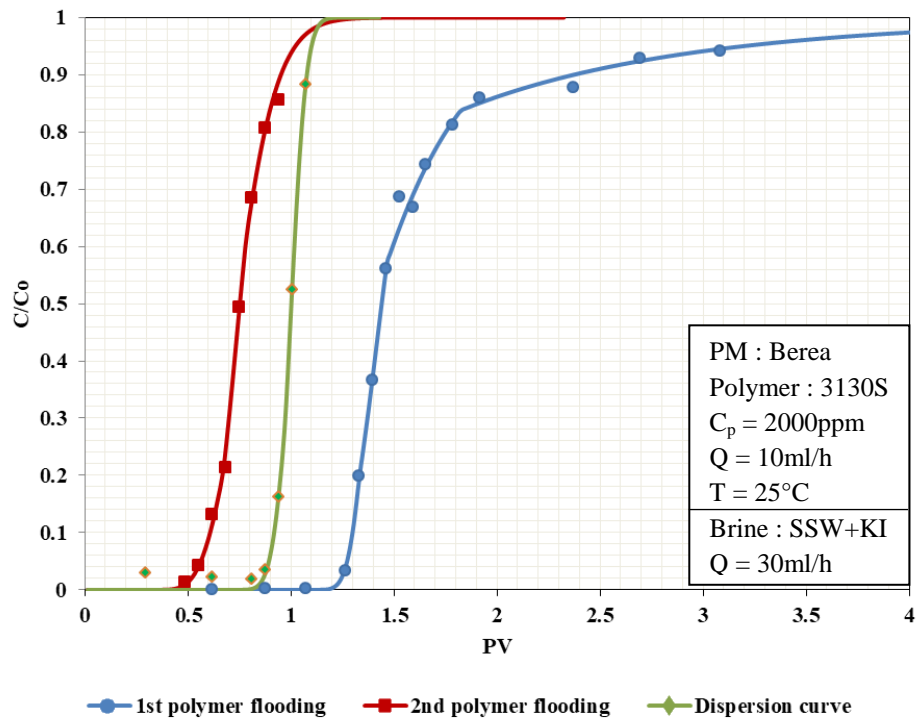


Figure 8-9. Breakthrough curves of first and second polymer flooding at $C_p=2000\text{ppm}$ of 3130S in Berea and KI dispersion

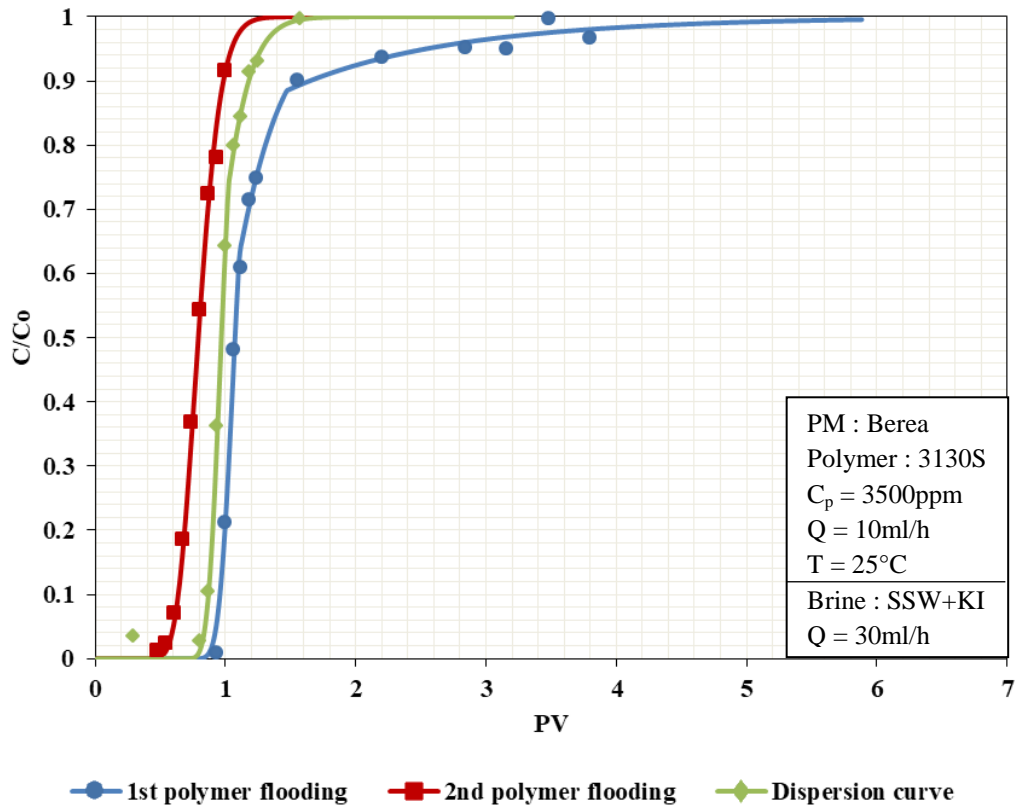


Figure 8-10. Breakthrough curves of first and second polymer flooding at $C_p=3500\text{ppm}$ of 3130S in Berea and KI dispersion

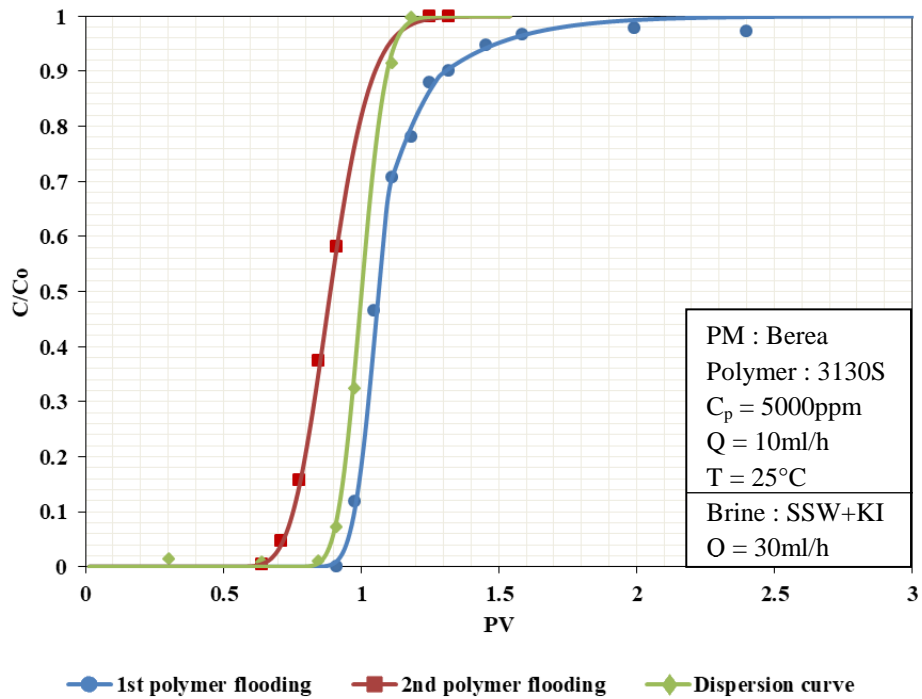


Figure 8-11. Breakthrough curves of first and second polymer flooding at $C_p=5000\text{ppm}$ of 3130S in Berea and KI dispersion

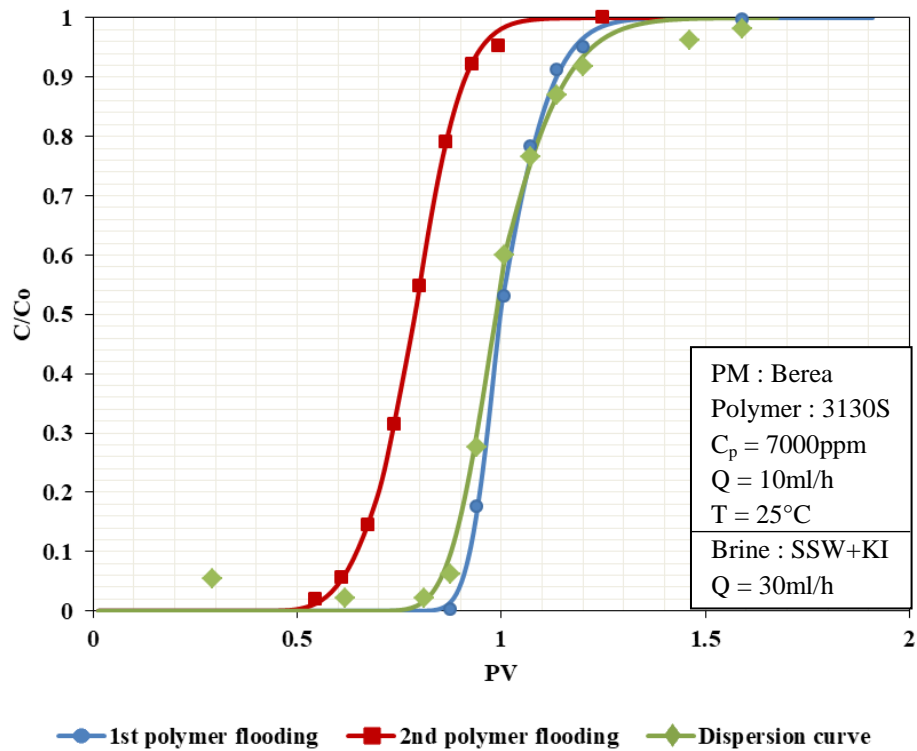


Figure 8-12. Breakthrough curves of first and second polymer flooding at $C_p=7000\text{ppm}$ of 3130S in Berea and KI dispersion

3130S in Bentheimer

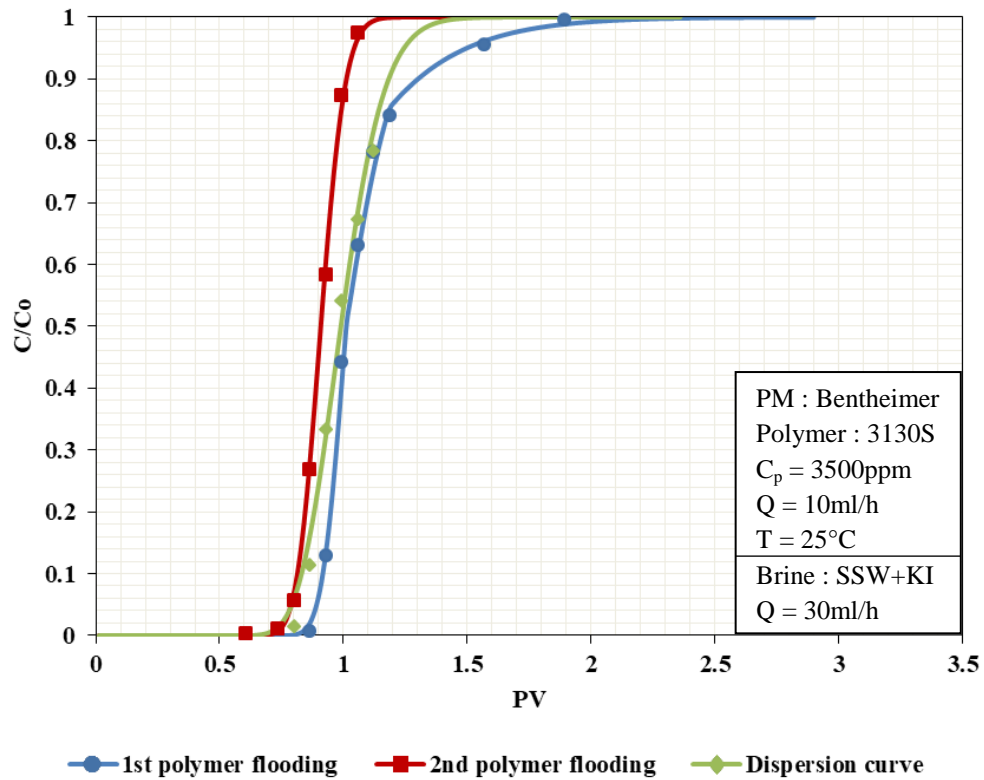


Figure 8-13. Breakthrough curves of first and second polymer flooding at $C_p=3500\text{ppm}$ of 3130S in Bentheimer and KI dispersion

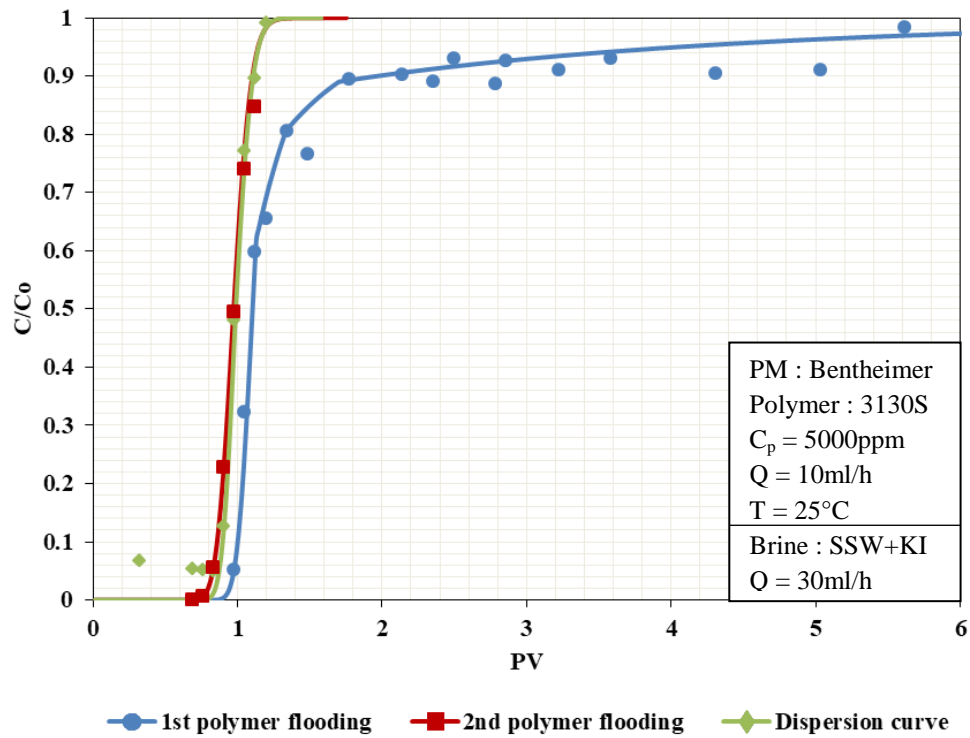


Figure 8-14. Breakthrough curves of first and second polymer flooding at $C_p=5000\text{ppm}$ of 3130S in Bentheimer and KI dispersion

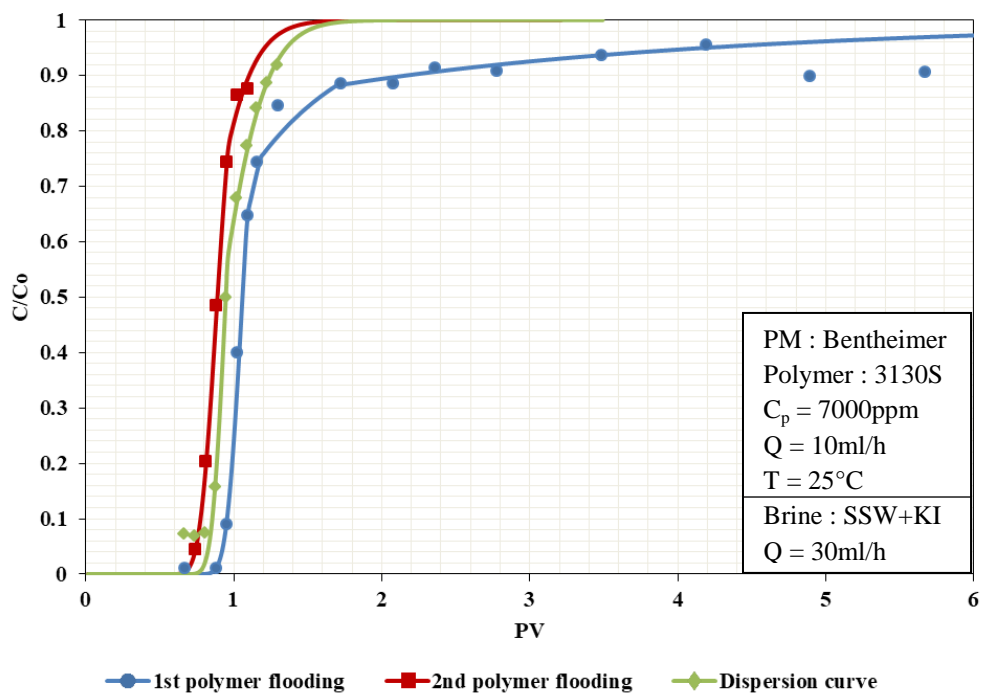


Figure 8-15. Breakthrough curves of first and second polymer flooding at $C_p=7000\text{ppm}$ of 3130S in Bentheimer and KI dispersion

5115XV and 5115BPM in Bentheimer

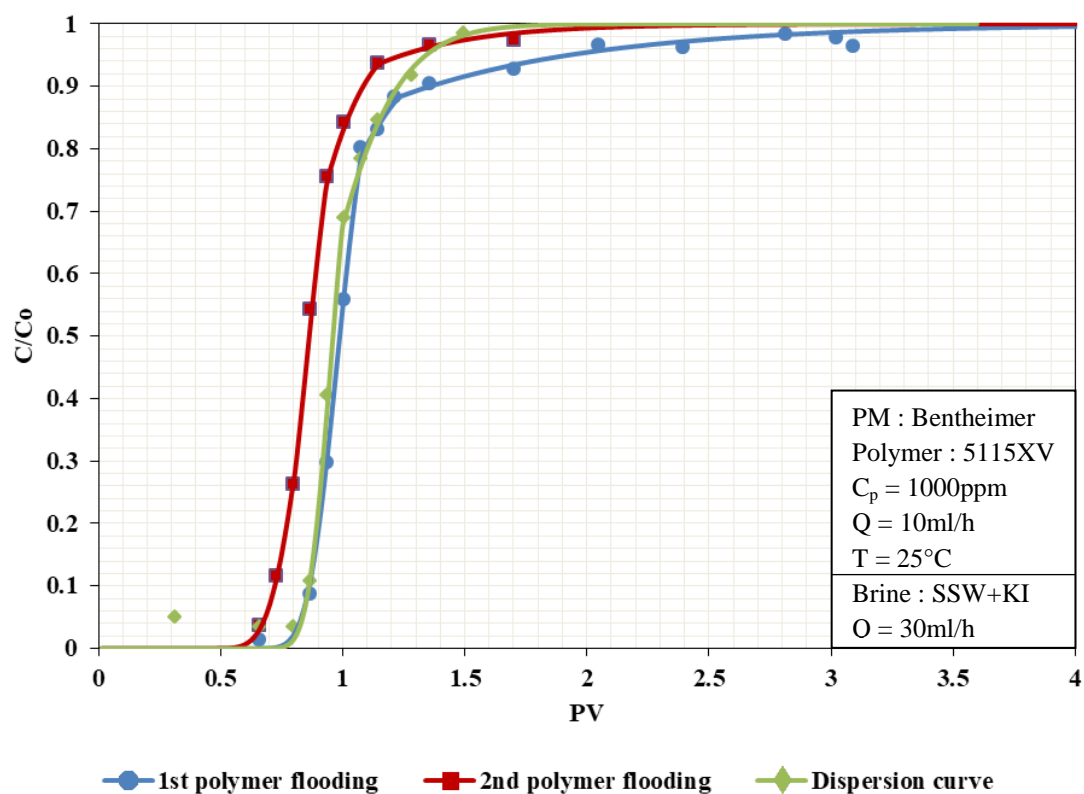


Figure 8-16. Breakthrough curves of first and second polymer flooding at $C_p=1000\text{ppm}$ of 5115XV in Bentheimer and KI dispersion

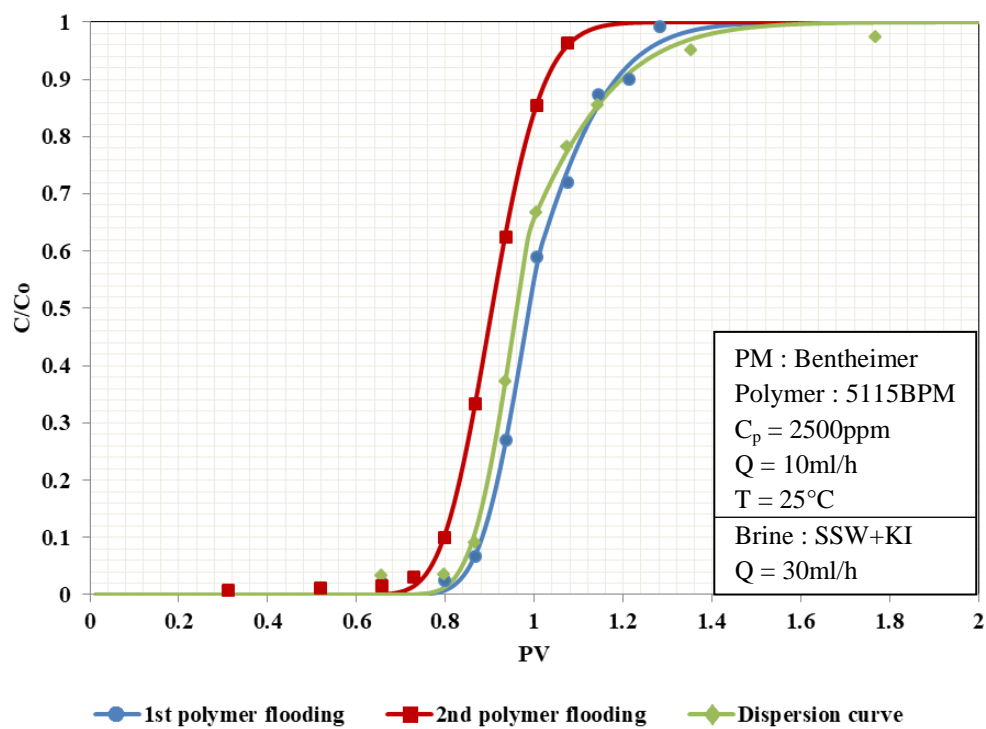


Figure 8-17. Breakthrough curves of first and second polymer flooding at $C_p=2500\text{ppm}$ of 5115BPM in Bentheimer and KI dispersion

Table 8-1. Experimental data from monophasic experiments in Bentheimer

Polymer	C _p , ppm	k, D	ϕ	PV, ml	Γ , $\mu\text{g/g}$	RM	IPV
3630S	200	2.91	0.234	75	21.9	1.9	4.8
	300	3.07	0.228	73	40.7	0.66	5
	500	2.48	0.234	75	41.5	4	8.13
	1000	2.54	0.249	71	54.2	8.6	10
	2000	3.33	0.234	69	63.9	40.9	11.4
	3000	2.75	0.22	65	61.8	68.5	8
	5000	2.68	0.244	72	77.5	258	16.6
3130S	3500	3.6	0.274	78	73	9	8.8
	5000	2.7	0.239	69	322	17	2
	7000	2.34	0.241	71	496	35	9
5115XV	1000	2.35	0.244	72	25	28	11
5115BPM	2500	2.3	0.244	72	33	10	9

Table 8-2. Experimental data from monophasic experiments with 3130S in Berea

C _p , ppm	k, mD	ϕ	PV, ml	Γ , $\mu\text{g/g}$	RM	IPV
500	168	0.209	78	104	2.2	21.6
700	132	0.206	79	173	2.7	21.4
2000	112	0.206	77	173	6.2	23.1
3500	108	0.217	81	163	12	19.5
5000	95	0.198	74	100	21	10
7000	120	0.201	77	155	37	22.1

Diphasic Experiments

3630S in Bentheimer

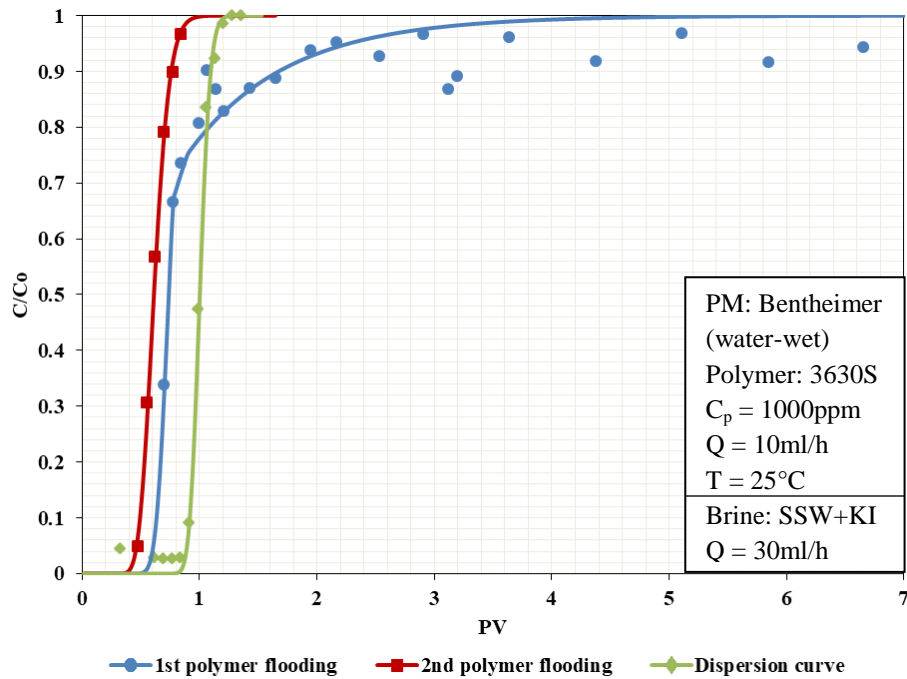


Figure 8-18. Breakthrough curves of first and second polymer flooding at $C_p=1000\text{ppm}$ of 3630S in Bentheimer (water-wet) and KI dispersion

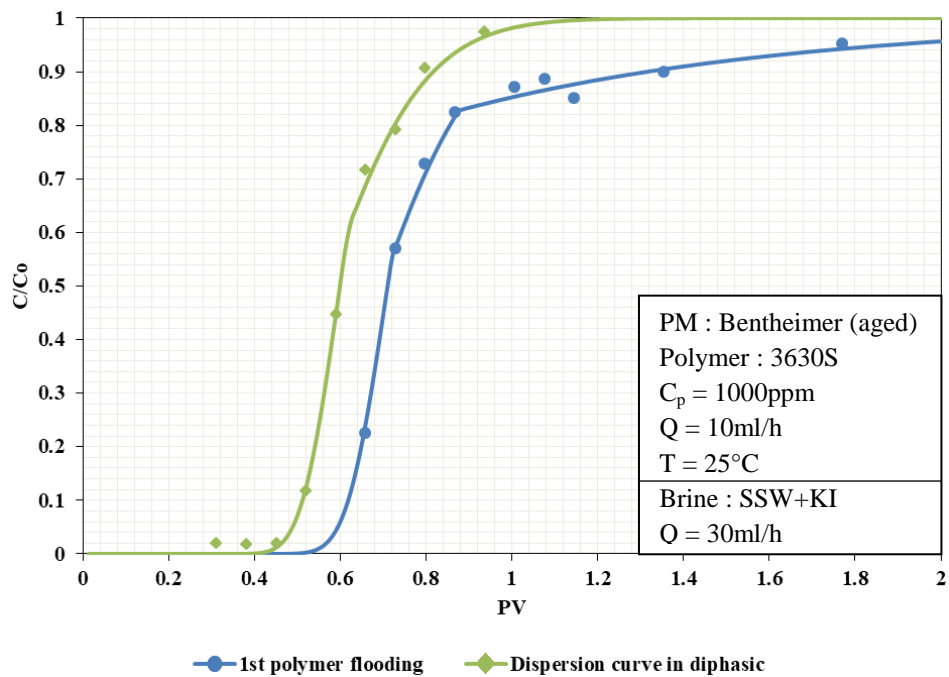


Figure 8-19. Breakthrough curves of first and second polymer flooding at $C_p=1000\text{ppm}$ of 3630S in Bentheimer (aged) and KI dispersion

5115XV in Bentheimer

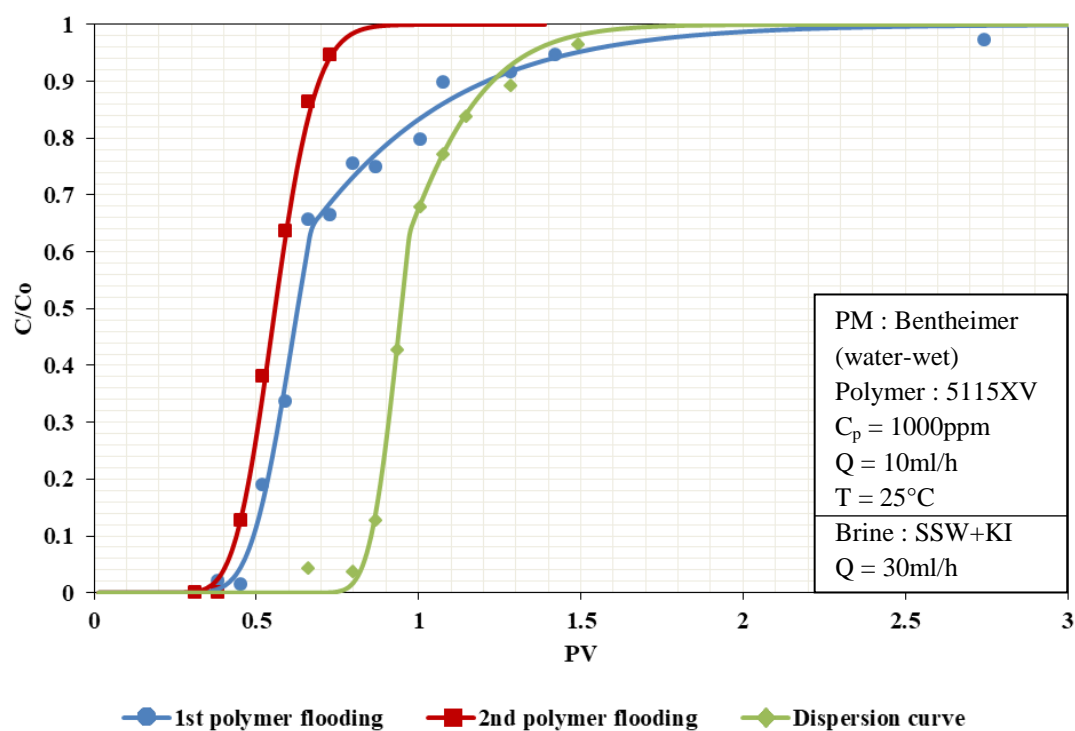


Figure 8-20. Breakthrough curves of first and second polymer flooding at $C_p=1000\text{ppm}$ of 5115XV in Bentheimer (water-wet) and KI dispersion

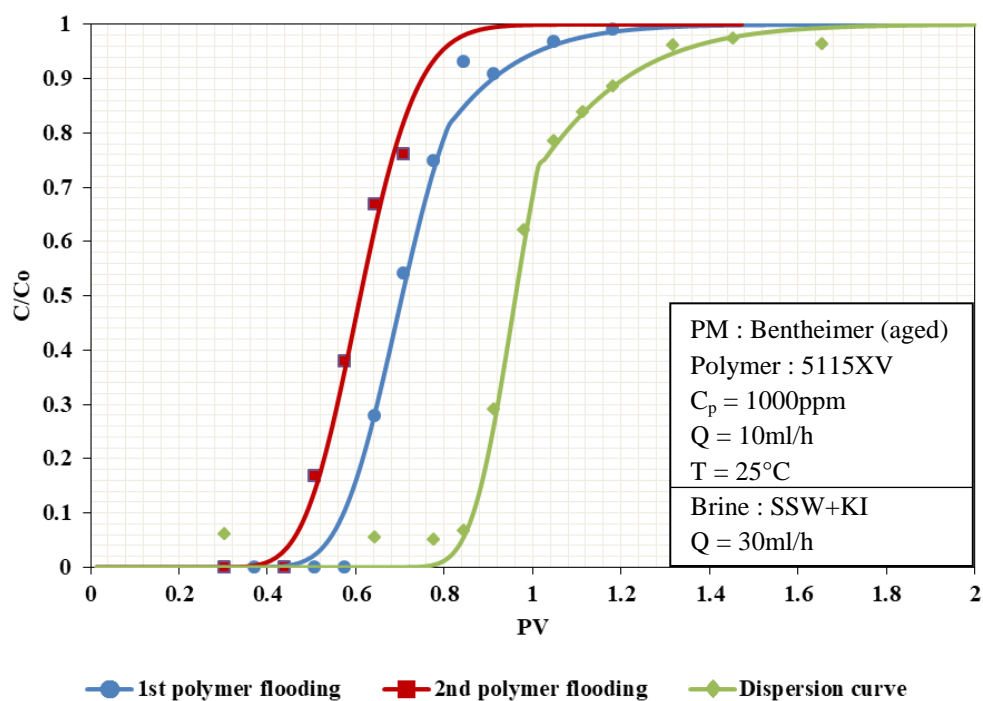


Figure 8-21. Breakthrough curves of first and second polymer flooding at $C_p=1000\text{ppm}$ of 5115XV in Bentheimer (aged) and KI dispersion